Université de Toulouse

THESE

En vue de l'obtention du

DOCTORAT DE L'UNIVERSITÉ DE TOULOUSE

Délivré par *l'Université Toulouse III - Paul Sabatier*
Discipline ou spécialité : *Biochimie et Biologie moléculaire*

Présentée et soutenue par *Lara KADDOUM*
Le *17 Décembre 2010*

Titre : *La protéine MeCP2: Etude de son implication dans la réponse aux dommages à l'ADN et développement de nouveaux outils pour sa détection*

JURY

Pr. Bernard SALLES - Professeur (UPS - Toulouse) - Président du Jury
Pr. Cristina CARDOSO - Professeur (Technische Universität - Darmstadt) - Rapporteur
Dr. Mario COSTA - Researcher (Institue of Neuroscience - Pisa) - Rapporteur
Dr. Frédéric COIN -Directeur de Reherche (IGBMC - Strasbourg) - Examinateur
Dr. Wim Vermeulen - Directeur de Recherche - (Erasmus MC - Rotterdam) - Examinateur
Dr. Giuseppina GIGLIA-MARI - Chargé de Recherche (IPBS - Toulouse) - Directrice de thèse
Dr. Etienne JOLY - Chargé de Recherche (IPBS - Toulouse) - Directeur de thèse

---

Ecole doctorale : *Biologie-Santé-Biotechnologies*
Unité de recherche : *IPBS CNRS - UMR5089*
Directeur(s) de Thèse : *Dr. Giuseppina GIGLIA-MARI et Dr. Etienne JOLY*
Rapporteurs : *Pr. Cristina CARDOSO et Dr. Mario COSTA*

Résumé

Le syndrome de Rett est une maladie neurodéveloppementale progressive conduisant à un polyhandicap lourd associé à des retards mentaux sévères. Cette pathologie a pour principale origine des mutations du gène codant pour la protéine Methyl-CpG Binding Protein 2 (MeCP2), localisé sur le chromosome X. Elle touche essentiellement les filles avec une fréquence d'environ 1/10 000 naissances. Différentes fonctions ont été attribuées à MeCP2 : modulateur transcriptionnel (active ou réprime la transcription), épissage alternatif de certains ARN, maintien de l'état de méthylation des gènes au cours de la réplication de l'ADN et modification de la structure tridimensionnelle et/ou du niveau de compaction de la chromatine.

Initialement, mes travaux de thèse ont consisté à explorer l'hypothèse que MeCP2 aurait la capacité de passer d'une cellule à l'autre. Les résultats obtenus suggèrent fortement que le transfert intercellulaire de MeCP2 ne se produit pas in vivo mais serait dû à une diffusion inter-cellulaire de la protéine suite à l'étape de fixation cellulaire à l'acétone nécessaire à la suite de l'expérimentation. Cependant, ces travaux nous ont permis de mettre au point une nouvelle méthode pour la détection des protéines dans les cellules de mammifères basée sur le système de split GFP.

Dans le cadre de mon projet de thèse, j'ai également produit et caractérisé des anticorps dirigés spécifiquement contre chacune des 2 isoformes de MeCP2. Ces anticorps originaux vont permettre d'étudier les niveaux d'expression et le rôle de chaque isoforme dans divers types cellulaires de l'organisme. Cela va pouvoir améliorer notre compréhension de la pathologie du syndrome de Rett.

Plus récemment, mes travaux se sont focalisés sur la relation entre MeCP2 et les mécanismes de réparation de l'ADN, et nous ont permis de mettre en évidence la capacité de MeCP2 de s'accumuler sur l'ADN endommagé. Cette accumulation est indépendante de la transcription et des voies GG-NER et TC-NER. Mais, elle dépend de la région C-terminal de la protéine MeCP2. Les futurs projets de l'équipe viseront à élucider les mécanismes impliqués dans cette nouvelle fonction de MeCP2.

Abstract

Rett syndrome is a severe and progressive X-linked neurodevelopmental disorder that affects 1/10000 female birth. RTT is caused by mutations in the mecp2 gene, encoding the Methyl CpG binding Protein 2. MeCP2 binds to methylated DNA and has several roles in: transcription activation or repression, chromatin remodeling, alternative splicing of mRNA, etc.

Initially, my thesis project was to explore the hypothesis that MeCP2 may be able to transfer between cells. My results suggest that this phenomenon appears after cell fixation with acetone and doesn't occur in vivo. This work, however, allowed us to develop a new staining method to detect and localize proteins in mammalian cells using the split GFP system.

Within the frame of this project, I have also produced antibodies specific for each of the two MeCP2 isoforms. These novel antibodies should prove to be interesting tools to understand the role of each isoform in the pathology of Rett syndrome.

More recently, my work was focalized on the relationship between MeCP2 and DNA damage. I was able to show that MeCP2 accumulates on DNA damage. This accumulation is independent from transcription, GG-NER and TC-NER pathways but depend on the C-terminal region of MeCP2. Future work will be aimed at understanding the mechanisms involved in this newly uncovered function of MeCP2, and will hopefully improve our understanding of Rett syndrome pathogenesis.

Many Thanks...

MA thèse a été réalisée au sein de l'Institut de Pharmacologie et de Biologie Structurale dirigée par Dr Jean-Philippe Girard. Je tiens à vous remercier pour votre accueil au sein du laboratoire.

I would like to thank Pr. Bernard Salles who accepted to be the president of my thesis jury.

I want also to thank Dr. Mario Costa, Dr. Frédéric Coin and Dr. Wim Vermeulen who accepted to evaluate my thesis work. I hope that you appreciated your journey in Toulouse besides all the weather and the airport problems. Dr. Cristina Cardoso, thank you for your careful evaluation of my thesis report. I regret that I haven't got the occasion to meet you in person but it was a pleasure to have a skype discussion with you during my thesis defence.

Ma thèse a été financée par l'Association Française du syndrome de Rett (AFSR) et la fondation pour la recherche médicale (FRM). Je vous exprime ma profonde gratitude pour les soutiens que vous m'avez accordés.

Je voudrais remercier mes deux directeurs de thèse pour leur soutien au quotidien durant ces quatre années de thèse.

Merci à Dr. Etienne JOLY pour m'avoir accueilli dans l'équipe dès mon DEA. Merci de m'avoir fait confiance et de m'avoir proposé de continuer en thèse sur le syndrome de Rett. Merci aussi de m'avoir laissé la liberté dans mon travail et de m'avoir poussé à aller toujours vers l'avant. Je souhaite aussi remercier Dr. Ambra Giglia-Mari pour son soutien et ses encouragements constants. Merci de m'avoir accepté dans ton équipe en milieu du chemin et d'avoir accepté de me guider sur ce nouveau projet. Merci pour ta patience et d'avoir pris le temps de m'expliquer les voies du DNA repair.

Merci à vous deux pour les discussions scientifiques si enrichissantes qu'on a pu avoir.

Je remercie chaleureusement toutes les personnes que j'ai côtoyé pendant ces quatre années et qui ont fait que les journées de travail ont été si agréables: Denis (Merci pour tes

conseils, ta disponibilité et ta gentillesse et pour toutes les discussions qu'on a pu partagées. En travaillant à côté de toi, j'ai appris comment on peut concilier enseignements, recherche et les moments en famille. Les mots d'ordre sont " Organisation et Efficacité!!! " Merci de m'avoir encourager à faire des enseignements et d'avoir été là jusqu'à la fin de ma thèse), Julie (Tu as été ma maman " MeCP2 ". Merci pour ton sourire, ta douceur et ta patience et pour tout ce que j'ai pu apprendre à tes côtés), Anne (Merci pour ton dynamisme et ta joie de vivre. Je retiendrais de toi ta philosophie sur la vie surtout concernant les enfants), Sandrine (Merci pour ton sourire et tes blagues parfois un peu à côté), Eddy (Merci pour ta gentillesse, ton calme, ta disponibilité et pour tout ce que tu m'as appris à l'animalerie. Merci pour ton amitié), Christine (Merci pour ton humour, ton sourire et ton dynamisme. Tu es la joie de vivre au labo au quotidien). Pierre-Olivier (Merci pour ta disponibilité et tout le temps que tu as passé à m'apprendre à utiliser le multiphoton), Magali (Ma voisine de bureau, Merci pour les discussions qu'on a pu avoir surtout sur les souris, tu m'a appris énormément), Sophie (Merci pour ta douceur, ta getillesse et ton sourire. J'espère que MeCP2 te sera de grande utilité dans tes mises au point de ChIP), Camille (ou Madame Godon pour les proches !!! Merci pour ta bonne humeur, ton humour décalé et ton efficacité à organiser un pot de dernières minutes. Je garderai un bon souvenir de tes expressions si étranges et de tes cours d'initiation au verlan), Julie et Joris (Merci d'avoir accepté mon anglais " si parfait ". Grâce à vous je m'améliore de jour en jour). Merci pour votre présence à tous, votre gentillesse et votre joie de vivre.

Merci à toutes les personnes de passage ou celles avec qui j'ai pu discuté dans un couloir ou autour d'un café, d'un repas ou une soirée. Ceux qui m'ont prêté un produit ou partagé un protocole ou des astuces: Florence, Roxane, Ludivine, Marielle, Aline, Luc, Cécile, Béatrice, Marlène. Je tiens à remercier mes voisins d'étage avec qui j'ai partagé de bons moments au cours de ces années : à celles qui sont déjà partie Audrey, Elisabeth, Claire, Dania, Claire, ceux qui sont encore là Isabelle (Merci pour tes encouragements constants), Leyre (Merci pour ta disponibilité pour nous tous, merci pour les nombreuses fois où tu as été ma motivation pour le travail tard le soir ou le WE, cela m'a évité le PTI), Pierre (Merci pour ta gentillesse et ta bonne humeur et tes encouragements au moment de la rédaction en plein été. Je te souhaite les meilleurs Western au monde !!!) et les derniers arrivés Thomas et Guillaume. Merci à tous pour vos aides et surtout le jour de la soutenance.

Je tiens à remercier l'équipe du Dr. Bernard Monsarrat et spécialement Sandrine qui

ont été les premiers à m'accueillir en master 1ère année. Merci de m'avoir donné l'envie de continuer dans la voie de la recherche. D'autre part je remercie l'équipe du Dr. Isabelle Maridonneau-Parini et surtout Arnaud pour avoir contribué à ma formation en DEA. Je garde un très bon souvenir de mon passage chez vous, merci pour tout ce que vous m'avez appris.

J'ai eu l'occasion de collaborer avec l'équipe du Dr Laurent Villard. Je tiens à les remercier pour leur accueil à Marseille et je remercie Dr. Jean-Christophe Roux et Nicolas Panayotis pour leur aide à réaliser les expériences d'immunohistochimie sur les tissus de souris.

Je remercie l'équipe pédagogique de biochimie de l'université Paul Sabatier à Toulouse. Merci pour m'avoir fait confiance et pour tous vos conseils qui m'ont été utiles pour mener à bien les enseignements. C'était une très belle expérience.

Grand merci à " mes copains du DEA " et " mes copains du Vendredi midi ". Aurel, Mitch et Caro, merci d'avoir été là dans les moments difficiles mais aussi pour tous les moments de joie qu'on a pu partager (surtout les kirs, pêches Melba.... et les chips !!! du Hoegarden les Vendredi soirs) . Aurel tu as été la plus courageuse et tu m'as supporté jusqu'au bout, merci pour toutes les discussions qu'on a pu avoir au biphoton pour faire passer le temps entre 2 acquisitions et les pauses cafés histoire de râler un peu. Mitch ou Mister Biblio, je ne sais toujours pas comment tu fais pour retenir le 5ème auteur d'une publi qui date de 1980 mais je te remercie pour toutes les discussions scientifiques qu'on a pu avoir autour de la pause café de 7h30 le matin. Caro, merci pour ta gentillesse et ton courage. Tu m'a appris que quand on veut quelque chose, il faut foncer et ne pas se laisser décourager. Gaelle, merci pour ta gentillesse et pour toutes les fois où tu m'as aidé à préparer mes oraux ou mes dossiers, pour les pauses de 16h agrémentées de quelques discussions protocoles, manips ou vacances. Le dernier " copain du Vendredi midi " Thomas merci pour tous les goûters et les pauses " expérimentations scientifiques " étranges mais intéressantes qu'on a pu partager.... Une thèse, ça fait aussi gagner des amis!!!

Toutes ces années, en France, n'auraient jamais été si agréables sans la présence des amis. Fred, Joel, Marion, Georgette, Joseph, Liliane, Cindy et Diana, merci pour tout ce que vous avez fait pour nous. Laurence, Claudia, Elodie, et bien sûr les loustics (Nath, Stéph fille et Stéph garçon, JB et Damien). Vous êtes des gens formidables. Merci pour les magnifiques soirées et les moments de délire qu'on a passé ensemble. Merci pour votre présence et

votre soutien pendant la rédaction de cette thèse. Le meilleur souvenir pour moi restera quand même le cochon et la chasse aux œufs sous la pluie. Avouez c'était la classe !!!! Et je n'oublierai pas bien sûr " Que font les rats sans Lara ?? " c'était génial !!!

Je ne serais pas arrivée là sans l'aide et l'encouragement de ma famille. à mes parents, merci de m'avoir fait confiance et d'avoir dit " oui " à mes projets : venir en France seule et me lancer dans une thèse. J'espère que vous ne m'en voudrez pas trop d'avoir encouragé Elsy et Achaya de venir continuer leurs études à mes côtés. Sœurette, qu'est ce que j'aurais fait sans toi. Pour moi tu as été ma sœur, mon amie, ma confidente, ma colocataire, mon défouloir... Merci pour ton sourire au quotidien, pour ton grand cœur et pour tous les moments qu'on a partagé et qu'on partagera ensemble. Merci pour toutes les aides informatiques que tu m'as apportées : sans toi je serai encore en train d'installer ma free et attendre des nuits et des nuits ce " chenillard " qui ne veut pas s'arrêter, surtout sans toi mon manuscrit n'aura jamais été aussi " Classe " !!!! Je te souhaite plein de courage pour que tu arrives toi aussi au bout de ta thèse et que tu réalises tes rêves. Frero, ces deux dernières années ont été superbes. Je suis contente que Toulouse t'ait plu. Je suis aussi très contente d'avoir pu partager ces deux années avec toi. Merci pour tout ce qu'on a fait ensemble. Rugby, Stade, pizza, bière, london town, fléchette.... Qui dit mieux !!!! Je te souhaite beaucoup de réussite pour tes projets futurs. Pense à moi quand tu seras riche, je suis toujours d'accord pour faire le tour du monde et " visiter la pierre ".

Enfin je remercie tous ceux que j'ai oubliés de citer et qui m'ont apporté leur soutien et leurs conseils à un moment donné de ma thèse.

≪ *Somewhere, something incredible is waiting to be known.* ≫

Dr. Carl Sagan

Résumé général des travaux de thèse et perspectives

LE syndrome de Rett est une maladie neuro-développementale progressive conduisant à un polyhandicap lourd associé à des retards mentaux sévères. Cette maladie touche principalement les filles avec une fréquence d'environ 1/10 000 naissances et représente la première cause de polyhandicap dans les sociétés occidentales. Après une première année asymptomatique, ce syndrome est caractérisé, entre autres, par l'apparition progressive de troubles moteurs, de mouvements stéréotypés, de dysfonctionnements massifs du système nerveux autonome, avec épilepsie, autisme et retard mental.

En 1999, l'équipe du Dr Huda Y. Zoghbi a découvert que le syndrome de Rett (RTT) est dû à des mutations dominantes du gène mecp2, localisé sur le chromosome X. La protéine MeCP2 appartient à la famille des MBP (Methyl-CpG-Binding Protein), qui sont des répresseurs de transcription se liant à l'ADN au niveau des dinucléotides CpG méthylés. Il existe 2 isoformes de MeCP2 (e1 et e2) issues de l'épissage alternatif d'un même ARNm ; la forme MeCP2e1 (ou MeCP2B) est majoritaire dans le cerveau. Différentes fonctions ont été attribuées à MeCP2 : modulateur transcriptionnel (active/réprime la transcription), épissage alternatif de certains ARN messagers, maintien de l'état de méthylation des gènes au cours de la réplication de l'ADN et modification de la structure tridimensionnelle et/ou du niveau de compaction de la chromatine. Ces différentes fonctions peuvent expliquer les larges variétés de symptômes observés chez les patientes atteintes du syndrome de Rett.

Au cours d'une étude, menée dans l'équipe de Dr Joly, visant à étudier la régulation, par MeCP2, de l'expression des gènes codant pour le complexe majeur d'histocompatibilité CMH I (cf. Appendix), l'équipe a observé que, dans des co-cultures de cellules neuronales transfectées par une forme étiquetée de MeCP2 et des cellules non transfectées, MeCP2 faisait l'objet d'un transfert intercellulaire.

Des données préliminaires indiquent que le passage de MeCP2 est rapide: un marquage du noyau des cellules receveuses adjacentes aux cellules donneuses est détectable après quelques dizaines de minutes. Ce passage est également spécifique car le transfert intercellulaire de MeCP2 s'opère vers d'autres cellules neuronales murines, mais pas vers des fibroblastes murins ou humains, ni vers des cellules neuronales humaines. De plus, dans les mêmes conditions, le répresseur transcriptionnel MBD2, qui appartient à la même famille, n'est pas transféré.

La première partie de ma thèse *(cf. Appendix et Chapitre 5)* a consisté à caractériser les mécanismes moléculaires impliqués dans ce phénomène et de caractériser la région de la protéine qui est nécessaire à ce transfert intercellulaire.

Les résultats préliminaires de ce projet ont été obtenus en réalisant des expériences d'immunofluorescences sur des cellules fixées. La première étape a donc été de confirmer ces résultats sur des cellules vivantes. Pour cela, MeCP2 a été fusionnée à la protéine fluorescente GFP. Après des expériences de co-cultures entre des cellules exprimant MeCP2-GFP et des cellules ne l'exprimant pas, nous n'avons pas pu observé le passage intercellulaire de MeCP2. Ces résultats peuvent être dus à la grande taille de la GFP qui peut gêner le transfert. Nous avons donc décidé d'utiliser le système de la split-GFP.

Le système « split-GFP » est basé sur l'auto-complémentation de deux fragments de la GFP : un fragment de 15 acides aminés appelé GFP 11, correspondant au dernier brin β de la GFP et le fragment complémentaire GFP 1-10 correspondant au reste de la molécule GFP. Ces deux fragments exprimés séparément ne sont pas fluorescents ; ce n'est que lorsqu'ils sont mis en commun qu'ils s'associent spontanément, permettant la reconstitution de la molécule GFP et la formation du chromophore.

Il a été montré que lorsque le fragment GFP 11 est fusionné avec une autre protéine, il est toujours capable de s'associer à GFP 1-10, et de restaurer la fluorescence GFP de façon quantitative au nombre de molécules étiquetées avec la GFP 11.

Pour notre projet, nous avons fusionné MeCP2 au petit fragment GFP 11. Cette construction a été exprimée d'une façon stable dans des cellules neuronales donneuses. Le fragment complémentaire de la GFP (GFP 1-10) a été exprimé dans d'autres cellules neuronales receveuses. Après co-culture, nous n'avons pas pu détecter l'apparition d'un signal fluorescent dans les cellules donneuses.

Malgré l'absence de contrôle positif lors des expériences de co-cultures cellulaires (par exemple les protéines Engrailed -1 ou 2, fusionnées à la GFP 11, connues pour transférer du noyau d'une cellule à l'autre), nous suspectons que le transfert inter-cellulaire de MeCP2 soit dû aux étapes de fixation et de perméabilisation instantanées avec l'acétone lors des expériences d'immunofluorescence. En effet, quand les cellules sont fixées avec le paraformaldéhyde et perméabilisées avec le Triton X100, nous n'observons plus le transfert de MeCP2.

Ce travail avec la split-GFP nous a permis de développer une nouvelle application à ce système. Nous avons montré que la protéine GFP1-10 recombinante peut être utilisée comme réactif en microscopie ou en cytométrie de flux pour détecter la présence de protéines fusionnées à la GFP 11 quelque soit leur localisation dans les cellules de mammifères. En comparaison avec les marquages avec des anticorps, cette technique s'avère être plus rapide et plus spécifique avec un ratio signal/bruit très élevé.

La deuxième partie de ma thèse *(cf. Chapitre 6)* a permis de produire et de caractériser, pour la première fois, de nouveaux anticorps capables de détecter séparément et spécifiquement chacune des deux isoformes de MeCP2.

Au laboratoire, nous avons montré que ces anticorps peuvent être utilisés pour des expériences de Western blot, d'immunofluorescence, d'immunohistochime et d'immunoprécipitation de la chromatine (ChIP).

Des expériences de western blot sur des extraits nucléaires issus de différents tissus (cerveau, poumon, coeur, foie, thymus, rate et rein) d'une souris âgée de 3 mois ont montré que l'isoforme MeCP2e1 est fortement exprimée dans le système nerveux central et moyennement exprimée dans les poumons et le rein. D'autre part, des expériences d'immunohistochimie sur des coupes de cerveau issues de cerveaux de souris âgées de 24 et de 55 jours, sauvages ou KO pour le gène mecp2, ont montré que l'isoforme MeCP2e1 est exprimée dans différentes structures du cerveau comme par exemple l'hippocampe, le noyau paraventriculaire et le noyau arque. Dans ces deux types d'experiences, nous n'avons pas pu détecter la présence de l'isoforme MeCP2e2 suggérant que cette isoforme n'est pas exprimée dans l'organisme ou bien elle est exprimée à un très faible niveau non détectable dans nos conditions expérimentales.

La troisième partie de ma thèse *(cf. Chapitre 7)* a consisté à étudier le rôle de MeCP2 dans la réponse aux dommages à l'ADN. En effet, quand nous avons induit des lésions à l'ADN

avec une micro-irradiation laser à 800 nm, nous avons observé une accumulation de MeCP2 dans la région du dommage. Nous avons aussi démontré que le recrutement de MeCP2 sur les lésions est indépendant de la transcription, et il est indépendant des 2 voies de réparation de l'ADN par excision des nucléotides : GG-NER et TC-NER. En revanche, nous avons observé que la partie C-terminale de MeCP2 (après l'acide aminé 308) est nécessaire pour ce recrutement. Cette partie de la protéine, qui est absente dans le modèle de souris de Dr. Zoghbi présentant des symptômes du syndrome de Rett, est importante pour la liaison de MeCP2 à l'ADN non méthylé et aux interactions protéines/ protéines.

En parallèle à ce travail nous avons pu montrer qu'en absence de la protéine CSB, l'interaction de MeCP2 avec la chromatine est diminuée.

La protéine CSB est une protéine de 168 kDa membre de la famille des hélicases SWI/SNF. Elle joue un rôle dans la réparation de l'ADN couplée à la transcription (TC-NER) en interagissant avec l'ARN polymérase II bloquée sur les lésions d'ADN. De plus, il a été montré que CSB joue un rôle dans le remodelage de la chromatine. Des mutations dans cette protéine ont été retrouvées chez des patients atteints du syndrome de Cockayne. Ces patients présentent un tableau de symptômes neurologiques très similaire à celui observé pour les patientes atteintes du syndrome de Rett. Ces symptômes neurologiques pourraient être causés par l'impossibilité pour MeCP2 de se lier correctement à la chromatine et d'effectuer sa fonction correctement dans le cerveau.

Il est maintenant important de comprendre le rôle de MeCP2 dans la réponse aux dommages à l'ADN. Est ce que MeCP2 agit directement au niveau d'une voie de réparation ? Est-elle capable de détecter une lésion et de recruter les protéines nécessaires pour la réparation du dommage ? Peut-elle jouer un rôle dans l'architecture de la chromatine autour de l'ADN endommagé ?

Ensuite, il est important de comprendre la relation entre MeCP2 et CSB. MeCP2 intéragit-elle directement avec CSB ? Sinon, se trouvent-elles dans le même complexe protéique ?

La découverte de ce nouveau rôle potentiel de MeCP2 dans la réponse aux dommages à l'ADN augmente la complexité des études réalisées sur cette protéine. Le fait que la partie C-terminal de la protéine soit impliquée dans le recrutement de MeCP2 sur les lésions de l'ADN et que des mutations dans cette région soient identifiées chez des patientes atteintes du syndrome de Rett implique que ce nouveau rôle pour la protéine doit être pris en compte dans la pathologie de Rett.

Les résultats de notre étude sont donc importants pour le syndrome de Rett mais aussi pour la maladie de Cockayne. À la fois ils pourraient permettre d'avancer dans la compréhension de ces deux maladies mais aussi de pouvoir envisager des thérapies communes, comme la supplémentation en anti-oxidants pour les patientes Rett.

Contents

Abreviation

- **Aa** : Amino acid
- **APE1** : APurinic/APyrimidinic Endonuclease1
- **AS** : Angelman Syndrome
- **ATM** : Ataxia Telangiectasia Mutated

- **BER** : Base Excision Repair
- **BFP** : Blue Fluorescent Protein
- **BRCA** : BReast CAncer

- **CDKL5** : Cyclin-Dependent Kinase-Like 5
- **CFP** : Cyan Fluorescent Protein
- **CPD** : Cyclobutane Pyrimidine Dimer
- **CpG** : Cytosine-phosphate-Guanine
- **cREB** : cAMP Response Element-Binding
- **CS** : Cockayne Syndrome

- **DNA** : DesoxyRibonucleic Acid
- **DNMT1** : DNA methyltransferase 1
- **DSB** : Double Strand Break

- **eGFP** : enhanced Green Fluorescent Protein
- **ES** : Embryonic Stem cells
- **Exol** : Exonuclease 1

- **FBP11** : Formin Binding Protein 11
- **FEN1** : Flap endonuclease 1
- **FOXG1** : Forkhead box protein G1

- **FRAP** : Fluorescence Recovery After Photobleaching

- **GG-NER** : Global Genome-Nucleotide Excision Repair
- **GGR** : Global Genome Repair

- **HDAC** : Histone Deacetylase Complex
- **HMGA1** : High Mobility Group A 1
- **HR** : Homologous Recombination

- **ID** : Insertion / Deletion

- **MBD** : Methyl Binding Domain
- **MeCP2** : Methyl CpG Binding Protein
- **MLH** : MutL Homolog
- **MMR** : Mismatch Repair
- **MSH** : MutS Homolog

- **N-COR** : Nuclear receptor corepressor
- **NER** : Nucleotide Excision Repair
- **NHEJ** : Non Homologous End Joining

- **Paf** : Patchy fur
- **PCNA** : Proliferating Cell Cuclear Antigen
- **6-4PP** : Pyrimidine-Pyrimidone (6-4) products

- **RFC** : Replication Factor C
- **RPA** : Replication Protein A
- **RTT** : Rett syndrome
- **RNA** : Ribonucleic Acid

- **STK9** : Serine/Threonine Kinase 9
- **SNE** : Severe neonatal encephalopathy
- **SWI/SNF** : SWItch/Sucrose NonFermentable

- **TC-NER** : Transcription Coupled- Nucleotide Excision Repair
- **TCR** : Transcription Coupled Repair

- TFIIB : Trancription Factor II B

- TFIIH : Trancription Factor II H

- TTD : TrichoThioDystrophy

- TRD : Transcription Repression Domain

- 3'-UTR : 3'-Untranslated Region

- XCI : X Chromosome Inactivation

- XLF : XRCC4-like factor

- XLMR : X-linked Mental retardation

- XP : Xeroderma Pigmentosum

- XRCC : *X-ray* repair cross-complementing

- Yb-1 : Y Box protein 1

- YFP : Yellow Fluorescent Protein

Studying the MeCP2 protein:
Exploring its involvement in the DNA Damage Response, and developing new tools for its detection.

Introduction

1 Rett Syndrome

1.1 Definition

Rett syndrome (RTT, MIM 312750) is a severe postnatal progressive neurodevelopmental disorder that manifests mainly in girls during early childhood. Rett syndrome is one of the most common causes of mental retardation in females with an incidence of 1 birth in 10000 to 20000.

This syndrome was described for the first time in 1966 by Andreas Rett, an Austrian neurologist in Vienna. But the syndrome became internationally recognised 17 years later when Dr. B. Hagberg, a Swedish neurologist, reported 35 cases of RTT [1, 2].

1.2 Clinical features

There is a large variability in the progression and the severity of Rett syndrome. We can distinguish between the classical and the atypical forms of RTT.

1.2.1 The classical form

At birth, girls with the classic form of the disease have a normal head circumference, appear to develop normally until 6-18 months and achieve the expected motor skills, language and social milestones. Nevertheless, some studies revealed subtle behavioural abnormalities soon after birth. After this period, the neurological development is arrested and the regression phase begins. This regression is commonly divided into four stages [2, 3, 4] and (Figure 1.1):

- Stage I: **The stagnation period** (6-18 months): In this stage, developmental progress

is stopped and the head growth undergoes deceleration that usually leads to microcephaly. Babies may show less eye contact and start to lose interest in toys. They may also show signs of hypotonia and have delays in the acquisition of sitting, crawling or walking.

- Stage II: **The regressive stage** (1-4 years): Children with Rett syndrome gradually lose the ability to speak and to use their hands purposefully. They show the classic "hand-washing" stereotypic activity. Some children with Rett syndrome hold their breath or hyperventilate and may scream or cry for no apparent reason. It's often difficult for them to move on their own. Girls show autistic features and half of them develop seizures.

- Stage III: **The relative stabilization period** (2-10 years): Although problems with movement continue, behavior may improve. Children in this stage often cry less and become less irritable. During this stage, the use of eye contact and hands for communication generally improve. Many people affected by Rett syndrome remain in stage III for the rest of their lives.

- Stage IV: **The late motor impairment period** (10-15 years): The last stage is marked by reduced mobility, muscle weakness and scoliosis. Understanding, communication and hand skills generally don't decline during this stage but repetitive hand movements may decrease.

1.2.2 The atypical form

Five distinct categories of atypical RTT have been described on the basis of clinical criteria. These variants can be either milder or more severe than the classic RTT phenotype. We can distinguish 3 types of milder variants [2, 3, 4] and (Figure 1.1):

- **the "forme fruste"** where regression begins later than classic RTT (between 1 and 3 years old). In this form the hand use is sometimes preserved with minimal stereotypic movement.

- **the preserved speech variant** where girls can speak a few words. Patients with this variant have a normal head size.

Classical RTT
Necessary criteria
1. Normal prenatal and perinatal history
2. Normal psychomotor development for the first 6 months
3. Normal head circumference at birth
4. Postnatal deceleration of head growth in most individuals
5. Loss of purposeful hand skills between 6 months and $2\frac{1}{2}$ years
6. Hand stereotypies
7. Evolving social withdrawal, communication dysfunction, loss of acquired speech, and cognitive impairment
8. Impairment or deterioration of locomotion

Supportive criteria
1. Breathing disturbances during waking hours
2. Bruxism
3. Impairment of sleeping pattern from early infancy
4. Abnormal muscle tone associated with muscle wasting and dystonia
5. Peripheral vasomotor disturbances
6. Progressive kyphosis or scoliosis
7. Growth retardation
8. Hypotrophic small and cold feet and/or hands

Exclusion criteria
1. Evidence of a storage disorder including organomegaly
2. Cataract, retinopathy, or optic atrophy
3. History of perinatal or postnatal brain damage
4. Confirmed inborn error of metabolism or neurodegenerative disorder
5. Acquired neurological disorder due to severe head trauma or infection

Variant RTT
Inclusion criteria
1. At least three of the six main criteria
2. At least five of the 11 supportive criteria

Main criteria
1. Reduction or absence of hand skills
2. Loss or reduction of speech (including babble)
3. Hand stereotypies
4. Loss or reduction of communication skills
5. Deceleration of head growth from early childhood
6. Regression followed by recovery of interaction

Supportive criteria
1. Breathing irregularities
2. Abdominal bloating or air swallowing
3. Bruxism
4. Abnormal locomotion
5. Kyphosis or scoliosis
6. Lower limb amyotrophy
7. Cold, discoloured and usually hypotrophic feet
8. Night time screaming and other sleep disturbances
9. Inexplicable episodes of screaming or laughing
10. Apparently diminished sensitivity to pain
11. Intense eye contact and/or eye pointing

[a]Modified from Hagberg *et al*: *Eur J Paediatr Neurol* 2002; 6: 293–297.

Figure 1.1 — Revised diagnostic criteria for classical and variant RTT. (Figure adapted from [2]).

▷ **the late regression variant** is characterized by normal head circumference and gradual loss of acquired speech and fine motor skills in late childhood.

And 2 types of more severe forms:

▷ **the congenital form** where patients show RTT features straight from birth. In addition to lacking the typical early normal period, they are floppy and very retarded.

▷ **the early seizure-onset variant**: In this variant, the normal perinatal period is soon followed by the appearance of seizures preceding the regression period.

1.3 Genetic origin of Rett Syndrome

Early reports suggested that RTT is an X-linked dominant disorder because of the almost exclusive occurrence in females, the high concordance rate among monozygotic twins and the rare familial cases with maternal inheritance.

The causes of RTT were difficult to determine because only 1 % of the RTT cases are familial (99% of RTT cases are sporadic). Genetic mapping studies on the X chromosome in familial cases identified the Xq28 locus as the origin of RTT [5, 6]. In 1999, Huda Zoghbi's

group carried out systematic mutational analysis of genes located in Xq28 in patients affected by the sporadic or the familial forms of RTT. They identified mutations in the *MeCP2* gene encoding for the X-linked methyl CpG binding protein 2 as the causes of some cases of RTT [7]. As many other genes located on the X chromosome, this gene undergoes X inactivation.

1.4 RTT causing mutations

1.4.1 Mutations in MeCP2 gene

MeCP2 mutations account for up to 95% of classic RTT cases [7, 8]. Almost all mutations occur *de novo* and they include missense, frameshift, nonsense and intragenic deletions ([9, 10] and Figure 1.2). About 70% of MeCP2 mutations are caused by a C to T transition at 8 CpG nucleotides located in the third and the fourth exons, whereas carboxy-terminal deletions occur in 10 to 15% of RTT patients [11].

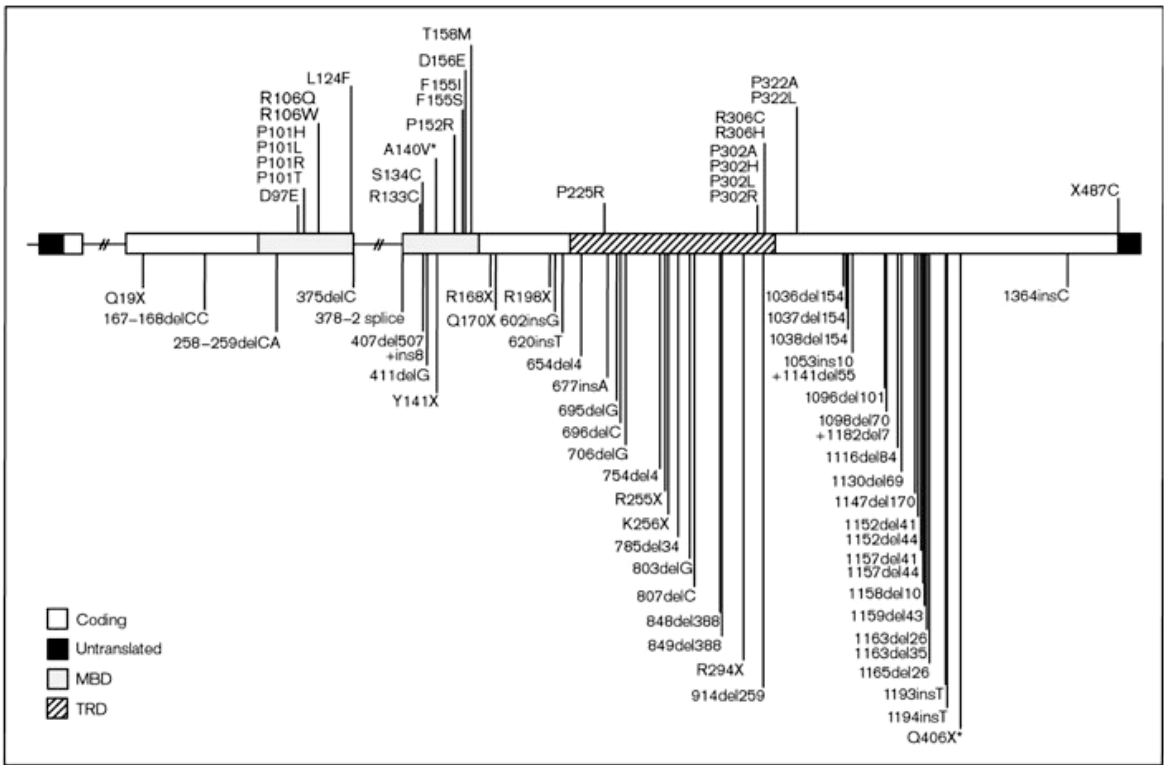

Figure 1.2 — **Summary of mutations found in coding region from exon 2 to exon 4 of MeCP2 gene**: Missense mutations are shown above the genomic structure of MeCP2 whereas nonsense or frameshift mutations are shown below. Asterisks represent mutations causing non-syndromic mental retardation. (Figure adapted from [10]).

1.4.2 Mutations in other genes

Some RTT patients don't show mutations in MeCP2 gene. It was proposed that there is at least one other gene responsible for RTT syndrome. Two groups showed that some cases of RTT-like phenotypes (with severe mental retardation and early seizure onset) are caused by truncating frameshift and missense mutations in the gene coding for the cyclin-dependant kinase-like 5 (CDKL5/ STK9) [12].

Another group reported that some mutations in the *FOXG1* gene are responsible for the congenital form of Rett syndrome, a severe variant where girls are retarded from the first months of life. The first studies revealed deletions and nonsense mutations in this gene as the origin of variant Rett syndrome [13, 14]. Recently a study revealed a frameshift point mutation in a boy with the congenital variant form of Rett syndrome [15].

1.5 Genotype/Phenotype correlations

RTT patients present a large phenotypic variability associated with different MeCP2 mutations. Recent genotype-phenotype studies showed that severity of RTT phenotype depends on the type of the mutation, the genetic background and the X-chromosome inactivation balance.

1.5.1 Type of mutations

Patients carrying mutations that truncate the protein in the C-terminal domain (late truncating mutations) present milder phenotype and are less typical of classical Rett Syndrome than those carrying missense or early truncating mutations. Jian *et al.* reported in 2005 that R270X mutation (X representing here a stop codon) is associated with elevated mortality. Wan *et al.* showed that girls carrying the same mutations could sometimes present different phenotypes. This observation is consistent with an important role for the X-chromosome inactivation (XCI) balance [16, 11].

1.5.2 Effect of XCI

The purpose of the inactivation of one of the X chromosome is to equalize X-linked gene products between XX females and XY males. This process occurs randomly in differenti-

ating embryonic cells in females, resulting in cells that are mosaic with respect to which chromosome is active.

MeCP2 gene is located on the X-chromosome and is subjected to XCI. Girls with Rett syndrome are thus mosaic for MeCP2 mutations, meaning that, on average, half of their cells express the wild-type MeCP2 allele and the other half express the mutated one. Some studies reported that healthy-carrier mothers or females with less severe RTT phenotype have a skewed XCI with inactivation of the mutated allele. This was illustrated, for example, with a study showing monozygotic twins with R294X mutation with very different phenotypes. While one of the twins with a severe phenotype presented a balanced XCI, the other one showed a less severe phenotype caused by a skewed XCI towards the maternal wild-type allele [17]. These results are, however, controversial because, in these studies, the XCI profile was determined on peripheral lymphocytes. In fact, it was demonstrated that the lymphocyte clone carrying the wild-type allele developed and proliferated faster than the clones carrying the mutated allele, thus biasing the XCI skewing [18]. Studies performed on RTT brain tissues suggest that balanced XCI patterns are prevalent [4].

1.5.3 MeCP2 Mutations in boys

At the beginning, RTT was considered to be an X-linked dominant disorder with male lethality. In 1999, Jan *et al.* identified males with Rett syndrome [19]. Screening of MeCP2 mutations in males with neurological pathologies revealed that these mutations can cause variable phenotypes such as:

- Classical RTT phenotype due to somatic mosaicism for mutations in MeCP2 or in cases of Klinefelter syndrome (XXY).

- Mild to severe mental retardation: These patients carry mutations different from the ones found in girls.

- Severe neonatal encephalopathy: These patients carry the same mutations identified in girls but the phenotype is more severe due to the presence of just one X chromosome in males. Male patients usually die in the first two years of life [20].

1.6 Mouse Models of Rett syndrome

To understand the molecular mechanisms implicated in RTT, different mouse models have been generated. These mouse models mimic the clinical features observed in RTT patients.

1.6.1 MeCP2-null mouse model

The first attempts to create MeCP2-null mice using male mouse embryonic stem (ES) cells lacking MeCP2 were unsuccessful. Chimeric embryos exhibited high lethality. In 2001, two groups directed by Dr Adrian Bird and Dr. Rudolph Jaenisch decided to use conditional knock-out approaches based on Cre-Lox technologies. Dr. Jaenisch generated the MeCP21lox mouse model with MeCP2 with conditionally deleted exon 3 [21] and Dr. Bird the $MeCP2^{tl1-1Bird}$ with MeCP2 with conditionally deleted exons 3 and 4 [22].

MeCP2-null male mice are apparently healthy at birth until 3 to 8 weeks of age. After this period, mice begin to show neurological symptoms like those observed in RTT patients: stiff and uncoordinated gait, hindlimb clasping, and irregular breathing. Uneven wearing of the teeth and misalignment of the jaws are also observed. Testes of MeCP2-null males were always internal. Symptoms progression leads to weight loss and early death around 54 days. Brain architecture in null mice is grossly normal, although a slight decrease in the size and weight can be noticed in comparison with wild-type littermates. This is due to neurons compaction in hippocampus, cerebral cortex and cerebellum.

$MeCP2^{+/-}$ females mice are viable, fertile and grow normally until adulthood. At 3 months, they start showing hind limb clasping and by 9 months they show RTT phenotypes such as breathing irregularity and inertia.

These results show that MeCP2-null mice can be a good model to study RTT because of delayed onset of neurological symptoms affecting posture, gait, breathing and spontaneous movements.

In 2006, Dr Patrick Tam generated mice with a targeted deletion of the methyl binding domain (MBD) resulting in complete loss of MeCP2 protein. $MeCP2^{tm1Tam}$ phenotype is comparable with that of the Jaenisch and Bird's mice phenotype. In addition, at 8 to 10 weeks after birth, they display reduced level of anxiety, locomotors activity and cerebellar

learning. In this study, authors wanted to verify if the Y chromosome has an effect on the mouse phenotype. For this heterozygous female, called $MeCP2^{tm1neoTam}$, were mated with Paf males on a C3H/HeSNJ background. Paf (or Patchy fur) is a mutation that provokes default in X and Y chromosome segregation during meiosis leading to a frequent loss of the Y chromosome. Comparison between $MeCP2^{tm1Tam}$ 39XO females and $MeCP2^{tm1Tam}$ 40XY males carrying mutated X alleles and differing only by expression of Y chromosome show similar profiles of postnatal viability and growth suggesting that Y chromosome has no impact on MeCP2-null phenotype [23].

1.6.2 MeCP2 conditional mutants

The group of Dr Jaenisch wanted to study the effect of specific deletion of MeCP2 in the central nervous system. MeCP2-null mice were hence crossed with transgenic mice carrying Nestin-Cre transgene. This crossing gave birth to mice in which MeCP2 was deleted specifically in neurons and glial cells. These mice displayed a phenotype similar to that observed in MeCP2-null mice suggesting that the primary site where the lack of MeCP2 is causing the Rett pathology is indeed in the brain. Chen et al also investigated the role of MeCP2 in postmitotic neurons. In order to do this, they introduced the Cam kinase Cre transgene which is active in the excitatory neurons in the postnatal forebrain, hippocampus and brainstem. For these conditional mutants the phenotype seemed to be less severe than null mice or Nestin-Cre conditional mutants. CamK-Cre conditional mutants were healthy until 3 months. After this period, they began to show symptoms including gain of body wait, ataxic gait and reduced nocturnal activity. The brain weight of these mice was reduced with smaller neuronal cell bodies in cortex and hippocampus [21].

1.6.3 MeCP2 truncation

In 2002, Dr Huda Zoghbi's group generated a mouse carrying a truncation at amino acid 308. This truncation eliminates the C-terminal region of MeCP2.

In these mice the phenotype is milder than those seen previously. MeCP2308/y are normal until 6 weeks and then they develop symptoms like tremors, kyphosis, learning and memory deficits, social behaviour abnormalities, etc. Heterozygote females MeCP2308/+ have impaired motor features starting at 35-39 weeks after birth. As in the case of human female patients, these mice show phenotypic variability due to the XCI. In this study, au-

thors show that the truncated protein has a normal nuclear localization on heterochromatic regions but histone H3 is hyperacetylated in the brain. In contrast, the acetylation level of histone H4 was the same as the one observed in their wild-type animals [24].

1.6.4 MeCP2 transgenic mice

In 2004, Luikenhuis et al. overexpressed a MeCP2 transgene, coding for MeCP2e2, in postmitotic neurons under the control of the Tau promoter [25]. Expression of tau-MeCP2 transgene in neurons is sufficient to rescue RTT phenotype as shown by the fact that when this transgene is expressed in MeCP2 deficient mice, the latter show a phenotype similar to wild-type animals. In 2007, Dr. Bird's group created a mouse model in which MeCP2 is silenced by the insertion of a lox-stop cassette [26]. The expression of MeCP2 can be re-activated by the addition of a transgene expressing a fusion between the Cre recombinase and a modified estrogen receptor (Cre-ER). The Cre-ER fusion protein remains in the cytoplasm until treatement with the estrogen analog tamoxifen. After treatement with tamoxifen, authors were able to rescue symptomatic animals suggesting that in the absence of MeCP2, neurons do not die and the phenotype can be reversible by delayed restoration of MeCP2 gene [26]. However, transgenic mice overexpressing MeCP2 show severe motor dysfunction: *Collins et al*. generated transgenic mice overexpressing the wild-type human MeCP2e2 protein at 2 fold the wild-type level. Early in the development, these mice show increased learning ability and synaptic plasticity. However, after the age of 10 weeks they developed seizures, hypoactivity and spasticity, dying by one year of age [27]

It was demonstrated that overexpression of MeCP2 in human males can cause autistic features and profound mental retardation [28, 29]. All these observations indicate that deficiency or elevated expression of MeCP2 cause neurodevelopmental disorders with a variability of phenotypes. These observations should be considered when attempting to develop therapies against Rett syndrome.

1.6.5 MeCP2-eGFP knock-in mice

This mouse was generated by Schmid *et al.* in 2007 [30]. In these mice, MeCP2 was tagged by eGFP in frame into exon 4 just before the stop-codon. These mice are viable, fertile and without any detectable abnormalities suggesting that MeCP2-GFP fusion is functional. Immunofluorescence colocalisation and confocal microscopy analysis revealed that MeCP2-

eGFP expression is restricted to the nucleus and targeted to heterochromatic regions. Results revealed that the fusion protein is expressed in all neurons, interneuron and astrocytes at different levels as described in other earlier studies. Authors didn't detect any MeCP2 expression in proliferative cells. In conclusion, this study revealed that MeCP2-eGFP expression matches endogenous MeCP2 expression suggesting that these mice can be an important tool to study MeCP2 expression or MeCP2 dynamics in vivo.

Bibliography

[1] B. Hagberg, J. Aicardi, K. Dias, and O. Ramos. A progressive syndrome of autism, dementia, ataxia, and loss of purposeful hand use in girls: Rett's Syndrome: report of 35 cases. *Ann Neurol*, 14(4):471–9, 1983.

[2] S. L. Williamson and J. Christodoulou. Rett Syndrome: new clinical and molecular insights. *Eur J Hum Genet*, 14(8):896–903, 2006.

[3] K. A. Jellinger. Rett Syndrome – an update. *J Neural Transm*, 110(6):681–701, 2003.

[4] M. D. Shahbazian and H. Y. Zoghbi. Rett Syndrome and MeCP2: Linking epigenetics and neuronal function. *Am J Hum Genet*, 71(6):1259–72, 2002.

[5] N. C. Schanen, E. J. Dahle, F. Capozzoli, V. A. Holm, H. Y. Zoghbi, and U. Francke. A new Rett Syndrome family consistent with X-linked inheritance expands the X chromosome exclusion map. *Am J Hum Genet*, 61(3):634–41, 1997.

[6] N. Sirianni, S. Naidu, J. Pereira, R. F. Pillotto, and E. P. Hoffman. Rett Syndrome: confirmation of X-linked dominant inheritance, and localization of the gene to Xq28. *Am J Hum Genet*, 63(5):1552–8, 1998.

[7] R. E. Amir, I. B. Van den Veyver, M. Wan, C. Q. Tran, U. Francke, and H. Y. Zoghbi. Rett Syndrome is caused by mutations in X-linked MECP2, encoding methyl-CpG-binding protein 2. *Nat Genet*, 23(2):185–8, 1999.

[8] T. Bienvenu, A. Carrie, N. de Roux, M. C. Vinet, P. Jonveaux, P. Couvert, L. Villard, A. Arzimanoglou, C. Beldjord, M. Fontes, M. Tardieu, and J. Chelly. MeCP2 mutations account for most cases of typical forms of Rett Syndrome. *Hum Mol Genet*, 9(9):1377–84, 2000.

[9] J. Christodoulou, A. Grimm, T. Maher, and B. Bennetts. RettBASE: The IRSA MeCP2 variation database-a new mutation database in evolution. *Hum Mutat*, 21(5):466–72, 2003.

[10] M. D. Shahbazian and H. Y. Zoghbi. Molecular genetics of Rett Syndrome and clinical spectrum of MeCP2 mutations. *Curr Opin Neurol*, 14(2):171–6, 2001.

[11] M. Wan, S. S. Lee, X. Zhang, I. Houwink-Manville, H. R. Song, R. E. Amir, S. Budden, S. Naidu, J. L. Pereira, I. F. Lo, H. Y. Zoghbi, N. C. Schanen, and U. Francke. Rett Syndrome and beyond: recurrent spontaneous and familial MeCP2 mutations at CpG hotspots. *Am J Hum Genet*, 65(6):1520–9, 1999.

[12] L. S. Weaving, J. Christodoulou, S. L. Williamson, K. L. Friend, O. L. McKenzie, H. Archer, J. Evans, A. Clarke, G. J. Pelka, P. P. Tam, C. Watson, H. Lahooti, C. J. Ellaway, B. Bennetts, H. Leonard, and J. Gecz. Mutations of CDKL5 cause a severe neurodevelopmental disorder with infantile spasms and mental retardation. *Am J Hum Genet*, 75(6):1079–93, 2004.

[13] F. Ariani, G. Hayek, D. Rondinella, R. Artuso, M. A. Mencarelli, A. Spanhol-Rosseto, M. Pollazzon, S. Buoni, O. Spiga, S. Ricciardi, I. Meloni, I. Longo, F. Mari, V. Broccoli, M. Zappella, and A. Renieri. FOXG1 is responsible for the congenital variant of Rett Syndrome. *Am J Hum Genet*, 83(1):89–93, 2008.

[14] F. T. Papa, M. A. Mencarelli, R. Caselli, E. Katzaki, K. Sampieri, I. Meloni, F. Ariani, I. Longo, A. Maggio, P. Balestri, S. Grosso, M. A. Farnetani, R. Berardi, F. Mari, and A. Renieri. A 3 Mb deletion in 14q12 causes severe mental retardation, mild facial dysmorphisms and Rett-like features. *Am J Med Genet A*, 146A(15):1994–8, 2008.

[15] T. Le Guen, N. Bahi-Buisson, J. Nectoux, N. Boddaert, Y. Fichou, B. Diebold, I. Desguerre, F. Raqbi, V. C. Daire, J. Chelly, and T. Bienvenu. A FOXG1 mutation in a boy with congenital variant of Rett Syndrome. *Neurogenetics*, 2010.

[16] L. Jian, H. L. Archer, D. Ravine, A. Kerr, N. de Klerk, J. Christodoulou, M. E. Bailey, C. Laurvick, and H. Leonard. p.R270X MeCP2 mutation and mortality in Rett Syndrome. *Eur J Hum Genet*, 13(11):1235–8, 2005.

[17] T. Ishii, Y. Makita, A. Ogawa, S. Amamiya, M. Yamamoto, A. Miyamoto, and J. Oki. The role of different X-inactivation pattern on the variable clinical phenotype with Rett Syndrome. *Brain Dev*, 23 Suppl 1:S161–4, 2001.

[18] D. Balmer, J. Arredondo, R. C. Samaco, and J. M. LaSalle. MeCP2 mutations in Rett Syndrome adversely affect lymphocyte growth, but do not affect imprinted gene expression in blood or brain. *Hum Genet*, 110(6):545–52, 2002.

[19] M. M. Jan, J. M. Dooley, and K. E. Gordon. Male Rett Syndrome variant: application of diagnostic criteria. *Pediatr Neurol*, 20(3):238–40, 1999.

[20] K. Ravn, J. B. Nielsen, P. Uldall, F. J. Hansen, and M. Schwartz. No correlation between phenotype and genotype in boys with a truncating MeCP2 mutation. *J Med Genet*, 40(1):e5, 2003.

[21] R. Z. Chen, S. Akbarian, M. Tudor, and R. Jaenisch. Deficiency of methyl-CpG binding protein-2 in CNS neurons results in a Rett-like phenotype in mice. *Nat Genet*, 27(3):327–31, 2001.

[22] J. Guy, B. Hendrich, M. Holmes, J. E. Martin, and A. Bird. A mouse MeCP2-null mutation causes neurological symptoms that mimic Rett Syndrome. *Nat Genet*, 27(3):322–6, 2001.

[23] G. J. Pelka, C. M. Watson, T. Radziewic, M. Hayward, H. Lahooti, J. Christodoulou, and P. P. Tam. MeCP2 deficiency is associated with learning and cognitive deficits and altered gene activity in the hippocampal region of mice. *Brain*, 129(Pt 4):887–98, 2006.

[24] M. Shahbazian, J. Young, L. Yuva-Paylor, C. Spencer, B. Antalffy, J. Noebels, D. Armstrong, R. Paylor, and H. Zoghbi. Mice with truncated MeCP2 recapitulate many Rett Syndrome features and display hyperacetylation of histone H3. *Neuron*, 35(2):243–54, 2002.

[25] S. Luikenhuis, E. Giacometti, C. F. Beard, and R. Jaenisch. Expression of MeCP2 in postmitotic neurons rescues Rett Syndrome in mice. *Proc Natl Acad Sci U S A*, 101(16):6033–8, 2004.

[26] J. Guy, J. Gan, J. Selfridge, S. Cobb, and A. Bird. Reversal of neurological defects in a mouse model of Rett Syndrome. *Science*, 315(5815):1143–7, 2007.

[27] A. L. Collins, J. M. Levenson, A. P. Vilaythong, R. Richman, D. L. Armstrong, J. L. Noebels, J. David Sweatt, and H. Y. Zoghbi. Mild overexpression of MeCP2 causes a progressive neurological disorder in mice. *Hum Mol Genet*, 13(21):2679–89, 2004.

[28] M. Meins, J. Lehmann, F. Gerresheim, J. Herchenbach, M. Hagedorn, K. Hameister, and J. T. Epplen. Submicroscopic duplication in Xq28 causes increased expression of the MeCP2 gene in a boy with severe mental retardation and features of Rett Syndrome. *J Med Genet*, 42(2):e12, 2005.

[29] H. Van Esch, M. Bauters, J. Ignatius, M. Jansen, M. Raynaud, K. Hollanders, D. Lugtenberg, T. Bienvenu, L. R. Jensen, J. Gecz, C. Moraine, P. Marynen, J. P. Fryns, and G. Froyen. Duplication of the MeCP2 region is a frequent cause of severe mental retardation and progressive neurological symptoms in males. *Am J Hum Genet*, 77(3):442–53, 2005.

[30] R. S. Schmid, N. Tsujimoto, Q. Qu, H. Lei, E. Li, T. Chen, and C. S. Blaustein. A methyl-CpG-binding protein 2-enhanced green fluorescent protein reporter mouse model provides a new tool for studying the neuronal basis of Rett Syndrome. *Neuroreport*, 19(4):393–8, 2008.

2 Methyl CpG Binding Protein 2 (MeCP2)

2.1 MeCP2 gene and protein

The *mecp2* protein was identified and purified for the first time in 1992 in Dr Adrian Bird's group based on its capacity to bind methylated DNA [1].

The *MeCP2* gene consists of four exons encoding for different variants of transcripts due to differential splicing or alternative usage of the polyadenylation sites in the highly conserved 3'-untranslated region (3'-UTR) [2, 3]. Northern blot analysis revealed the presence of 3 transcripts of 1.8, 7.5 and 10 kb. 1.8 and 10kb are the major transcripts. They have similar half-lives but differ by their translation efficiency [2, 4, 5]. The functional significance of these different transcripts is unknown (Figure 2.1).

In 2004, two studies revealed the presence of two isoforms of MeCP2 that differ in their N-terminal region [6, 7]. This is due to an alternative splicing of exon 2. The first transcript (MeCP2e1 or MeCP2α in mice or MeCP2B in human) lacks exon 2 and the initiation site is in exon 1. The second transcript (MeCP2e2 or MeCP2β in mouse or MeCP2A in human) contains the 4 exons and the initiation site is in exon 2 (Figure 2.1). The two splice variants differ in translation efficiency and are expressed at different relative amounts in different tissues. MeCP2e1 is more abundant in the brain, thymus and lung and during neuronal differentiation.

MeCP2e1 protein (498 aa) is 12 amino acids longer than MeCP2e2 (486 aa). It contains 21 amino acids encoded by exon 1 and lacks the 9 amino acids encoded by exon 2. The major difference between the two isoforms is the presence of a poly-alanine and a poly-glycine repeats in the N-terminal region of the longer isoform, MeCP2e1. Both MeCP2 isoforms are

nuclear and colocalize with methylated heterochromatic foci in mouse cells [6, 7].

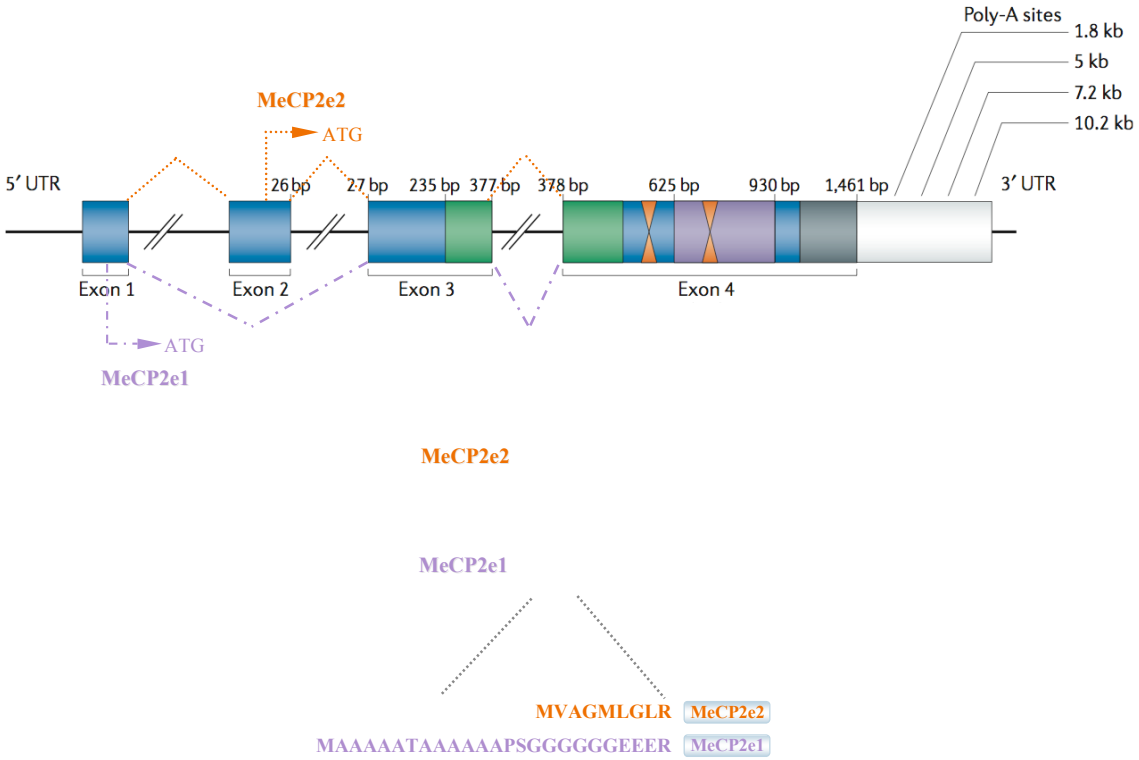

***Figure 2.1* — The MeCP2 gene and its splicing isoforms**: Structure of the MeCP2 gene with its four exons and the different polyadenylation sites generating transcripts of 1.8, 5, 7.2 and 10.2 Kb. The presence of the 5Kb transcript remains controversial (8). The two main protein isoforms, MeCP2e2 (486 amino acids) and MeCP2e1 (498 amino acids) are produced by alternative splicing of the MeCP2 transcript and differ in their N-terminal regions which are encoded by exon 1 in the case of MeCP2e1 and exon 2 for MeP2e2. (Figure adapted from [8]).

2.2 MeCP2 function domain

MeCP2 belongs to a family of proteins that contain a MBD domain which binds to methylated DNA (Figure 2.2).

Three domains compose MeCP2: the methyl binding domain (MBD), the transcription repression domain (TRD) and the C-terminal domain (Figure 2.1).

The MBD, an 85 amino acids domain (from amino acid 78 to 162 in MeCP2) [10], specifically binds to symmetrically methylated CpG dinucleotides, with a preference for CpG sequences with adjacent A/T-rich motifs [11]. The MBD can also bind to four-way DNA junctions (also called Holliday junctions formed during homologous recombination) on unmethylated DNA with the same affinity as on methylated CpG [12].

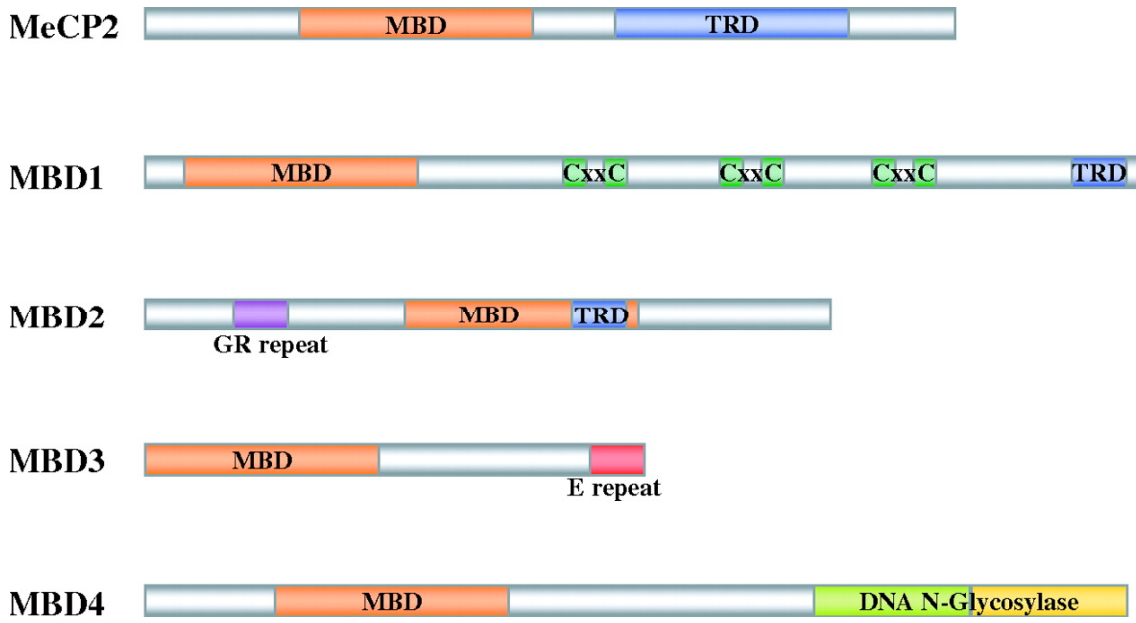

Figure 2.2 — **Characteristic domains of the methyl CpG binding (MBD) protein family**: MBD proteins display homology within their MBD domain. The family contains five members: MBD1 and MBD2 are transcriptional repressors, MeCP2, the founding member, plays different roles as transcription modulator or mRNA splicing factor. MBD3 is a member of the Mi2/NuRD co-repressor complex and MBD4 is a G-T mismatch glycosylase playing a role in DNA repair. (Figure adapted from [9])

The TRD, a 104 amino acids domain (from amino acid 207 to 310), is very basic containing 26% lysine and arginine. It also contains non-polar amino acids (12.5% alanine, 10.5% valine and 8% proline) [13]. TRD is required to repress transcription by recruiting transcriptional co-repressors such as Sin3a, c-ski, N-COR and histone deactylase complex HDAC 1 and 2 [14, 15, 16]. The TRD can repress transcription at long-range distance ranging from 500 to 1500 bp away from the promoter [13]. The TRD contains also the MeCP2 nuclear localisation signal between amino acids 255 and 271 [17].

Although the C-terminal region is not well characterized, this region is very important for MeCP2 function. In fact, the mouse model carrying the R308X mutation (X is a stop codon) reproduces many features of RTT phenotype [18]. MeCP2 C-terminus presents a WDR domain (amino acids 325 to 486) containing a poly-proline rich sequence (amino acids 376 to 405). This region can bind to splicing factors containing a group II WW domain like the FBP11 (Formin binding protein 11) and HYPC proteins [19]. Furthermore, the C-terminal region allows MeCP2 fixation on naked DNA and on nucleosomal cores [20, 21].

Amino acids 188-194, between the MBD and the TRD, are identical to those found within the AT hook DNA binding domains of HMGA1 [22]. This region can bind to the xenopus

protein p20, this interaction reduces the turnover and stabilize MeCP2 [23].

2.3 MeCP2 expression profile

Several studies, carried out in rodents [24, 25, 5], monkeys [26] and human [5], aimed to analyse the expression profile of MeCP2. From these studies, it appears that MeCP2 is expressed in many tissues. Western blot analysis on mice tissue samples revealed that the MeCP2 protein is not abundant in liver, stomach and small intestine, moderately expressed in kidney and heart and highly abundant in brain, lung and spleen [5]. Within the cerebral tissue, MeCP2 is not abundant in astrocytes [27] and immature neurons. However its expression increases to be highest in mature neurons and it is maintained high in these cells throughout life. LaSalle *et al.* showed that MeCP2 expression varies between neuronal populations from different regions and different structures within the central nervous system (CNS) [28]. In this study, they characterised two populations of cells: The $MeCP2^{lo}$ cells, expressing low levels of MeCP2, were found in the brain (glial and neuronal cells) and in the periphery whereas the $MeCP2^{hi}$ cells, expressing high levels of MeCP2, were found in a higher proportion in the layer IV of the cerebral cortex and in the molecular layer of the cerebellum.

MeCP2 expression is regulated in a developmental stage and cell type specific manner. Few things are known about molecular mechanisms implicated in this regulation. It was shown that the *mecp2* gene contains multiple transcription starting sites embedded in a region that is GC rich and contains CpG islands. In this study, they showed that the mouse *mecp2* promoter does not contain any canonical boxes like TATA or CAAT. They also identified a promoter region (-677/+56) that is responsible for the expression of MeCP2 in neuronal cells. In this region, there is a positive regulatory element of 19 bp (-64 to +46) that controls the major activity of the promoter region [29].

In 2006, a study focused on mapping the regulatory regions of the locus of human MeCP2 showed that the locus is characterized by a very large intron 2 (60 Kb), a 3'- UTR of 8,5 kb with highly conserved domains and different polyadenylation sites and a 40 kb intergenic region separating MeCP2 from the nearest upstream gene [30]. It also identified a region supposed to be the core promoter (-179 to -309 bp upstream the initiation site) supporting basal gene expression. Two positive regulatory elements were characterized

(-681/-847) and (-847/-1071) as well as two negative regulatory elements (-309/-370) and (-553/-681). In order to identify potential Cis-regulatory elements able to control spatio-temporal expression of MeCP2, authors performed an interspecies sequence comparison and identified four enhancers and two silencer elements in the 210 kb surrounding MeCP2 locus [30].

2.4 MeCP2 biological function

2.4.1 Transcription repression

As previously mentioned, MeCP2 contains two domains: The MBD domain that binds to methylated DNA and a TRD domain that represses transcription by interacting with different partners. It was shown that MeCP2 could repress transcription by different mechanisms:

2.4.1.1 Histone deactylation

Transcription can be regulated by histone modifications: histone acetylation contributes to gene activation whereas histone deacetylation is accompanied by transcription repression. It was shown that MeCP2 can repress transcription by deacetylating histones. In fact, the transcription repression domain of MeCP2 interacts with the co-repressor Sin3a complex. This complex contains the histone deacetylase complex (HDAC 1 and HDAC 2). This interaction leads to the chromatin remodelling and compaction causing transcription repression [14, 16]. MeCP2 interacts also with c-ski and NCOR that are components of the HDAC complex [15].

Uta Francke's group analysed the histone acetylation profile in clonal lymphoblastoid cell culture from RTT female carrying the R168X and in cells from hemizygous male carrying the V288X mutation. Western blot analysis showed that histone H4 was hyperacetylated on residue 16, whilst histone H3 acetylation profile was not modified [31]. In contrast, another study done in the $MeCP2^{308/y}$ mice showed an elevated level of histone H3 acetylation [18].

Finally, Thatcher and Lasalle demonstrated that H3K9 acetylation (H3K9ac) shows a dynamic developmental localization pattern coincident with MeCP2 increase. Nuclei with mature neuronal phenotype characterized by a large euchromatic nucleus and a single large nucleolus presented concomitantly a high level of MeCP2 and a reduced level of H3K9ac

[32].

However some studies revealed that transcription repression by MeCP2 is partially alleviated by treatment with Trichostatin A (TSA), an inhibitor of the histone deacetylase activity. This partial inhibition suggests that an alternative mechanism probably exists, independent from the histone deacetylase complex, and able to repress transcription [33].

2.4.1.2 Histone methylation

MeCP2 can inhibit transcription by histone methylation. In fact, it was suggested that methylation at lysine 9 of histone H3 (H3K9me) is associated with gene silencing. In 2003, Fuks *et al*, showed that MeCP2 associates with histone H3 methyltransferase activity to induce H3K9 methylation on gene H19 [34].

2.4.1.3 Chromatin Compaction and architecture

Additionally it has been found that MeCP2 binds *in vitro* to 12-mer nucleosomal array (12 octamers/DNA) and can induce its compaction. MeCP2 carrying the R133C mutation (affecting the binding to methylated DNA) or R168X mutation lacking the C-terminal region of the protein are unable to compact the chromatin showing that the chromatin-condensing domain resides in the TRD and/or C-terminal regions of MeCP2 [21].

Another study showed that the C-terminal region of MeCP2 (amino acids 294 to 370 and 371 to 453) is important for chromatin compaction in a methylation-independent manner. This compaction is due to a nucleosome-MeCP2-nucleosome interaction [21].

It was also shown that MeCP2, like H1, binds to the linker DNA very close to the DNA entry and exit sites of the nucleosome forming a "stem"motif [35, 36, 21].

In 2005, Horike *et al.* showed also that MeCP2 can repress transcription of the *Dlx5-Dlx6* locus by forming a silent chromatin loop [37].

2.4.1.4 Direct interaction with the transcriptional machinery

An *in vitro* study revealed that the TRD can interact with TFIIB and prevent the formation of the pre-initiation complex [38].

2.4.2 Transcription activator

In contrast to the data showing that MeCP2 is a transcription inhibitor, in 2008, Chahrour *et al.* carried out a study to examine gene expression patterns in the hypothalamus of MeCP2-null and transgenic mice. Surprisingly, in this study, authors showed that MeCP2 binds to promoters of activated genes and associates with the transcription activator CREB1. Moreover, they showed that MeCP2 can activate the expression of the *Creb1* gene. An increased level of CREB1 induces miR132 microRNA and represses MeCP2 translation suggesting a negative regulatory loop between MeCP2 and CREB1 [39]. These results confirm another study, in which, by using Chip-chip analysis in SH-SY5Y cells, MeCP2 has been found associated more frequently with promoters that are also associated with RNA polymerase II [40].

All these data suggest that MeCP2 would be a "transcriptional modulator" rather than a repressor.

2.4.3 Alternative splicing of mRNA

By co-immunoprecipitation and mass spectrometry analysis, Young *et al.* characterized an RNA dependant interaction between MeCP2 and the Y box binding protein1 (YB-1) [41]. YB-1 is implicated in transcription and translation regulation, in DNA repair and in response to stress. The region of MeCP2 required for this interaction is between amino acid 195 and 329. C-terminal truncation of MeCP2 after amino acid 308 (the same as $MeCP2^{308}$ mice generated by Zoghbi's group (cf. chapter 1 section 1.6.3)) decreases this interaction from 50 to 70% indicating that sequence beyond the TRD is important for this interaction. Analysis of mRNA splicing profile in cerebral cortex of wild-type and $MeCP2^{308/y}$ mice showed aberration in alternative splicing of different genes like *Dlx5* and *NR1* (an NMDA receptor subunit). Interaction of MeCP2 with YB-1 and with FBP11 and HYPC (two others splicing factors) [19] suggests an important role of MeCP2 in splicing regulation.

2.4.4 Maintaining of DNA methylation

In vertebrates, DNA methylation is very important to maintain the chromatin structure and gene silencing [42]. DNA methylation occurs at position 5 of cytosine. During DNA replication, eukaryotic cells should maintain the methylation pattern along the newly synthesized

DNA strand. This epigenetic "mark" is preserved by DNA methyltransferase 1 (DNMT1). This protein lacks a DNA binding domain.

To understand how this enzyme is recruited to hemi-methylated DNA, Kimura and Shiota carried out a study in 2003 and they revealed that MeCP2 interacts with DNMT1 *via* its TRD. However, MBD deletion decreases the interaction between MeCP2 and DNMT1 suggesting that the MBD also contributes to this interaction [43].

2.5 MeCP2 mutations and other diseases

MeCP2 mutations were also found in pathologies other than Rett syndrome like:

2.5.1 The Angelman syndrome (AS)

The AS is a neuro-developmental disorder with some phenotypic similarities to RTT. It occurs in 1:12,000 to 1:20,000 in the general population (affecting girls and boys equally). Unlike RTT, AS is characterized by an earlier onset (like hypotonicity at birth). However, there is no developmental regression, and purposeful hand movements are retained. Angelman Syndrome is primarily caused by deletions, mutations or imprinting errors in *UBE3A* gene on chromosome 15 coding for the ubiquitin protein ligase E3A. MeCP2 mutations causing RTT have been diagnosed in girls and boys presenting AS features [44].

2.5.2 The severe neonatal encephalopathy (SNE)

The SNE is characterized by a static encephalopathy, seizures and respiratory abnormalities. It affects boys that inherit MeCP2 mutation from their mother who present a favorable XCI skewing towards the non-mutated allele. Frequently, these boys die at an early age.

2.5.3 The X-linked Mental retardation (XLMR)

It's an inherited condition that causes failure to develop cognitive abilities because of mutations or duplications of genes across the X chromosome. Couvert *et al.* identified MeCP2 point mutations in up to 2% of individuals with XLMR. These mutations were not observed in RTT patients [45]. Lugtenberg *et al.* also showed that duplication of the region Xq28, including MeCP2, is identified in 1% of patients with XLMR and in 2% of patients

with severe progressive neurological symptoms [46].

2.5.4 Autism

Autism is relatively rare in girls. Autism is characterized by severe impairments in social interaction and communication. The onset of symptoms generally occurs around 1 to 3 years of age and phenotypic features overlap with those of Rett syndrome.

A study identified two females with autistic disorder carrying mutations in *MeCP2* gene. The first one is a 1157del41 mutation resulting in a MeCP2 protein truncated to 389 amino acids from the normal 486. This mutation has previously been reported in two females with classic RTT. The second one is a nonsense mutation (R294X) which is one of the most frequent mutations found in RTT [47, 48].

2.6 Conclusions

MeCP2 is highly abundant in mature neurons, with a number of molecules approaching the number of histone octamers [49]. Its expression level is tightly regulated and the slightest perturbation results in deleterious neurological consequences. This chromatin-associated protein is widely distributed in the genome. It interacts with a high number of different partners: proteins, chromatin, DNA and RNA, suggesting that it is a multifunctional protein, with roles in chromatin remodeling and RNA splicing. Significant progress has been made over the last 10 years but the complex situation still remains to be clarified. Diverse questions remained unanswered, such as: Do the two isoforms of MeCP2 exist in significant amounts, and what are their respective roles? What is the function of MeCP2 outside the nervous system? What are the fundamental molecular interactions between MeCP2 and chromatin? Are there cellular functions of MeCP2 that have yet to be discovered?

To understand precisely the molecular mechanisms behind the Rett syndrome and to consider potential treatment for the affected girls, it is important to understand the exact function of MeCP2 in the cell.

Bibliography

[1] J. D. Lewis, R. R. Meehan, W. J. Henzel, I. Maurer-Fogy, P. Jeppesen, F. Klein, and A. Bird. Purification, sequence, and cellular localization of a novel chromosomal protein that binds to methylated DNA. *Cell*, 69(6):905–14, 1992.

[2] J. F. Coy, Z. Sedlacek, D. Bachner, H. Delius, and A. Poustka. A complex pattern of evolutionary conservation and alternative polyadenylation within the long 3"-untranslated region of the methyl-CpG-binding protein 2 gene (*mecp2*) suggests a regulatory role in gene expression. *Hum Mol Genet*, 8(7):1253–62, 1999.

[3] K. Reichwald, J. Thiesen, T. Wiehe, J. Weitzel, W. A. Poustka, A. Rosenthal, M. Platzer, W. H. Stratling, and P. Kioschis. Comparative sequence analysis of the MeCP2-locus in human and mouse reveals new transcribed regions. *Mamm Genome*, 11(3):182–90, 2000.

[4] G. J. Pelka, C. M. Watson, J. Christodoulou, and P. P. Tam. Distinct expression profiles of MeCP2 transcripts with different lengths of 3'UTR in the brain and visceral organs during mouse development. *Genomics*, 85(4):441–52, 2005.

[5] M. D. Shahbazian, B. Antalffy, D. L. Armstrong, and H. Y. Zoghbi. Insight into Rett Syndrome: MeCP2 levels display tissue- and cell-specific differences and correlate with neuronal maturation. *Hum Mol Genet*, 11(2):115–24, 2002.

[6] S. Kriaucionis and A. Bird. The major form of MeCP2 has a novel N-terminus generated by alternative splicing. *Nucleic Acids Res*, 32(5):1818–23, 2004.

[7] G. N. Mnatzakanian, H. Lohi, I. Munteanu, S. E. Alfred, T. Yamada, P. J. MacLeod, J. R. Jones, S. W. Scherer, N. C. Schanen, M. J. Friez, J. B. Vincent, and B. A. Minassian. A previously unidentified MeCP2 open reading frame defines a new protein isoform relevant to Rett Syndrome. *Nat Genet*, 36(4):339–41, 2004.

[8] T. Bienvenu and J. Chelly. Molecular genetics of Rett Syndrome: when DNA methylation goes unrecognized. *Nat Rev Genet*, 7(6):415–26, 2006.

[9] M. Fatemi and P. A. Wade. MBD family proteins: reading the epigenetic code. *J Cell Sci*, 119(Pt 15):3033–7, 2006.

[10] X. Nan, R. R. Meehan, and A. Bird. Dissection of the methyl-CpG binding domain from the chromosomal protein MeCP2. *Nucleic Acids Res*, 21(21):4886–92, 1993.

[11] R. J. Klose, S. A. Sarraf, L. Schmiedeberg, S. M. McDermott, I. Stancheva, and A. P. Bird. DNA binding selectivity of MeCP2 due to a requirement for A/T sequences adjacent to methyl-CpG. *Mol Cell*, 19(5):667–78, 2005.

[12] T. C. Galvao and J. O. Thomas. Structure-specific binding of MeCP2 to four-way junction DNA through its methyl CpG-binding domain. *Nucleic Acids Res*, 33(20):6603–9, 2005.

[13] X. Nan, F. J. Campoy, and A. Bird. MeCP2 is a transcriptional repressor with abundant binding sites in genomic chromatin. *Cell*, 88(4):471–81, 1997.

[14] P. L. Jones, G. J. Veenstra, P. A. Wade, D. Vermaak, S. U. Kass, N. Landsberger, J. Strouboulis, and A. P. Wolffe. Methylated DNA and MeCP2 recruit histone deacetylase to repress transcription. *Nat Genet*, 19(2):187–91, 1998.

[15] K. Kokura, S. C. Kaul, R. Wadhwa, T. Nomura, M. M. Khan, T. Shinagawa, T. Yasukawa, C. Colmenares, and S. Ishii. The Ski protein family is required for MeCP2-mediated transcriptional repression. *J Biol Chem*, 276(36):34115–21, 2001.

[16] X. Nan, H. H. Ng, C. A. Johnson, C. D. Laherty, B. M. Turner, R. N. Eisenman, and A. Bird. Transcriptional repression by the methyl-CpG-binding protein MeCP2 involves a histone deacetylase complex. *Nature*, 393(6683):386–9, 1998.

[17] X. Nan, P. Tate, E. Li, and A. Bird. DNA methylation specifies chromosomal localization of MeCP2. *Mol Cell Biol*, 16(1):414–21, 1996.

[18] M. Shahbazian, J. Young, L. Yuva-Paylor, C. Spencer, B. Antalffy, J. Noebels, D. Armstrong, R. Paylor, and H. Zoghbi. Mice with truncated MeCP2 recapitulate many Rett Syndrome features and display hyperacetylation of histone H3. *Neuron*, 35(2):243–54, 2002.

[19] J. P. Buschdorf and W. H. Stratling. A WW domain binding region in methyl-CpG-binding protein MeCP2: impact on Rett Syndrome. *J Mol Med*, 82(2):135–43, 2004.

[20] T. Nikitina, R. P. Ghosh, R. A. Horowitz-Scherer, J. C. Hansen, S. A. Grigoryev, and C. L. Woodcock. MeCP2-chromatin interactions include the formation of chromatosome-like structures and are altered in mutations causing Rett Syndrome. *J Biol Chem*, 282(38):28237–45, 2007.

[21] T. Nikitina, X. Shi, R. P. Ghosh, R. A. Horowitz-Scherer, J. C. Hansen, and C. L. Woodcock. Multiple modes of interaction between the methylated DNA binding protein MeCP2 and chromatin. *Mol Cell Biol*, 27(3):864–77, 2007.

[22] V. H. Adams, S. J. McBryant, P. A. Wade, C. L. Woodcock, and J. C. Hansen. Intrinsic disorder and autonomous domain function in the multifunctional nuclear protein, MeCP2. *J Biol Chem*, 282(20):15057–64, 2007.

[23] S. Carro, A. Bergo, M. Mengoni, A. Bachi, G. Badaracco, C. Kilstrup-Nielsen, and N. Landsberger. A novel protein, Xenopus p20, influences the stability of MeCP2 through direct interaction. *J Biol Chem*, 279(24):25623–31, 2004.

[24] S. Cassel, M. O. Revel, C. Kelche, and J. Zwiller. Expression of the methyl-CpG-binding protein MeCP2 in rat brain. An ontogenetic study. *Neurobiol Dis*, 15(2):206–11, 2004.

[25] B. C. Mullaney, M. V. Johnston, and M. E. Blue. Developmental expression of methyl-CpG binding protein 2 is dynamically regulated in the rodent brain. *Neuroscience*, 123(4):939–49, 2004.

[26] S. Akbarian, R. Z. Chen, J. Gribnau, T. P. Rasmussen, H. Fong, R. Jaenisch, and E. G. Jones. Expression pattern of the Rett Syndrome gene *mecp2* in primate prefrontal cortex. *Neurobiol Dis*, 8(5):784–91, 2001.

[27] I. Maezawa, S. Swanberg, D. Harvey, J. M. LaSalle, and L. W. Jin. Rett Syndrome astrocytes are abnormal and spread MeCP2 deficiency through gap junctions. *J Neurosci*, 29(16):5051–61, 2009.

[28] J. M. LaSalle, J. Goldstine, D. Balmer, and C. M. Greco. Quantitative localization of heterogeneous methyl-CpG-binding protein 2 (MeCP2) expression phenotypes in normal and Rett Syndrome brain by laser scanning cytometry. *Hum Mol Genet*, 10(17):1729–40, 2001.

[29] M. Adachi, E. W. Keefer, and F. S. Jones. A segment of the Mecp2 promoter is sufficient to drive expression in neurons. *Hum Mol Genet*, 14(23):3709–22, 2005.

[30] J. Liu and U. Francke. Identification of cis-regulatory elements for MeCP2 expression. *Hum Mol Genet*, 15(11):1769–82, 2006.

[31] M. Wan, K. Zhao, S. S. Lee, and U. Francke. MeCP2 truncating mutations cause histone H4 hyperacetylation in Rett Syndrome. *Hum Mol Genet*, 10(10):1085–92, 2001.

[32] K. N. Thatcher and J. M. LaSalle. Dynamic changes in Histone H3 lysine 9 acetylation localization patterns during neuronal maturation require MeCP2. *Epigenetics*, 1(1):24–31, 2006.

[33] F. Yu, J. Thiesen, and W. H. Stratling. Histone deacetylase-independent transcriptional repression by methyl-CpG-binding protein 2. *Nucleic Acids Res*, 28(10):2201–6, 2000.

[34] F. Fuks, P. J. Hurd, D. Wolf, X. Nan, A. P. Bird, and T. Kouzarides. The methyl-CpG-binding protein MeCP2 links DNA methylation to histone methylation. *J Biol Chem*, 278(6):4035–40, 2003.

[35] P. T. Georgel, R. A. Horowitz-Scherer, N. Adkins, C. L. Woodcock, P. A. Wade, and J. C. Hansen. Chromatin compaction by human MeCP2. Assembly of novel secondary chromatin structures in the absence of DNA methylation. *J Biol Chem*, 278(34):32181–8, 2003.

[36] T. Ishibashi, A. A. Thambirajah, and J. Ausio. MeCP2 preferentially binds to methylated linker DNA in the absence of the terminal tail of histone H3 and independently of histone acetylation. *FEBS Lett*, 582(7):1157–62, 2008.

[37] S. Horike, S. Cai, M. Miyano, J. F. Cheng, and T. Kohwi-Shigematsu. Loss of silent-chromatin looping and impaired imprinting of DLX5 in Rett Syndrome. *Nat Genet*, 37(1):31–40, 2005.

[38] N. K. Kaludov and A. P. Wolffe. MeCP2 driven transcriptional repression in vitro: selectivity for methylated DNA, action at a distance and contacts with the basal transcription machinery. *Nucleic Acids Res*, 28(9):1921–8, 2000.

[39] M. Chahrour, S. Y. Jung, C. Shaw, X. Zhou, S. T. Wong, J. Qin, and H. Y. Zoghbi. MeCP2, a key contributor to neurological disease, activates and represses transcription. *Science*, 320(5880):1224–9, 2008.

[40] D. H. Yasui, S. Peddada, M. C. Bieda, R. O. Vallero, A. Hogart, R. P. Nagarajan, K. N. Thatcher, P. J. Farnham, and J. M. Lasalle. Integrated epigenomic analyses of neuronal MeCP2 reveal a role for long-range interaction with active genes. *Proc Natl Acad Sci U S A*, 104(49):19416–21, 2007.

[41] J. I. Young, E. P. Hong, J. C. Castle, J. Crespo-Barreto, A. B. Bowman, M. F. Rose, D. Kang, R. Richman, J. M. Johnson, S. Berget, and H. Y. Zoghbi. Regulation of RNA splicing by the methylation-dependent transcriptional repressor methyl-CpG binding protein 2. *Proc Natl Acad Sci U S A*, 102(49):17551–8, 2005.

[42] T. Kouzarides. Histone methylation in transcriptional control. *Curr Opin Genet Dev*, 12(2):198–209, 2002.

[43] H. Kimura and K. Shiota. Methyl-CpG-binding protein, MeCP2, is a target molecule for maintenance DNA methyltransferase, Dnmt1. *J Biol Chem*, 278(7):4806–12, 2003.

[44] P. Watson, G. Black, S. Ramsden, M. Barrow, M. Super, B. Kerr, and J. Clayton-Smith. Angelman Syndrome phenotype associated with mutations in MeCP2, a gene encoding a methyl CpG binding protein. *J Med Genet*, 38(4):224–8, 2001.

[45] P. Couvert, T. Bienvenu, C. Aquaviva, K. Poirier, C. Moraine, C. Gendrot, A. Verloes, C. Andres, A. C. Le Fevre, I. Souville, J. Steffann, V. des Portes, H. H. Ropers, H. G. Yntema, J. P. Fryns, S. Briault, J. Chelly, and B. Cherif. MeCP2 is highly mutated in X-linked mental retardation. *Hum Mol Genet*, 10(9):941–6, 2001.

[46] D. Lugtenberg, T. Kleefstra, A. R. Oudakker, W. M. Nillesen, H. G. Yntema, A. Tzschach, M. Raynaud, D. Rating, H. Journel, J. Chelly, C. Goizet, D. Lacombe, J. M.

Pedespan, B. Echenne, G. Tariverdian, D. O'Rourke, M. D. King, A. Green, M. van Kogelenberg, H. Van Esch, J. Gecz, B. C. Hamel, H. van Bokhoven, and A. P. de Brouwer. Structural variation in Xq28: MeCP2 duplications in 1% of patients with unexplained XLMR and in 2% of male patients with severe encephalopathy. *Eur J Hum Genet*, 17(4):444–53, 2009.

[47] R. M. Carney, C. M. Wolpert, S. A. Ravan, M. Shahbazian, A. Ashley-Koch, M. L. Cuccaro, J. M. Vance, and M. A. Pericak-Vance. Identification of MeCP2 mutations in a series of females with autistic disorder. *Pediatr Neurol*, 28(3):205–11, 2003.

[48] J. M. Lasalle and D. H. Yasui. Evolving role of MeCP2 in Rett Syndrome and autism. *Epigenomics*, 1(1):119–130, 2009.

[49] P. J. Skene, R. S. Illingworth, S. Webb, A. R. Kerr, K. D. James, D. J. Turner, R. Andrews, and A. P. Bird. Neuronal MeCP2 is expressed at near histone-octamer levels and globally alters the chromatin state. *Mol Cell*, 37(4):457–68, 2010.

3 Green Fluorescent protein and Microscopy

3.1 Introduction

Visualization of proteins in cells was performed using techniques like histochemistry and immunohistochemistry. To detect native intra-cellular proteins, monoclonal antibodies are sometimes available. Otherwise, a large choice of epitope tags (myc, His, HA, Flag) is nowadays available to specifically detect or isolate proteins in cells. Detection of such tags either involves specific monoclonal antibodies directly linked to a fluorochrome, or successive steps of unlabelled antibody and fluorochrome-conjugated secondary reagents. The major drawback of these techniques is that they need cells fixation and permeabilization, that they can affect the behaviour of some proteins. Understanding protein dynamics and measuring spatio-temporal modifications of protein expression and/or localization require sensitive and quantitative tools adapted to studies in living cells. One of the most important recent technological development in cell biology has been the use of the Green Fluorescent Protein (GFP) isolated from the jellyfish *Aequorea victoria* [1]. Fusion to GFP enables direct visualization of intracellular proteins in their biological environment without the need for secondary reagents, cofactors or treatments of the cells.

3.2 Green Fluorescent Protein (GFP)

GFP is a 27 kDa protein (238 amino acids) [2]. It absorbs blue light with an excitation maximum of 395 nm, with a smaller peak at 475 nm, and fluoresces with an emission maximum at 510 nm [3]. GFP owes its visible absorbance and fluorescence to a chromophore formed by the cyclization and subsequent oxidation of three amino acids: Ser65, Tyr66 and

Gly67. These posttranslational modifications are established in an autocatalytic way and allow formation of fluorescent molecule when the protein is expressed in other species from prokaryotes to eukaryotes [4].

The crystal structure of GFP was solved in 1996. Analysis of this structure revealed the presence of eleven β-sheets that form a barrel with a diagonal α-helix in the inside of the barrel. The chromophore is located in the middle of the α-helix chain [5, 6] (Figure 3.1).

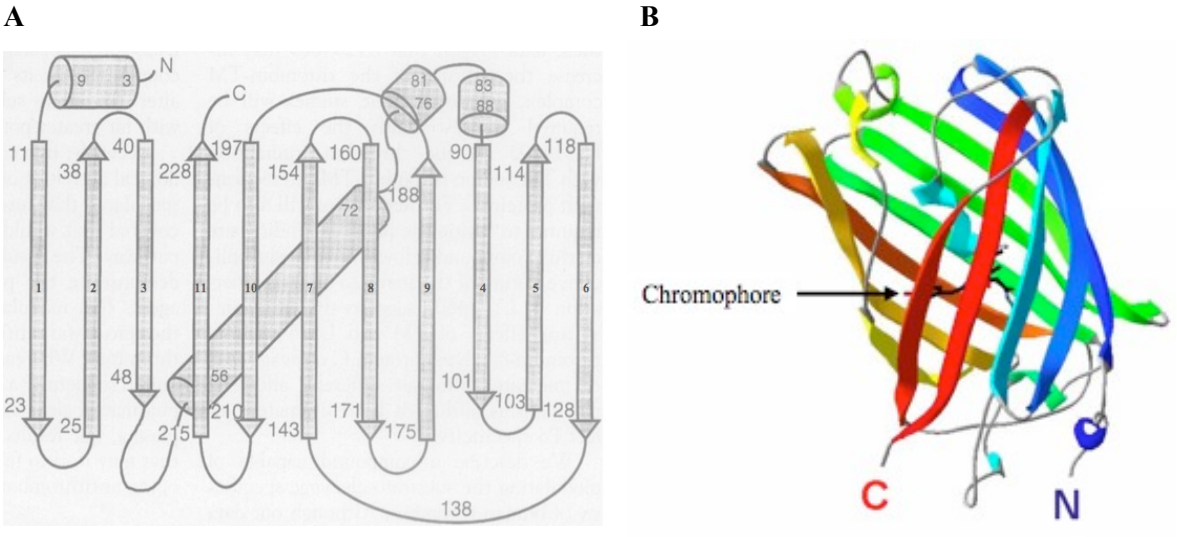

Figure 3.1 — Two representations of the Green Fluorescent Protein: A) Schematic representation and amino acid residue number, at the beginning and the end, of each of the 11 β-sheets and the α-helix constituting the GFP. B) β-barrel representation of the GFP. The chromophore is embedded inside the barrel. Adapted from [5] and captured from `http://fr.academic.ru/pictures/frwiki/71/GFP.png`

Wild-type GFP presents poor expression in certain mammalian species and low fluorescence intensity when excited with the 488 nm line of an argon laser, the standard laser used for live cell imaging studies by microscopy or by flow cytometry. Mutagenesis experiments were performed on wild-type GFP and different mutants have been selected. For example the mutant carrying a double mutation on Serine 65 (S65T) and Phenylalanine 64 (F64L) results in a 30-fold increase of fluorescence intensity over WT. The excitation maxima of this mutant was also red-shifted by about 100 nm, permitting efficient excitation at 488 nm (Figure 3.2) [7]. Finally the gene sequence of this mutant was re-engineered with codons preferentially found in human proteins, providing an enhanced GFP (eGFP) that combined increased fluorescence activity and high expression levels in mammalian cells [8]. The screen of different mutants has also lead to the identification of different colour variants like the Blue, the Cyan and the Yellow Fluorescent Protein (BFP, CFP and YFP) [3, 5]. All

these variants provide interesting tools to study the dynamic of particular protein in living cells (Figure 3.2).

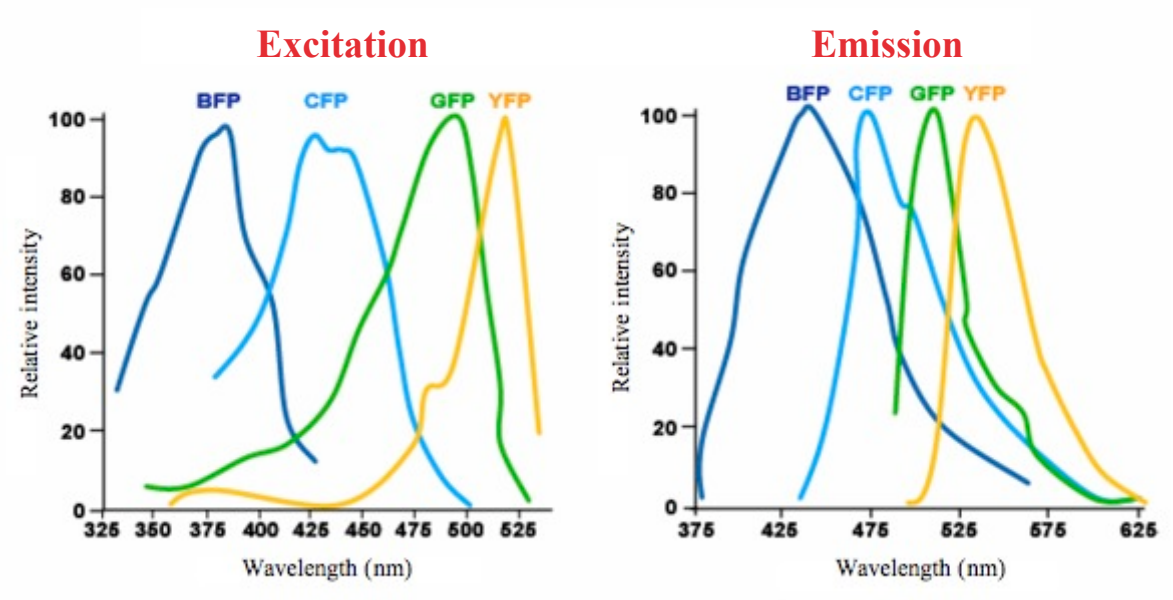

Figure 3.2 — Excitation and emission spectra of eGFP and its variants BFP, CFP and YFP. Captured from `http://fr.academic.ru/pictures/frwiki/71/GFP.png`

3.3 Split GFP system

Sometimes, the large size of GFP may alter protein localization and behaviour, and in some cases the permanent fluorescence of the reporter can be a hindrance to detect other markers.

In 2005, Cabantous *et al.* engineered soluble, self-associating fragments of GFP that can be used to tag and detect either soluble or insoluble proteins in living cells or cell lysates. The split GFP system is simple and is based on the auto-assembly capacity of two non-fluorescent portions of GFP, GFP 1-10 and GFP11, to restore a fully fluorescent GFP. The GFP11 tag, which is only 15 amino-acids long (β-strand 11, residues 215-230), is fused to the N or C-terminus of the coding sequence of the protein of interest, and can then be expressed in eukaryotic cells. The GFP 1-10 detector fragment (β-strands 1-10, residues 1-214) is expressed separately. Neither fragment alone is fluorescent. When mixed, the small and the large GFP fragments spontaneously associate, resulting in GFP folding and formation of the fluorophore [9] (Figure 3.3).

During my thesis, I used the split GFP tagging system in which the GFP 1-10 was used

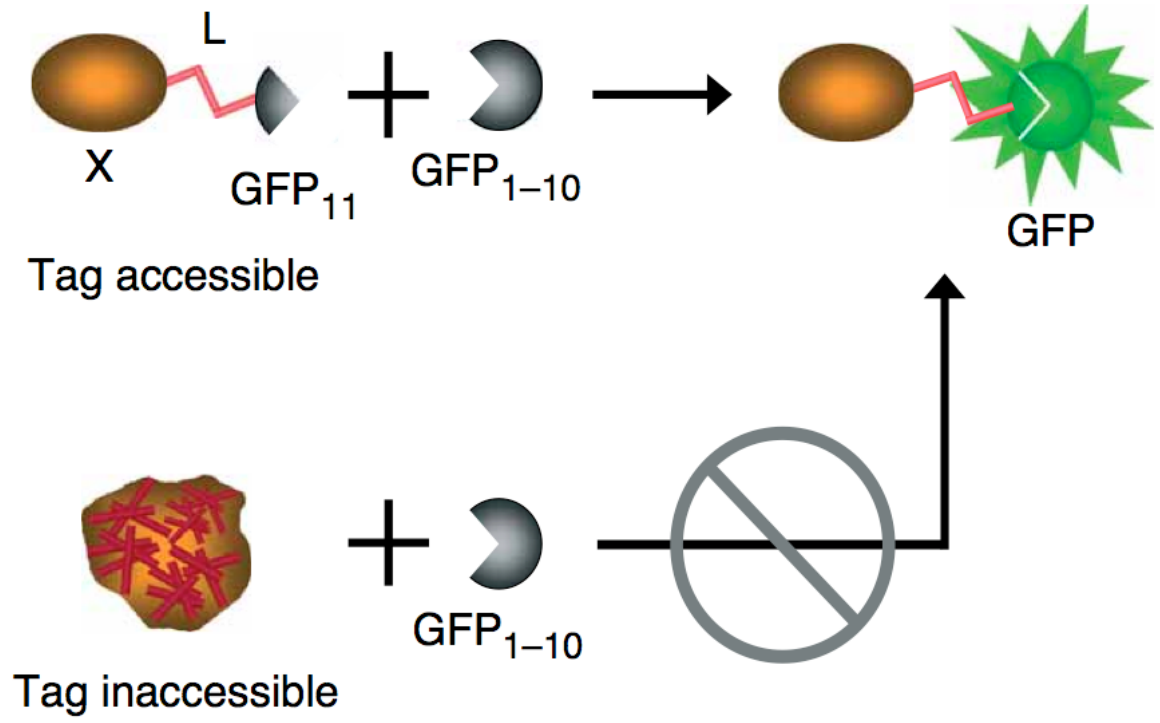

Figure 3.3 — Principle of the split GFP complementation system: the protein of interest (X) is fused to the GFP11 fragment (β-strand 11) via a linker (L). The GFP 1-10 fragment (β-strand 1-10) is expressed and purified separatly. When these two fragments are separated, there is no fluorescence. On the other side, when mixed, these two fragments associate spontaneously resulting in GFP folding and forming of the fluophore. When the GFP11 is not accessible, due to aggregation or misfolding of protein X, the fluorescence is abolished. Adapted from [9]

as a reagent for the detection of GFP11-tagged proteins in mammalian cells. The GFP1-10 fragment was produced separately in *Escherichia coli* and purified from inclusion bodies. This new application allows fast and sensitive detection of proteins by both flow cytometry and microscopy analysis.

3.4 Fluorescence Recovery After Photobleaching (FRAP)

Fluorescence is the process that occurs when fluorescent molecules absorb photons of certain wavelength and, following this absorption, emit light at a higher wavelength. When the GFP (or other fluorophores) is excited with a high intensity laser pulse, it becomes non-fluorescent due to the limited number of excitation-emission cycles that it can undergo. This process is called photobleaching [10]. This property allowed the development of an interesting technique called Fluorescence Recovery After Photobleaching (FRAP). It is an important technique to study the dynamic of proteins in living cells [11, 12].

It consists on photobleaching molecules in a small area of the cell with a high intensity laser pulse. Then the redistribution of fluorescence in the photobleached area is monitored over time. Results will provide information on the mobility parameters of fluorescently tagged proteins and allow the identification of possible bound or transient immobile fractions.

Immediately after the bleach-pulse, the majority of the GFP will lose their fluorescence, and we can then distinguish between three different situations (Figure 3.4):

- When the GFP-tagged proteins are very mobile; the photobleached area becomes green again rapidly after photobleaching.
- In contrast, if the GFP-tagged proteins are immobile they will not diffuse back into the bleached area and the bleached area will recover its intensity very slowly.
- When a GFP-tagged protein is transiently immobile due to its interaction with other molecules; it will result in a biphasic recovery plot. First, the plot will show a relatively fast recovery of fluorescence caused by free diffusing proteins. Then the bleached molecules that are released from their bound state will increase the fluorescence recovery in the strip.

FRAP is an important tool and if combined with GFP or GFP-variants, as a fluorescent tag, it allows the characterization and the determination of the localization, activity and the dynamics of proteins in their biological environment: the living cell.

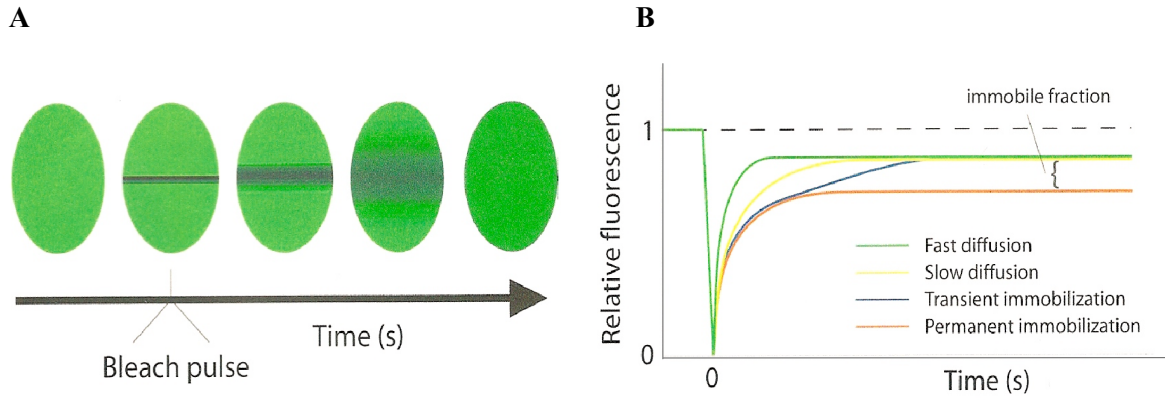

Figure 3.4 — Schematic representation of strip-FRAP experiments: A) The green ellipsoids represent a cell nucleus expressing GFP. The experiment consists on defining a small strip in the middle of the nucleus which is photobleached. Then the fluorescence recovery is monitored along time. This results in different curves B) with multiple shapes that characterize the mobility of each protein of interest.

Bibliography

[1] O. Shimomura, F. H. Johnson, and Y. Saiga. Extraction, purification and properties of aequorin, a bioluminescent protein from the luminous hydromedusan, Aequorea. *J Cell Comp Physiol*, 59:223–39, 1962.

[2] D. C. Prasher, V. K. Eckenrode, W. W. Ward, F. G. Prendergast, and M. J. Cormier. Primary structure of the Aequorea victoria green-fluorescent protein. *Gene*, 111(2):229–33, 1992.

[3] R. Heim, D. C. Prasher, and R. Y. Tsien. Wavelength mutations and posttranslational autoxidation of green fluorescent protein. *Proc Natl Acad Sci U S A*, 91(26):12501–4, 1994.

[4] A. B. Cubitt, R. Heim, S. R. Adams, A. E. Boyd, L. A. Gross, and R. Y. Tsien. Understanding, improving and using green fluorescent proteins. *Trends Biochem Sci*, 20(11):448–55, 1995.

[5] M. Ormo, A. B. Cubitt, K. Kallio, L. A. Gross, R. Y. Tsien, and S. J. Remington. Crystal structure of the *Aequorea victoria* green fluorescent protein. *Science*, 273(5280):1392–5, 1996.

[6] F. Yang, L. G. Moss, and Jr. Phillips, G. N. The molecular structure of green fluorescent protein. *Nat Biotechnol*, 14(10):1246–51, 1996.

[7] B. P. Cormack, R. H. Valdivia, and S. Falkow. FACS-optimized mutants of the green fluorescent protein (GFP). *Gene*, 173(1 Spec No):33–8, 1996.

[8] T. T. Yang, L. Cheng, and S. R. Kain. Optimized codon usage and chromophore mutations provide enhanced sensitivity with the green fluorescent protein. *Nucleic Acids Res*, 24(22):4592–3, 1996.

[9] S. Cabantous, T. C. Terwilliger, and G. S. Waldo. Protein tagging and detection with engineered self-assembling fragments of green fluorescent protein. *Nat Biotechnol*, 23(1):102–7, 2005.

[10] U. Kubitscheck, O. Kuckmann, T. Kues, and R. Peters. Imaging and tracking of single GFP molecules in solution. *Biophys J*, 78(4):2170–9, 2000.

[11] A. B. Houtsmuller and W. Vermeulen. Macromolecular dynamics in living cell nuclei revealed by fluorescence redistribution after photobleaching. *Histochem Cell Biol*, 115(1):13–21, 2001.

[12] E. A. Reits and J. J. Neefjes. From fixed to FRAP: measuring protein mobility and activity in living cells. *Nat Cell Biol*, 3(6):E145–7, 2001.

4 DNA Damage Repair

4.1 Introduction

DNA is located mostly in the nucleus of living cells. It contains all the genetic information needed by the cell to develop and function properly. Therefore it is vital for the cell to maintain and protect the integrity of genomic DNA. Nevertheless, cellular DNA is continuously exposed to genotoxic stress producing a large variety of DNA lesions. This stress can be caused by [1] (Figure 4.1):

- Endogenous damaging sources produced by normal cellular metabolism (like reactive oxygen species or lipid peroxidation), errors made during DNA replication or from spontaneous hydrolysis of nucleotides resulting in the loss of bases (abasic sites) or deamination of cytosine, 5-methylcytosine, adenine and guanine.

- Environmental agents such as ionizing radiation, ultra-violet light or cigarette smoke etc.

Many of these lesions block transcription or interfere with DNA replication. If these lesions remained unrepaired, they can cause mutations that enhance cancer risk or cell death. In order to counteract the deleterious effects of DNA damage, cells developed five major repair pathways that detect and repair different kinds of DNA damage. Double strand breaks are repaired by Homologous Recombination (HR) or NonHomologous End Joining (NHEJ), base-base mismatches and insertion/deletion mutations are repaired by Mismatch Repair (MMR). Base Excision Repair (BER) repairs single strand breaks, oxidative or alkylating damages. Nucleotide Excision Repair (NER), is responsible for eliminating helix distorting lesions, bulky adducts and intra-strand crosslinks ([1, 2]).

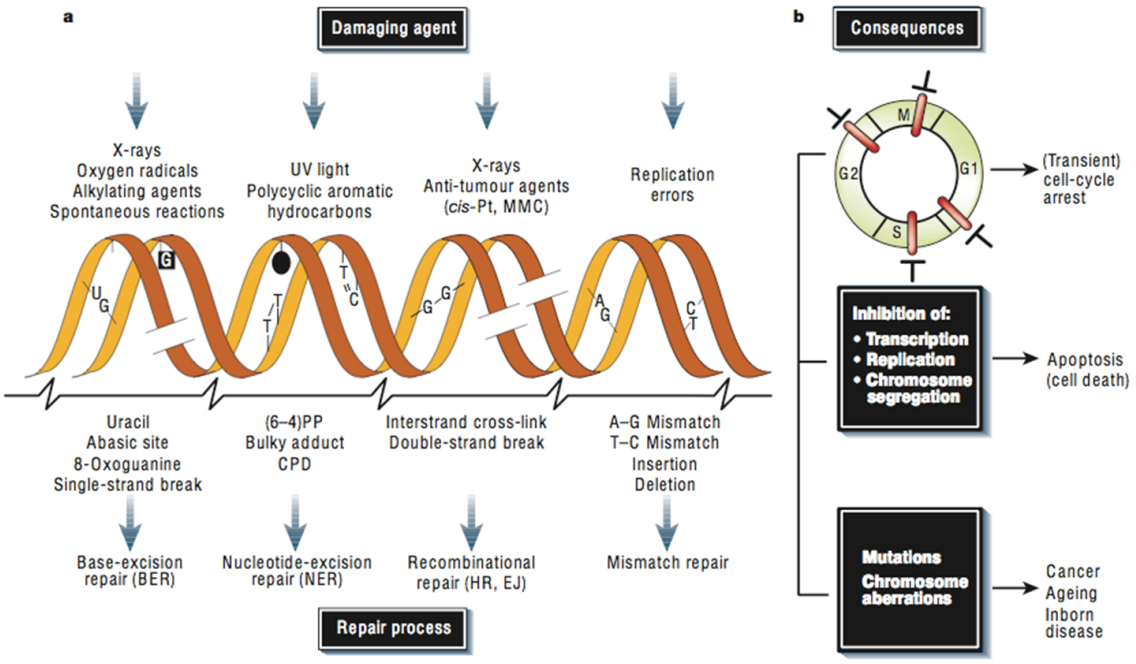

Figure 4.1 — **DNA damage, repair mechanisms and consequences.** a) DNA damages are caused by a variety of damaging agents, that when left unrepaired, cause mutations that can either induce cancer or accelerate ageing. To face this problem, cells developed five major repair pathways to deal with these different lesions. b) Upon damage sensing, cell cycle is arrested to allow the DNA repair. If the damage still remain unrepaired, cells undergo apoptosis (Figure adapted from [1]).

4.2 DNA repair pathways

4.2.1 DNA Double Strand Breaks (DSB) repair

Around 10 DSBs are produced daily per cell. These breaks can result from either endogenous sources:

1. When the replication fork encounters a damaged template.
2. When topoisomerases II accidently breaks DNA both strands.
3. During VDJ recombination.

Or exogenous sources when the cell is exposed to ionizing radiation (X-rays or gamma rays), topoisomerase poisons and radiomimetic drugs. Cells developed two major pathways to repair DSB: the Non Homologous End Joining (NHEJ) and the Homologous Recombination (HR) [3, 4].

4.2.1.1 Non Homologous End Joining (NHEJ)

NHEJ is the dominant pathway to remove DSBs in higher eukaryotes. It allows the ligation of the two ends of DSBs independently of the cell cycle because the presence of a sister chromatid is not required [5]. NHEJ is initiated by the binding of the heterodimer Ku70/Ku80 to the broken ends followed by the recruitment of DNA-PKcs (DNA dependant protein kinase catalytic subunit) and Artemis [6, 7]. Artemis-DNA-PKcs complex is able to cut DNA overhangs in the region of DSBs [8]. This allows the recruitment of XRCC4 and the DNA ligase IV complex that carry out the ligation step to complete repair. This step is stimulated by the XLF protein (also called Cernunnos) that stabilizes the XRCC4/DNA ligase IV complex on the DSB site [9, 10, 4] and (Figure 4.2).

NHEJ is considered as an error-prone mechanism because the Artemis-DNA-PKcs complex is required to process DNA ends before ligation causing loss of some genetic material.

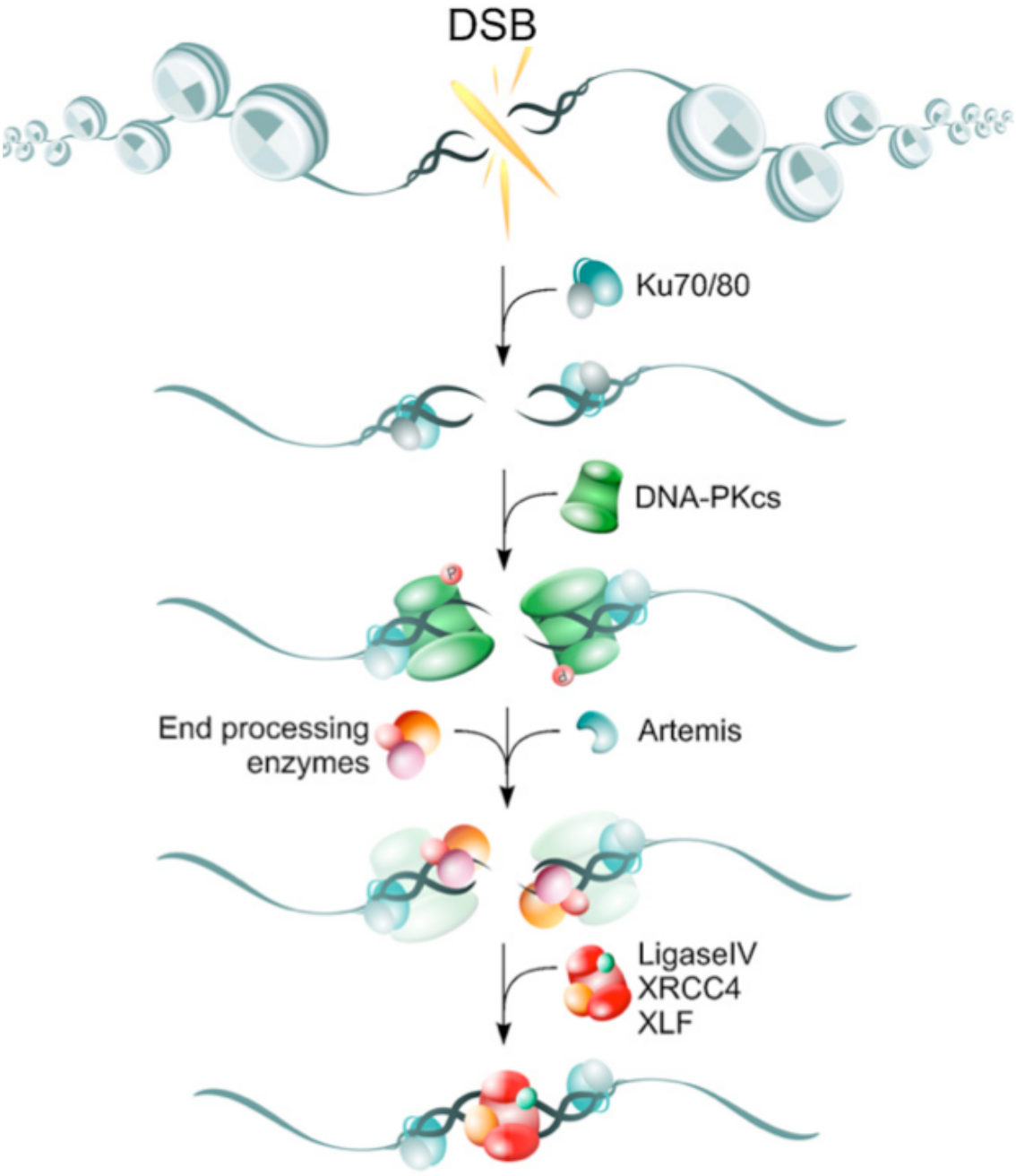

Figure 4.2 — **Schematic representation of the Non Homologous End Joining pathway.** DNA double strand breaks are recognised by Ku proteins that recruit DNA-PKcs followed by Artemis that allowed DNA overhangs resection. The ligation step is performed by the DNA ligase IV associated to XRCC4 and XLF. (Figure adapted from ([11])).

4.2.1.2 Homologous Recombination (HR)

Another mechanism involved in the repair of DSBs is the Homologous Recombination (HR). HR is an error-free repair mechanisms that occurs dominantly in S and G2 phases because it requires the presence of a homologous template such as the sister chromatid ([5, 12])). In HR (Figure 4.3), broken ends are recognized by the Mre11-Rad50-NBS1 (MRN) complex which can activate and recruit ATM (via its direct interaction with Nbs1), a protein kinase that phosphorylate numerous substrates in the DNA damage response, including histone H2AX (an early marker of DSB formation) ([13, 14]). MRN complex carries also a 5'-3' exonuclease activity creating free 3'-ends on both sides of the break [15]. The newly synthesized 3' overhangs ends are stabilized by RPA and, in cooperation with RAD52, BRCA1 and BRCA2, it allows the recruitment of RAD51 to form the nucleoprotein filament. The RAD51 filament (with RAD52 and RAD54) is required to find homologous sequences like the neighbouring intact sister chromatid. Strand invasion into a homologous sequence forms a D-loop intermediate and allow the 3'-end to be extended by polymerase. Intersection between DNA strands, also called Holliday junction, are resolved by resolvases like BLM-topoisomerase III complex, MUS81-EME1 complex or GEN1 ([1, 16]).

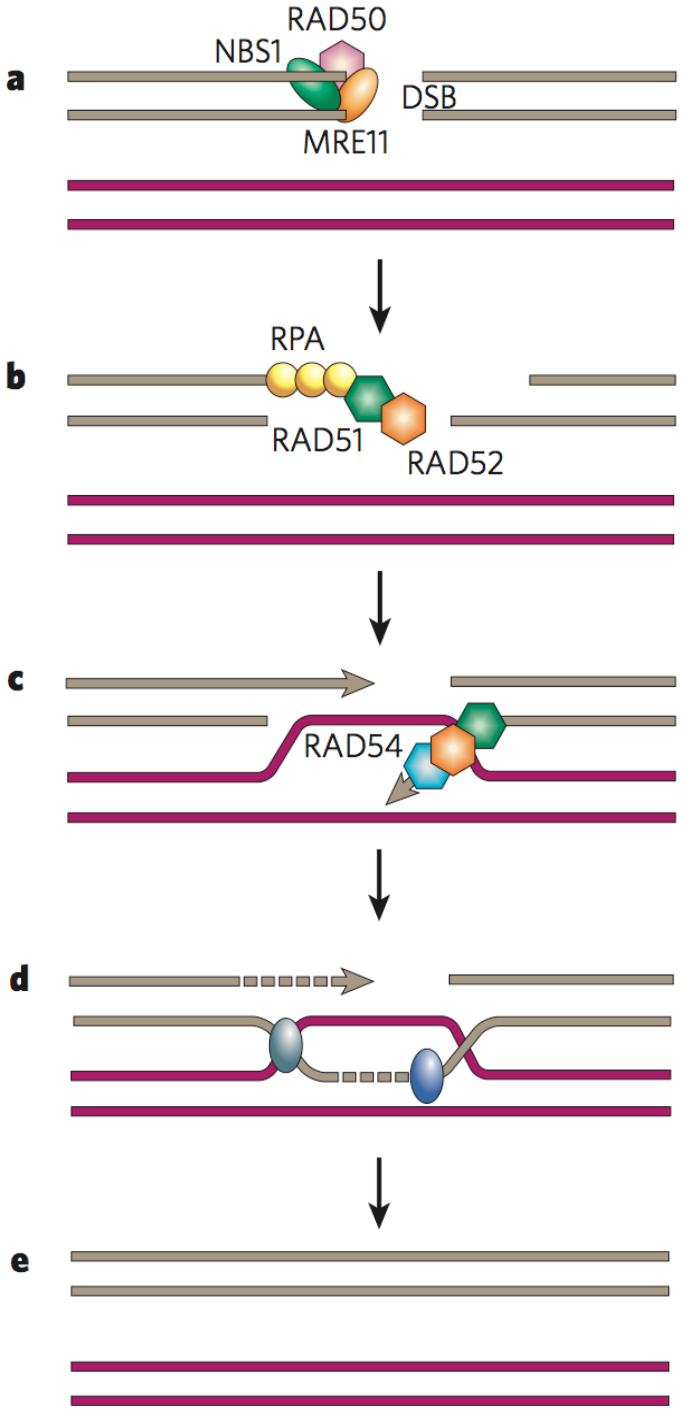

Figure 4.3 — **Schematic representation of the Homologous Recombination pathway.** a) DNA double strand breaks are recognized by the MRN complex (Mre11-Rad50-NBS11) which generates single strand DNA by resection. Single strand ends are protected by RPA. RAD52 and RAD51 are then required to find homologous sequences (Figure adapted from [17]).

4.2.2 Mismatch repair (MMR)

MMR corrects base-base mismatches and insertion/deletion (ID) mispairs generated during DNA replication and/or recombination [1].

In higher eukaryotes, repair of base-base mismatches or IDs of 1 to 2 nucleotides are initiated by MutSα (composed by MSH2 and MSH6) whereas the repair of larger ID is preferentially initiated by MutSβ (composed by MSH2 and MSH3) ([18, 19]). MutSα moves along the DNA and after the detection of a mismatch, it recruits MutLα (composed by hMLH1 and hPMS2). MutSα- MutLα dissociates from the mismatch and translocate along the DNA to encounter a DNA strand break bound by PCNA in 3′ and by RFC in 5′. If the complex moves upstream (Figure 4.4a), it encounters RFC, displaces it and recruits EXO1 that degrades DNA from 5′ to 3′. Complex that migrates downstream (Figure 4.4b), encounters PCNA. The RFC molecule at 5′ extremity would not be displaced preventing degradation of the 5′ to 3′ strand. The degradation occurs from 3′ to 5′ towards the mismatch. In both cases, single strand DNA is protected by RPA and the gap is filled by DNA pol δ. Finally, the remaining nick is ligated by the DNA ligase I [16].

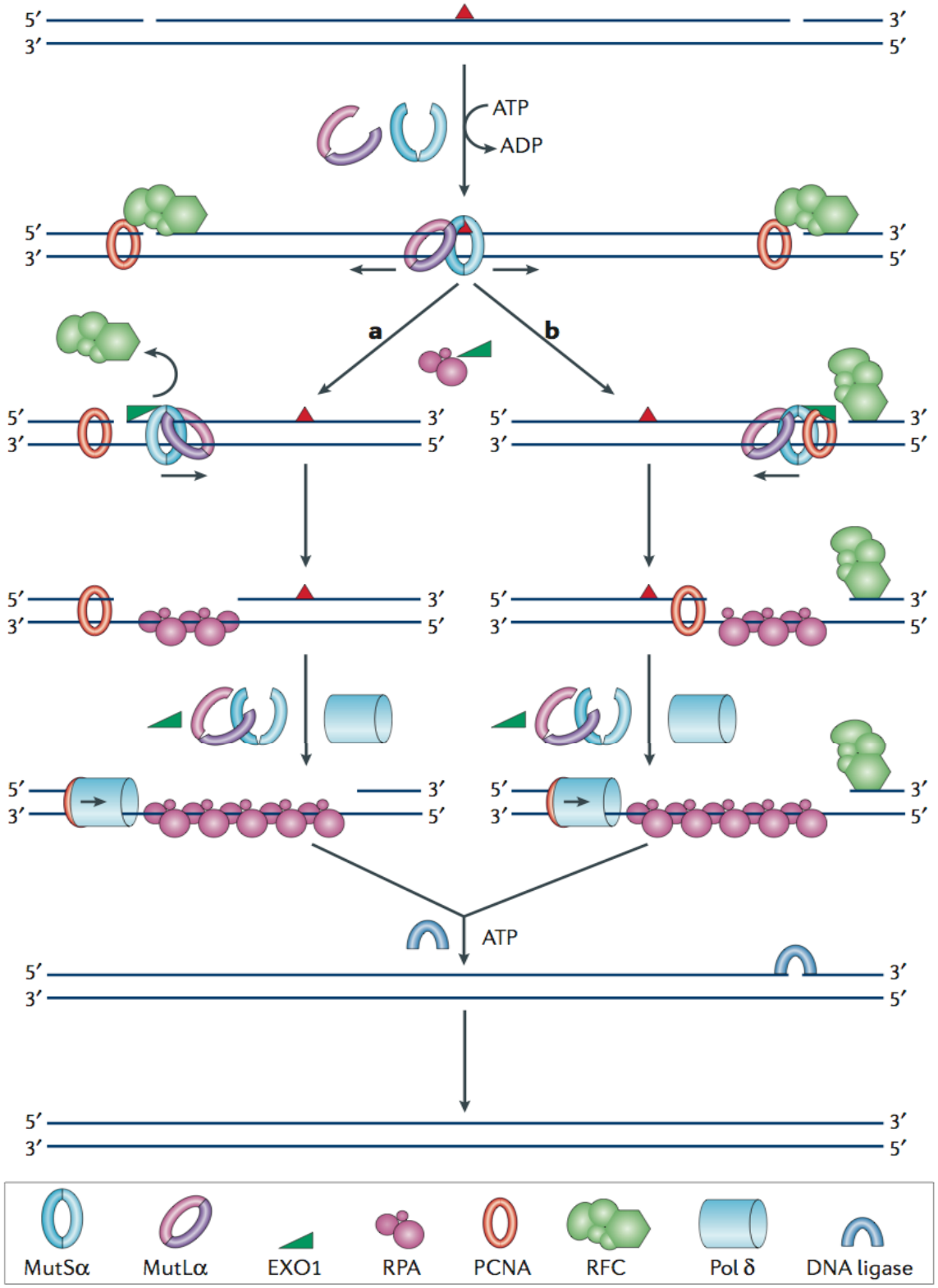

Figure 4.4 — **Schematic representation of the Mismatch Repair pathway.** DNA damage is recognized by MutSα. MutLα is then recruited followed by the exonuclease EXO1 which degrades DNA to eliminate the mismatch. Gap is filled by the DNA polymerase δ bound to PCNA. The last step is the ligation by the DNA ligase I (Figure adapted from [16]).

4.2.3 Base Excision Repair (BER)

BER is required to correct lesions caused by oxidative, alkylation, deamination, depurination or depyrimidation damages. These lesions cause base modifications that can induce the incorporation of an incorrect base by DNA polymerase during replication causing mutations. The first step in BER consists of lesion recognition by a DNA glycosylase, which removes the damaged base by cleaving the N-glycosidic bond and generating an apurinic/apyrimidic site (AP). This site is recognized and cut by the endonuclease APE1 which creates a single strand break (or a gap). After this step, two sub-pathways exist that carry on the repair ([20, 21, 22], Figure 4.5):

1. The short-patch BER: in this pathway, the DNA polymerase β fills the single nucleotide gap and removes the sugar moiety remaining after incision by APE1, the nick is sealed by the DNA ligase III and XRCC1 complex.

2. The long-patch BER: in this pathway, the gap is recognized by PCNA and DNA polymerase δ/ϵ which fill the gap by synthesizing multiple nucleotides (2-20 bases). The DNA flap is removed by the endonuclease FEN1 and the nick is sealed by the DNA ligase I. Additionally, when BER is initiated by a single strand breaks on DNA caused by irradiation or incomplete topoisomerase action, the lesion is recognized by PARP1.

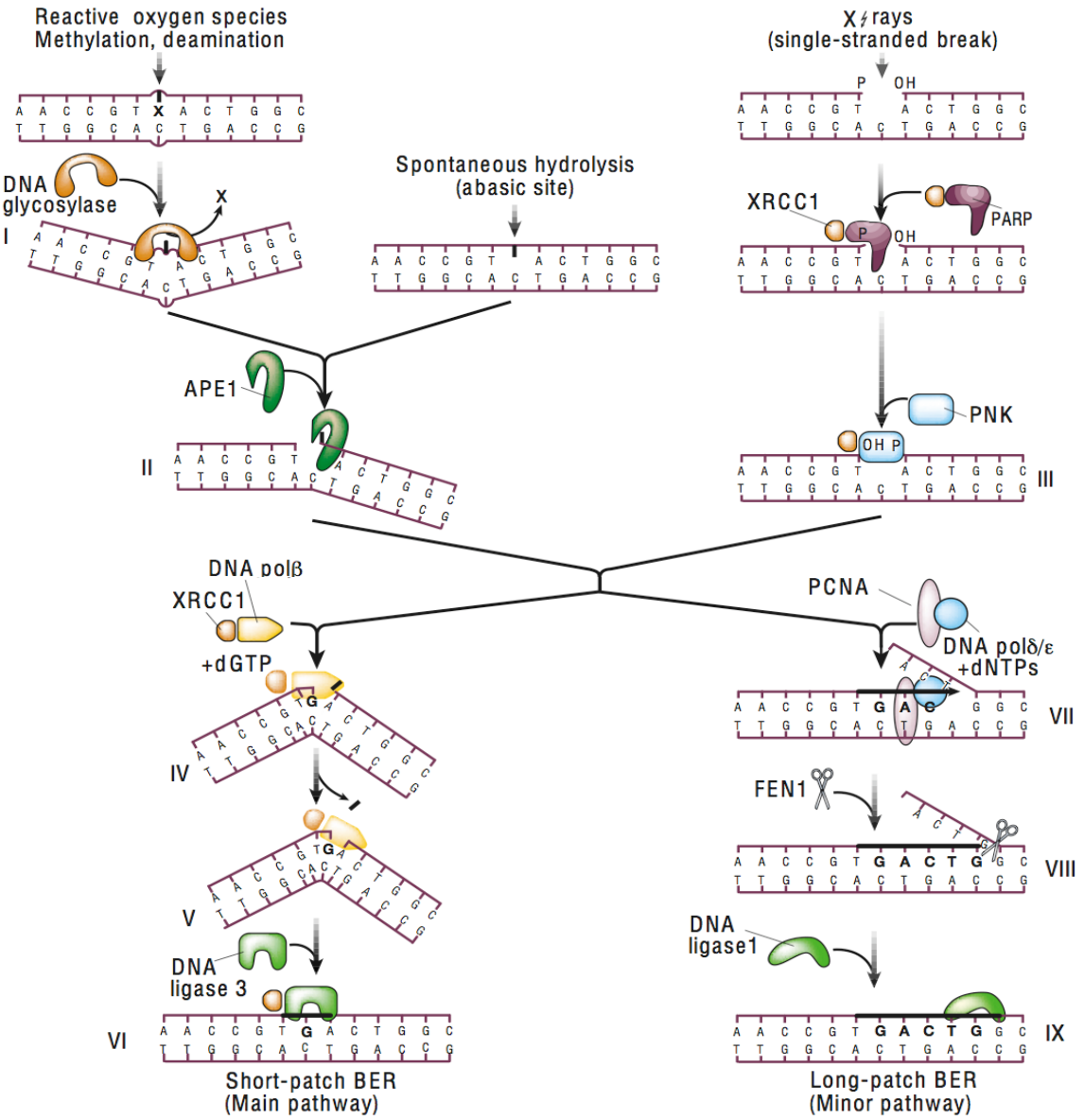

Figure 4.5 — **Schematic representation of the Base Excision Repair pathway.** In BER; damage is recognized by DNA glycosylase and APE1 in the case of base modifications and by XRCC1, PARP and PNK when the damage is a single strand break. Thereafter, there are two pathways: the Short-patch BER (at the left) that requires DNA pol β XRCC1 and DNA ligase 3 to perform a one-nucleotide gap-filling reaction. Or the Long-patch BER (at the right) involving by PCNA, DNA pol δ/ϵ FEN1 and the DNA ligase I to fill the gap with multiple nucleotides (2-20 bases) (Figure adapted from [1]).

4.2.4 Nucleotide Excision Repair (NER)

The NER pathway is specifically responsible for recognition and elimination of lesions that cause distortion to the DNA structure such as pyrimidine (6-4) pyrimidone Photo-Products (6-4PPs) and cyclobutane pyrimidine dimers (CPDs) [23]. NER is divided in two sub-pathways depending on the localization of the damage and the damage detection step ([24, 25], Figure 4.6):

- Global genome repair (GGR) pathway repairs damages located on untranscribed region of active genes or unexpressed regions of the genome. In this pathway, the lesion is detected by the binding of XPC-HRad23-centrin2 complex.
- Transcription coupled repair (TCR) pathway repairs lesions located in an active transcribed region. In this case, lesion detection is initiated by the stalling of the RNA polymerase II elongation complex. Two TCR-specific factors: CSB and CSA participate in coordinating the pre-incision and the post-incision reactions.

After the recognition step, TCR and GGR funnel into a common mechanismin which TFIIH complex is recruited to the lesion site. TFIIH is a basal transcription factor that is able to open up a region of approximately 20 nucleotides around the lesion thanks to the helicase activities of its two subunits XPB and XPD. Subsequently, XPA and RPA are recruited to the site of damage to stabilize the open intermediates and protect the single strand DNA. Then, the two nucleases XPG and XPF (associated to ERCC1) excise the damaged strand respectively in 3′ and 5′.

At the end, the gap is filled by DNA polymerase δ/ϵ and the remaining nick is sealed by the DNA ligase I or the DNA ligase III [26].

Defect in NER pathways is manifested by rare autosomal recessive human disorders all charachterized by sun sensitivity such as Xeroderma pigmentosum (XP), trichothiodystrophy (TTD) and Cockayne syndrome (CS). While XP patients have more than 1000-fold increase in susceptibility to skin cancer; TTD and CS patients have normal skin cancer risk [27].

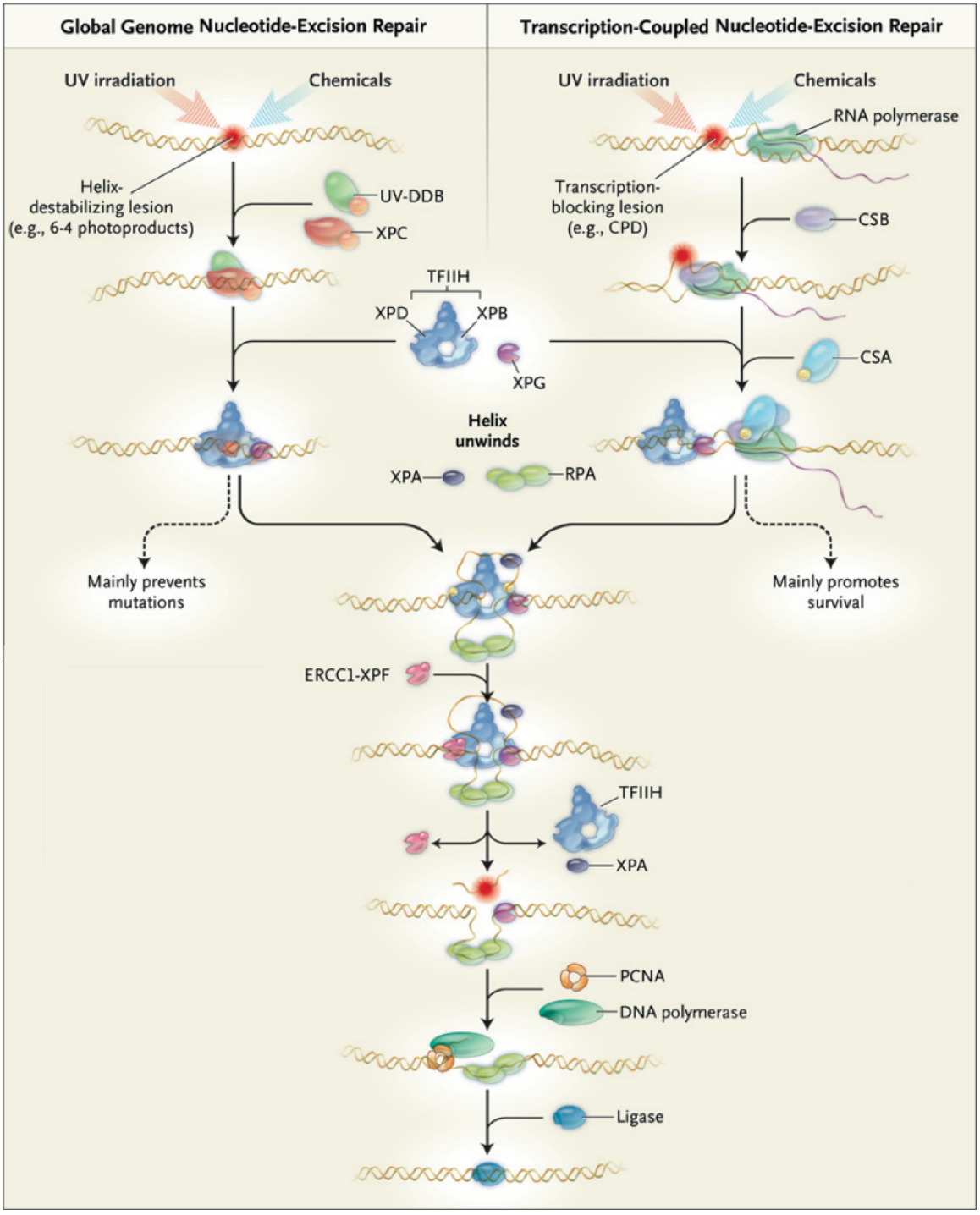

***Figure 4.6* — Schematic representation of the Nucleotide Excision Repair pathway.** Helix distorting lesions are detected by XPC-HR23B complex in Global Genome Repair (GGR) or by RNA pol II elongation complex blocked at the damage in Transcription Coupled Repair (TCR). After DNA damage recognition, TFIIH complex is recruited to open the helix of DNA. The endonucleases XPG and XPF/ERCC1 excise the damaged strand. Finally, the replication machinery performs gap-filling DNA synthesis and the nick is sealed (Figure adapted from [28])

4.2.4.1 Xeroderma pigmentosum (XP)

Mutations in either one of the seven different genes encoding for XPA to XPG cause Xeroderma pigmentosum (XP). XP patients present burns or freckles-like pigmentation on skin regions exposed to the sun. They develop skin cancer at a mean age of less than 10 years old [29, 30] (29). In addition to skin abnormalities, about 30% of XP patients exhibit progressive neurological degeneration characterized by symptoms that include microcephaly, ataxia, mental retardation, reduced tendon reflexes, hearing loss, deafness and swallowing difficulties, etc. [31]

4.2.4.2 Trichothiodystrophy (TTD)

TTD patients are characterized by sulfur-deficient brittle hair and ichthyosis. Clinical features of this syndrome vary between patients from mild cases, with only hair problems to severe cases presenting growth retardation, microcephaly, intellectual impairement, skeletal abnormalities and decreased fertility. Although some TTD patients show photosensitivity, they do not have cutaneous lesions and skin cancer predisposition [27].

4.2.4.3 Cockayne Syndrome (CS)

Mutations in CSA or CSB genes, disrupting TCR pathway, give rise to the severe Cockayne Syndrome. CS patients appear normal at birth and then suffer from severe neurological problems like neurodemyelinnation, mental retardation, and hearing loss. In addition, they present developmental pathologies like growth failure, microcephaly. Unlike XP and TTD patients, they show immature sexual development. They are sun sensitive but do not have the pigmentary changes or increased skin cancer frequencies seen in XP. The average life span of CS patients is 12,5 years and the main causes of death are pneumonia and respiratory infections which could well be due to the generally poor condition of the patients [27, 32].

A mouse model for CS-B was generated by mimicking a mutation found in a CSB patient (CS1AN mutation: Lys337 stop), resulting in a truncated form of the protein [33]. This modification of the CSB gene is analogous to the mutation found in CS1AN CSB-deficient human fibroblasts. $CSB^{-/-}$ mice show similar repair features as CS patients.

The Cockayne Syndrome B (CS-B) gene encodes for a 168 kDa protein and is a mem-

ber of the SWI/SNF family of putative helicases [34]. This family of proteins is involved in transcription, chromatin remodeling, DNA repair and translesion synthesis processes. CSB protein contains an Snf2-like helicase domain, an acidic stretch (aa 356-394), a glycin-rich region (aa442-446) and a nuclear localization signal (aa446-481). In addition, two putative casein kinase II phosphorylation sites are found close to the NLS motif [34]. CSB displays DNA-dependant ATPase and DNA binding activities, but not a helicase activity [35]. Besides its role in TC-NER, CSB is implicated in RNA Polymerases I, II and III transcription. It can act as a chromatin remodeling factor and can interact with core histones, inducing negative supercoiling [35]. CSB cells have been shown to be sensitive to genotoxic agents such as IR and Paraquat that give rise to oxidative damage suggesting a role for CSB in the removal of this kind of lesions [36]. Taken together, CSB represents a versatile protein with many different functions involved in a diversity of distinct and overlapping processes.

Bibliography

[1] J. H. Hoeijmakers. Genome maintenance mechanisms for preventing cancer. *Nature*, 411(6835):366–74, 2001.

[2] T. Lindahl and R. D. Wood. Quality control by DNA repair. *Science*, 286(5446):1897–905, 1999.

[3] A. J. Hartlerode and R. Scully. Mechanisms of double-strand break repair in somatic mammalian cells. *Biochem J*, 423(2):157–68, 2009.

[4] M. R. Lieber. The mechanism of double-strand DNA break repair by the NonHomologous DNA End-Joining pathway. *Annu Rev Biochem*, 79:181–211, 2010.

[5] F. Delacote and B. S. Lopez. Importance of the cell cycle phase for the choice of the appropriate DSB repair pathway, for genome stability maintenance: the trans-S double-strand break repair model. *Cell Cycle*, 7(1):33–8, 2008.

[6] P. O. Mari, B. I. Florea, S. P. Persengiev, N. S. Verkaik, H. T. Bruggenwirth, M. Modesti, G. Giglia-Mari, K. Bezstarosti, J. A. Demmers, T. M. Luider, A. B. Houtsmuller, and D. C. van Gent. Dynamic assembly of end-joining complexes requires interaction between Ku70/80 and XRCC4. *Proc Natl Acad Sci U S A*, 103(49):18597–602, 2006.

[7] C. Poinsignon, R. de Chasseval, S. Soubeyrand, D. Moshous, A. Fischer, R. J. Hache, and J. P. de Villartay. Phosphorylation of Artemis following irradiation-induced DNA damage. *Eur J Immunol*, 34(11):3146–55, 2004.

[8] A. A. Goodarzi, Y. Yu, E. Riballo, P. Douglas, S. A. Walker, R. Ye, C. Harer, C. Marchetti, N. Morrice, P. A. Jeggo, and S. P. Lees-Miller. DNA-PK autophosphorylation facilitates Artemis endonuclease activity. *Embo J*, 25(16):3880–9, 2006.

[9] P. Ahnesorg, P. Smith, and S. P. Jackson. XLF interacts with the XRCC4-DNA ligase IV complex to promote DNA NonHomologous End-Joining. *Cell*, 124(2):301–13, 2006.

[10] D. Buck, L. Malivert, R. de Chasseval, A. Barraud, M. C. Fondaneche, O. Sanal, A. Plebani, J. L. Stephan, M. Hufnagel, F. le Deist, A. Fischer, A. Durandy, J. P. de Villartay, and P. Revy. Cernunnos, a novel NonHomologous End-Joining factor, is mutated in human immunodeficiency with microcephaly. *Cell*, 124(2):287–99, 2006.

[11] E. Mladenov and G. Iliakis. Induction and repair of DNA double strand breaks: The increasing spectrum of non-homologous end joining pathways. *Mutat Res*, 2011. Journal article.

[12] N. Saleh-Gohari and T. Helleday. Conservative homologous recombination preferentially repairs DNA double-strand breaks in the S phase of the cell cycle in human cells. *Nucleic Acids Res*, 32(12):3683–8, 2004.

[13] C. T. Carson, R. A. Schwartz, T. H. Stracker, C. E. Lilley, D. V. Lee, and M. D. Weitzman. The MRE11 complex is required for ATM activation and the G2/M checkpoint. *Embo J*, 22(24):6610–20, 2003.

[14] C. Wyman and R. Kanaar. DNA double-strand break repair: all's well that ends well. *Annu Rev Genet*, 40:363–83, 2006.

[15] D. D'Amours and S. P. Jackson. The MRE11 complex: at the crossroads of dna repair and checkpoint signalling. *Nat Rev Mol Cell Biol*, 3(5):317–27, 2002.

[16] J. Jiricny. The multifaceted mismatch-repair system. *Nat Rev Mol Cell Biol*, 7(5):335–46, 2006.

[17] J. A. Downs, M. C. Nussenzweig, and A. Nussenzweig. Chromatin dynamics and the preservation of genetic information. *Nature*, 447(7147):951–8, 2007.

[18] S. Acharya, T. Wilson, S. Gradia, M. F. Kane, S. Guerrette, G. T. Marsischky, R. Kolodner, and R. Fishel. hMSH2 forms specific mispair-binding complexes with hMSH3 and hMSH6. *Proc Natl Acad Sci U S A*, 93(24):13629–34, 1996.

[19] F. Palombo, I. Iaccarino, E. Nakajima, M. Ikejima, T. Shimada, and J. Jiricny. hMutSbeta, a heterodimer of hMSH2 and hMSH3, binds to insertion/deletion loops in DNA. *Curr Biol*, 6(9):1181–4, 1996.

[20] K. H. Almeida and R. W. Sobol. A unified view of base excision repair: lesion-dependent protein complexes regulated by post-translational modification. *DNA Repair (Amst)*, 6(6):695–711, 2007.

[21] P. Fortini and E. Dogliotti. Base damage and single-strand break repair: mechanisms and functional significance of short- and long-patch repair subpathways. *DNA Repair (Amst)*, 6(4):398–409, 2007.

[22] A. B. Robertson, A. Klungland, T. Rognes, and I. Leiros. DNA repair in mammalian cells: Base excision repair: the long and short of it. *Cell Mol Life Sci*, 66(6):981–93, 2009.

[23] T. Nouspikel. DNA repair in mammalian cells : Nucleotide excision repair: variations on versatility. *Cell Mol Life Sci*, 66(6):994–1009, 2009.

[24] M. Fousteri and L. H. Mullenders. Transcription-coupled nucleotide excision repair in mammalian cells: molecular mechanisms and biological effects. *Cell Res*, 18(1):73–84, 2008.

[25] V. Mocquet, J. P. Laine, T. Riedl, Z. Yajin, M. Y. Lee, and J. M. Egly. Sequential recruitment of the repair factors during NER: the role of XPG in initiating the resynthesis step. *Embo J*, 27(1):155–67, 2008.

[26] J. Moser, H. Kool, I. Giakzidis, K. Caldecott, L. H. Mullenders, and M. I. Fousteri. Sealing of chromosomal DNA nicks during nucleotide excision repair requires XRCC1 and DNA ligase III α in a cell-cycle-specific manner. *Mol Cell*, 27(2):311–23, 2007.

[27] J. de Boer and J. H. Hoeijmakers. Nucleotide excision repair and human syndromes. *Carcinogenesis*, 21(3):453–60, 2000.

[28] J. H. Hoeijmakers. DNA damage, aging, and cancer. *N Engl J Med*, 361(15):1475–85, 2009. Journal Article Review United States.

[29] K. H. Kraemer. Sunlight and skin cancer: another link revealed. *Proc Natl Acad Sci U S A*, 94(1):11–4, 1997.

[30] K. H. Kraemer, M. M. Lee, and J. Scotto. DNA repair protects against cutaneous and internal neoplasia: evidence from Xeroderma Pigmentosum. *Carcinogenesis*, 5(4):511–4, 1984.

[31] J. H. Robbins, R. A. Brumback, M. Mendiones, S. F. Barrett, J. R. Carl, S. Cho, M. B. Denckla, M. B. Ganges, L. H. Gerber, R. A. Guthrie, and et al. Neurological disease in Xeroderma Pigmentosum. Documentation of a late onset type of the juvenile onset form. *Brain*, 114 (Pt 3):1335–61, 1991.

[32] M. A. Nance and S. A. Berry. Cockayne Syndrome: review of 140 cases. *Am J Med Genet*, 42(1):68–84, 1992.

[33] G. T. van der Horst, H. van Steeg, R. J. Berg, A. J. van Gool, J. de Wit, G. Weeda, H. Morreau, R. B. Beems, C. F. van Kreijl, F. R. de Gruijl, D. Bootsma, and J. H. Hoeijmakers. Defective transcription-coupled repair in Cockayne Syndrome B mice is associated with skin cancer predisposition. *Cell*, 89(3):425–35, 1997.

[34] C. Troelstra, A. van Gool, J. de Wit, W. Vermeulen, D. Bootsma, and J. H. Hoeijmakers. ERCC6, a member of a subfamily of putative helicases, is involved in Cockayne's Syndrome and preferential repair of active genes. *Cell*, 71(6):939–53, 1992.

[35] E. Citterio, V. Van Den Boom, G. Schnitzler, R. Kanaar, E. Bonte, R. E. Kingston, J. H. Hoeijmakers, and W. Vermeulen. ATP-dependent chromatin remodeling by the Cockayne Syndrome B DNA repair-transcription-coupling factor. *Mol Cell Biol*, 20(20):7643–53, 2000.

[36] C. L. Licht, T. Stevnsner, and V. A. Bohr. Cockayne Syndrome group B cellular and biochemical functions. *Am J Hum Genet*, 73(6):1217–39, 2003.

Working Context

In 1999 Huda Zoghbi's group identified different mutations in the Mecp2 gene as the origin of Rett syndrome. To understand this pathology, it was essential to identify and characterize the function of the protein. Early studies revealed that MeCP2 is a transcriptional repressor due to its capacity to bind to CpG methylated DNA and to compact the chromatin, thus preventing recruitment of the transcription machinery. These results suggest that pathologies associated with *mecp2* mutations are due to the misregulation of neuronal genes. That's why different groups tried to identify MeCP2 target genes.

In the laboratory, the group was interested to explore the hypothesis that genes encoding for the Major Histocompatibilty Complex class I molecules (MHC I) are regulated by MeCP2 in the central nervous system (CNS). This hypothesis stemmed from the report by the group of Carla Shatz that MHC I molecules are important for the activity-dependant synaptic rearrangements that occur during normal brain development [1]. Furthermore, these genes have a particularly high GC content and they are expressed during the post-natal development and are repressed in adult brain except in response to cytokines or injuries. For all these reasons, it was tempting to think that *mecp2* mutations could induce misregulations of CMH I genes that would provoke abnormal neuronal connection in the brain giving rise to neurodevelopmental disorders of RTT [2, 1, 3].

Although initial results showed that overexpression of either of the two isoforms of MeCP2 by transient transfection of neuronal and fibroblastic cell lines resulted in reduced levels of MHC class I and β2-microglobulin at the cell surface, the same results were obtained after overexpression of mutated MeCP2 proteins, carrying mutations in the MBD domain (R133C and T158M) and in the TRD domain (R306C and the truncated form R308X). These mutations, however, do not affect the capacity of MeCP2 to condense chromatin by binding to linker DNA and bringing nucleosome together in a "stem" conformation through DNA-protein interactions. A possible interpretation of these results was thus that effects of MeCP2 on MHC class I are independent from the methylation status of the genes' promoters but could involve conformational changes in chromatin preventing the access of transcriptional machinery. These data suggest also that repression of MHC class I expression by the over-expression of MeCP2 in cells cultured in vitro is not relevant for the pathogenesis of RTT, at least for the mutations tested in this study (Cf Appendix).

During this work, Julie Miralvès used fluorescence microscopy to verify the localization of MeCP2 in murine neuroblastoma (N2A) cells overexpressing the wild-type and the mu-

tated forms of the protein. After immunofluorescence staining against MeCP2, she noticed that very bright cells (expressing a high level of MeCP2) were surrounded by cells expressing a lower level of MeCP2, with this level decreasing progressively with the distance from the brightest cell. This observation suggested that, either expression of MeCP2 in transfected cell resulted in the activation of endogenous gene in neighbouring cells or MeCP2 protein was able to transfer from the transfected cell to the adjacent ones, similarly to what has been previously described for the homeoproteins [4].

To discriminate between these two mechanisms, she tagged the human MeCP2 protein by a myc epitope recognized by the 9E10 monoclonal antibody. These constructs were transfected in N2A cells. She then labelled transfected cells with CMTMR and co-cultivated them with unlabelled and untransfected N2A cells. After immunostaining experiments against myc epitope, she noticed that nuclei of untransfected cells inherited myc-tagged MeCP2 from neighbouring cells expressing a high level of MeCP2 and this could be detected as early as 1h after co-culture. These results suggested that MeCP2 could have the capacity to transfer from cell to cell. She noticed also that mouse fibroblastic cell lines (such as MC57 and L cells) failed to transmit MeCP2 to adjacent neighbouring cells.

Preliminary experiments allowed the goup to suggest that MeCP2 can have the capacity to transfer between the nucleus of adjacent cells and this phenomenon is specific to neuronal cells.

Initially, the main direction of my PhD project was to identify the mechanism responsible for this inter-neuronal transfer and to characterize the portion of the MeCP2 protein required for this function.

Before my arrival, all experiments were performed by immunostaining on fixed cell. To verify if this mechanism occurred in living cells, we tagged MeCP2 with GFP but we were unable to detect the intercellular transfer. The problem can arise from the size of the GFP which can block the mechanism of transfer. To overcome this problem, we decided to use the split GFP complementation system: when separated these two parts of the GFP are not fluorescent but when together, they can assemble spontaneously to regenerate a fluorescent protein. We thus tagged MeCP2 with GFP11, the small peptide of 15 amino acids corresponding to the β-strand 11 of the GFP. This construct was stably expressed in "donor" cells, and the other part of the GFP (GFP1-10) was stably expressed in "receiver" cells, co-culture experiments did not reveal any increase in fluorescence, which led us to

suspect that there may not be a transfer of MeCP2 between living cells.

Although we did not have a positive control in our experiments, such as a GFP11-tagged homeoprotein (like Engrailed-1 or 2) which is a nuclear protein like MeCP2 that has been characterised as having the capacity to pass from cell to cell, we have come to suspect that the inter-cellular transfer of MeCP2 we were seeing may be related to the protocol of acetone fixation which was being used. Indeed, when the cells were treated with formaldehyde before the acetone treatment, there was no longer any detectable transfer. We thus envisage that in cells expressing high levels of MeCP2, some molecules are not irreversibly fixed by the acetone treatment and can thus go back into in solution. Since these molecules have a strong affinity for chromatin, they would be recruited to the chromatin of neighbouring nuclei, but their transfer would have taken place after fixation, and not between living cells.

Working with split GFP, we also developed a new application for this system, whereby recombinant GFP1-10 is used as a staining reagent. This enables us to detect GFP11-tagged proteins by microscopy and flow cytometry in the mammalian cells via a one-step assay which allows detection of protein with high specificity and with very low background of fluorescence in comparison with antibodies.

Bibliography

[1] G. S. Huh, L. M. Boulanger, H. Du, P. A. Riquelme, T. M. Brotz, and C. J. Shatz. Functional requirement for class I MHC in CNS development and plasticity. *Science*, 290(5499):2155–9, 2000.

[2] R. A. Corriveau, G. S. Huh, and C. J. Shatz. Regulation of class I MHC gene expression in the developing and mature CNS by neural activity. *Neuron*, 21(3):505–20, 1998.

[3] H. Neumann, A. Cavalie, D. E. Jenne, and H. Wekerle. Induction of MHC class I genes in neurons. *Science*, 269(5223):549–52, 1995.

[4] A. Prochiantz and A. Joliot. Can transcription factors function as cell-cell signalling molecules? *Nat Rev Mol Cell Biol*, 4(10):814–9, 2003.

Studying the MeCP2 protein:
Exploring its involvement in the DNA Damage Response, and developing new tools for its detection.

Results

5 One-step split GFP staining for sensitive protein detection and localization in mammalian cells

Lara *Kaddoum*[1,3], Eddy *Magdeleine*[1,3], Geoffrey S. *Waldo*[4], Etienne *Joly*[1,3], and Stéphanie *Cabantous*[2,3]

[1]CNRS, Institute of Pharmacology and Structural Biology (IPBS), Toulouse, France

[2]INSERM U563, Département Innovation Thérapeutique et Oncologie Moléculaire, Institut Claudius Régaud, Université Paul Sabatier, Toulouse, France

[3]Université Paul Sabatier, IPBS, Toulouse, France

[4]Bioscience Division, MS-M888, Los Alamos National Laboratory, Los Alamos, NM, USA

Adapted from **BioTechniques, Vol. 49, No. 4, October 2010, pp. 727-73**

5.1 Abstract

Although epitope tags are useful to detect intracellular proteins and follow their localization with antibodies, background and nonspecific staining often remain problematic. We describe a simple assay based on the split GFP complementation system. Proteins tagged with the 15-amino acid GFP 11 fragment are detected with a solution of the recombinant nonfluorescent complementary GFP 1-10 fragment to reconstitute a fluorescent GFP. In contrast to antibody-based staining methods, this one-step assay presents high specificity and very low background of fluorescence, thus conferring higher signal-to-noise ratios. We demonstrate that this new application of the split GFP tagging system facilitates detection of proteins displaying various subcellular localizations using flow cytometry and microscopy analysis.

5.2 Introduction

Understanding protein dynamics in living cells requires sensitive and quantitative tools for measuring spatiotemporal modifications of protein expression and/or localization. Fusion to green fluorescent protein (GFP) or its derivatives enables direct visualization of intracellular proteins without the need for secondary reagents or treatment of the cell [1]. However, the large size of GFP may alter protein localization and behavior [2], and the permanent fluorescence of the reporter can be a hindrance to detect other markers. To detect native intracellular proteins, monoclonal or polyclonal antibodies are sometimes available, but they need to recognize an epitope conserved after fixation. Alternatively, various epitope tags (myc, His, HA, Flag) have been developed to specifically detect or isolate proteins in cells [3]. Detection of such tags either involves specific monoclonal antibodies directly linked to a fluorochrome or successive steps of unlabeled antibody and fluorochrome-conjugated secondary reagents [4]. Such protocols are often time-consuming, as they require several washing steps to remove all unbound reagents between binding reactions. Moreover, low signal-to-noise ratios are often observed, due to the presence of nonspecifically bound antibodies, especially for polyclonal antibodies, or due to endogenous expression of the epitope in the parent cell [5].

As a possible alternative, we have investigated whether we could use the split GFP tagging system for the intracellular detection of proteins [6], which is based on the auto-

assembly capacity of two nonfluorescent portions of GFP-GFP 1-10 and GFP 11-to restore a fully fluorescent GFP. The GFP 11 tag, which is only 15 amino acids long, is fused to the N or C terminus of the coding sequence of the protein of interest and can then be expressed in eukaryotic cells. The GFP 1-10 detector fragment is produced separately in Escherichia coli and purified from inclusion bodies as previously described [7]. After fixation and permeabilization of cells expressing the GFP 11-tagged protein, the refolded GFP 1-10 protein is added in trans, allowing the two split GFP fragments to associate spontaneously and restore the GFP fluorescence (Figure 5.1A). Here, we describe the application of the split GFP protein complementation assay for detecting GFP 11-tagged proteins in mammalian cells relative to antibody staining using FACS and microscopy analysis.

5.3 Materials and methods

5.3.1 Plasmids

pcDNA 3.1 vector expressing human MeCP2e1-Myc-His was provided by Dr. Berge A. Minassian of the Hospital for Sick Children, Toronto, Ontario, Canada [8]. For FK506 binding protein 12 and MeCP2e1, the respective coding sequences were inserted at the N terminus of GFP 11, in a vector derived from pEGFP_N3 (Clontech Laboratories, Saint-Germain-en-Laye, France) (see sequence of the mammalian GFP 11 cassette below). To generate GFP 11-H-Ras, full-length GFP was replaced by the 15-amino acid mammalian GFP 11 peptide (GFP11m) in the pEGFP-H-Ras plasmid kindly provided by J. Lippincot-Schwartz [9].

5.3.2 DNA sequence of the GFP11m vector cassette

5.3.2.1 GFP11m N-terminal fusion

5'ATGGGCCGGGACCACATGGTGCTGCACGAGTACGTGAACGCCGCCGGCAT
CACAGACGGCGGCAGCGGCGGCGGCAGC-3'.

5.3.2.2 GFP11m C-terminal fusion

5'GGCGACGGCGGCAGCGGCGGCGGCAGCCGGGACCACATGGTGCTGCACGA
GTACGTGAACGCCGCCGGCATCACATAA-3'.

5.3.2.3 Recombinant GFP 1-10

Expression of GFP 1-10 detection reagent was performed in E. *coli* BL21 (DE3). Recombinant protein was purified from inclusion bodies as described previously [7]. For each set of assays, 37.5 mg purified inclusion bodies were used to prepare 15 mL GFP 1-10 solution (2.5 mg/mL) in 50 mM Tris, pH 7.4, 0.1 M NaCl, 10% glycerol (TNG).

5.3.3 Cell culture

Neuro2A (N2A) cells were maintained in DMEM supplemented with 10% FCS, 100 U/mL penicillin, 100 μg/mL streptomycin, 10 mM HEPES, 0.1 mM nonessential amino acids, and 1 mM sodium pyruvate. Human embryonic kidney (HEK) 293 cells were grown in RPMI-1640 medium supplemented with 10% FCS, 100 U/mL penicillin, 100 μg/mL streptomycin, and 2 mM L-glutamine.

5.3.4 Transfection

Transfections were carried out using JetPEI (Polyplus Transfection, Illkirch, France) following the manufacturer's instructions. Depending on the resistance gene carried by the plasmid vector, stable clones were selected with either 500 μg /mL G418 (Invitrogen, Cergy Pontoise, France) or 125 μg/mL Zeocin (InvivoGen, Toulouse, France) and thereafter maintained at these concentrations. Monoclonal cell lines were obtained by single cell dilution in 96-well plates. Cells used as negative control were untransfected, and were thereby not cultured in the presence of selecting drugs.

5.3.5 Antibodies

5.3.5.1 Primary antibodies

Rabbit polyclonal anti-MeCP2 antibody (crude serum) was generated after immunization of a rabbit with a synthetic peptide corresponding to amino acids 465-478 of mouse MeCP2 (C-PRPNREEPVDSRTP; performed by Millegen, Labège, France). Mouse anti-Myc IgG1 antibody was purified with protein A beads (Pierce, Thermo Scientific, Brebières, France) from clone 9E10 hybridoma supernatants (purchased from ATCC, Manassas, VA, USA). Rat monoclonal anti-H-Ras antibody was purchased from Santa Cruz Biotechnology

(Cat. no. sc-35; Santa Cruz, CA, USA).

5.3.5.2 Secondary antibodies

Alexa Fluor 488-conjugated goat anti-rabbit, Alexa Fluor 647-conjugated goat anti-rabbit, rhodamine-conjugated goat anti-rabbit, Alexa Fluor 488-conjugated goat anti-mouse, Alexa Fluor 647-conjugated goat anti-rat, and rhodamine-conjugated goat anti-rat were obtained from Molecular Probes, Invitrogen.

5.3.6 Flow cytometry analysis

For each condition, 2×10^5 cells were trypsinized, washed three times with PBS, then fixed with 4% paraformaldehyde for 10 min at 4°C. After two washes with PBS, cells were permeabilized in 0.1% Triton-X 100 in PBS for 10 min at 4°C. Cells were then washed twice with 2% FCS PBS before incubation with the primary antibody (rabbit anti-MeCP2 serum, dilution 1/300, or mouse anti-Myc, dilution 1/300, home-purified solution at 4 mg/mL, or rat anti-H-Ras, dilution 1/200) for 45 min at 4°C (dilution in 2% FCS PBS). After three washes with 2% FCS PBS, cells were incubated with secondary antibody (dilution 1/200) for 30 min at 4°C. Cells were washed again three times with 2% FCS PBS buffer and then analyzed using a FACS Calibur cytometer and CellQuest software (BD Biosciences, Le Pont de Claix, France).

For GFP 1-10 detection, the recombinant protein solution was diluted to 0.15 mg/mL in 2% FCS PBS and directly added to the fixed/permeabilized cells. After incubation at room temperature (RT) for 3 h, fluorescence was analyzed using a FACScalibur flow cytometer. For double staining, cells were labeled with GFP 1-10 for 3 h at RT, washed twice with 2% FCS PBS buffer, and then incubated with the appropriate antibodies.

5.3.7 Immunofluorescence staining and microscopy

N2A cells (1×10^5 cells per well) or HEK 293 cells (1×10^5 cells per well) stably expressing MeCP2, FKBP, or H-Ras tagged with either GFP 11 or GFP were plated overnight on glass coverslips in 24-well plates. Cells were washed twice with PBS and fixed with 3.7% paraformaldehyde (PFA) in PBS for 30 min at RT. After two washes with PBS, cells were permeabilized in 0.3% Triton-X 100 for 10 min at RT. For GFP fusions, cells were washed

twice with 2% FCS PBS, and after a final wash with PBS, coverslips were mounted in 4',6'-diamidino-2-phenylindole (DAPI)-containing ProLong Gold antifading reagent (Molecular Probes, Invitrogen). For GFP 1-10 detection, GFP 11-expressing cells were incubated for 3 h at RT with GFP 1-10 protein solution diluted to 0.15 mg/mL in 2% FCS PBS. Cells were washed with PBS and mounted in DAPI-containing ProLong Gold antifading reagent. For double staining, cells were labeled with GFP 1-10, washed twice with 2% FCS PBS and then incubated with primary antibody (rabbit anti-MeCP2 diluted to 1/300 and rat anti-H-R as diluted to 1/200) for 1h at RT. After three washes with 2% FCS PBS, cells were incubated with secondary antibodies (anti-rabbit IgG, rhodamine, and anti-rat IgG, rhodamine, diluted to 1/400) for 1 h at RT. Cells were washed with PBS and mounted in DAPI-containing ProLong Gold antifading reagent. We used a DM-RB fluorescence microscope (Leica, Nanterre, France) with a 40× and 100× oil immersion objective to visualize the stained cells. Images were acquired with a CoolSNAP HQ camera (Photometrics, Roper Scientific, Evry, France) and analyzed with MetaMorph (Molecular Devices, Sunnyvale, CA, USA) or ImageJ (`http://rsbweb.nih.gov/ij`).

5.3.8 Microplate assay

Cells (5× 10^6) were trypsinized and washed three times with PBS. The cell pellet was flash-frozen in liquid nitrogen. The frozen pellet was resuspended in 40 μL extraction buffer (25% glycerol, 0.42 M NaCl, 1.5 mM MgCl2, 0.2 mM EDTA, 20 mM HEPES, pH 7.9, 0.5 mM DTT).In a 96-well fluorescence plate, 50 μL total cell extracts were serial diluted in 100 μL final volume of TNG buffer. These dilutions (50 μL) were mixed with 100 μL 0.3 mg/mL GFP 1-10 protein solution. The plate was incubated overnight at 4°C. Fluorescence was measured using a FLx800 Fluorescence Microplate Reader (BioTek, Colmar, France). For titration curves, starting concentrations of GFP 11 peptide (0.03 mg/mL) were used and diluted serially in 50 μL TNG buffer.

5.4 Results and discussion

5.4.1 Characterization of the GFP 1-10 staining assay for FACS

We initially developed this method for the detection of the nuclear methyl-CpG binding protein 2 (hMeCP2e1) in mammalian cells [8]. The results shown in Figures 5.1 and 5.2 were obtained with a monoclonal cell line that expresses homogenous levels of MeCP2-GFP 11, as detected with an anti-MeCP2 polyclonal antibody. Cells in suspension were fixed in 4% PFA, permeabilized with 0.1% Triton, and then incubated in a solution of 0.3 mg/mL GFP 1-10 protein at 4°, 20°, and 37°C. Fluorescence increase was followed by flow cytometry (FACS) at different time intervals for 24h. Kinetic plots demonstrated a first order reaction with temperature-dependent rates (Figure 5.1B). A slower kinetic of complementation was observed at 4°C, reaching a plateau after overnight incubation (Figure 5.1B and Figure 5.5). At 37°C, a faster reaction rate was observed, but final fluorescence value was considerably reduced, probably because of unfolding of the renatured GFP 1-10 protein. Our optimal condition was obtained at RT, in which maximum fluorescence was reached after 12h, similarly to what had been observed previously in *E. coli* [6]. Background fluorescence, determined by incubating nontransfected N2A cells with GFP 1-10 was very low, but increased slightly over time, and the best signal-to-noise ratios, in excess of 130, were thus attained after 3-4h of staining (Figure 5.5).

5.4.2 Sensitivity of the GFP 1-10 staining in microplate assay

To evaluate the sensitivity of the split GFP assay with eukaryotic cell extracts, we performed the complementation in 96-well plates. N2A cells (6×10^6) expressing MeCP2-GFP 11 were used to obtain a final volume of 100 μL total cell extract. Serial 2-fold dilutions of the sample were performed in 50 μL TNG buffer and then incubated with GFP 1-10 at 4°C. Fluorescence was measured on a microplate reader after overnight incubation. As a control, cell extract from N2A cells was also measured in the same dilution range and was substracted from the signal. As observed previously with bacterially produced proteins [7], sensitivity plots showed an excellent linear relationship between fluorescence and protein quantity (Figure 5.1C, left). To evaluate protein concentration of MeCP2-GFP 11, a standard titration curve was performed using GFP 11 peptide (Figure 5.1C, right). From this, we eval-

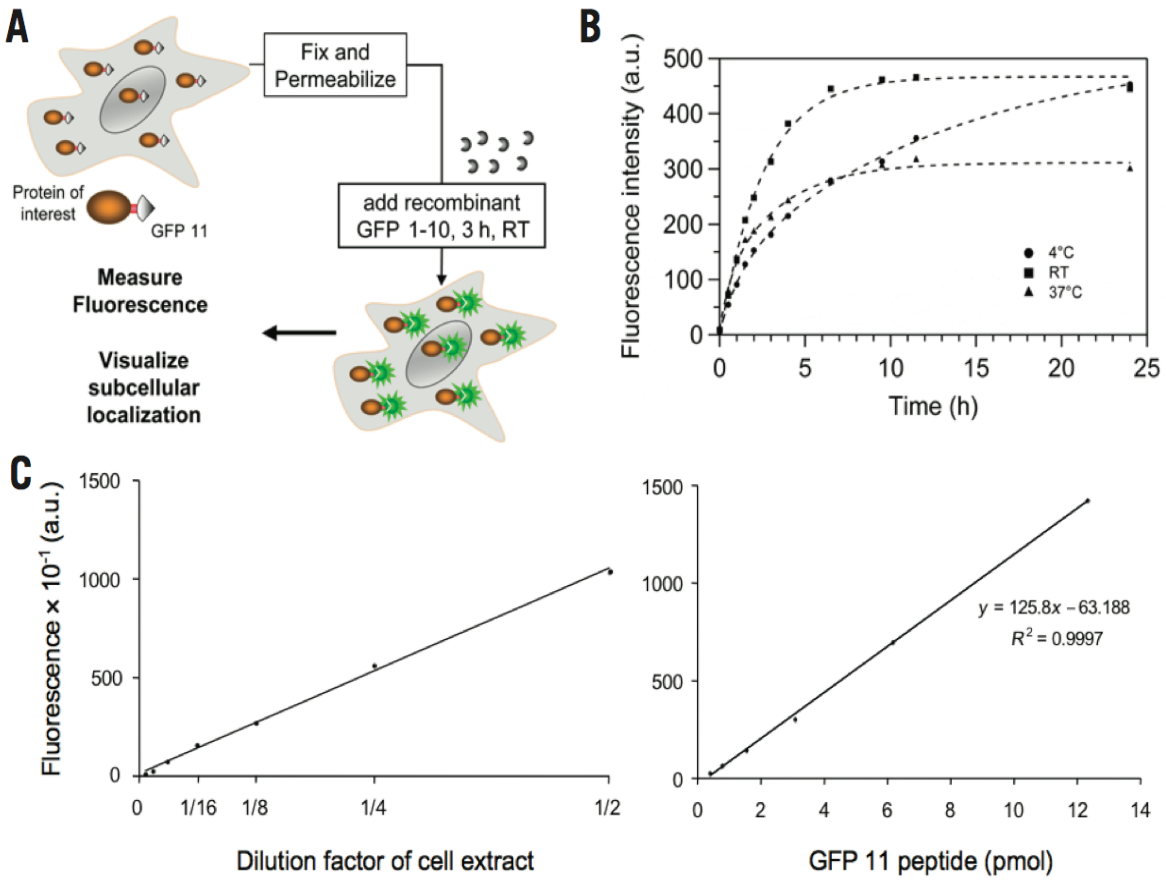

Figure 5.1 — **Characterization of the GFP 1-10 in vitro assay in mammalian cells.** (A) Cells expressing GFP 11-tagged protein are fixed and permeabilized. Reconstituted GFP 1-10 protein solution is added and incubated at RT for 3 h. Fluorescence is measured and compared with control cells. (B) Kinetic profiles of complementation reaction of N2A-MeCP2-GFP 11 cells incubated with GFP 1-10 at three temperatures: 4°C (•), 20°C (■), and 37°C (▲). FACS measurements of fluorescence intensity were performed at various time intervals. (C) Using the GFP 1-10 complementation assay to evaluate the amounts of protein in cell extracts. Cell extracts (left graph) and peptide dilutions (right graph) were complemented with recombinant GFP 1-10 in solution in a 96-well plate, and fluorescence was measured after an overnight incubation at 4°C. The quantity of GFP 11-tagged protein in cell extract dilutions was then deduced from a standard calibration curve with GFP 11 peptide solution (right graph). a.u., arbitrary units.

5

uated that this particular clone of N2A transfectants contained, on average, 1.5×10^6 copies of GFP 11-tagged MeCP2 protein of the same order of magnitude as levels reported in physiological conditions [10]. The limit of sensitivity of the plate-based assay was 0.5 pmol GFP 11 peptide, as previously observed with bacterially produced proteins [6], and this corresponded to a 1/100 dilution of the starting cellular extract (8 μg total protein) (Figure 5.1C). These results demonstrate that the linearity and the sensitivity of the assay are suited for monitoring protein expression in mammalian cells.

5.4.3 Comparison with MAb staining

Using FACS, we then compared the sensitivity of the split GFP detection system with antibody staining [5] (Figure 5.2A). We used another clone of N2A cells transfected with a vector coding for MeCP2 tagged with the myc-His double epitope, which expresses protein levels similarly to the MeCP2-GFP 11 clone, as detected by anti-MeCP2 antibody (Figure 5.2A, bottom row, middle panel). As expected with polyclonal antibodies, staining with the rabbit pre-immune serum gave some background compared with cells reacted solely with the secondary anti-rabbit antibody. Staining with immune anti-MeCP2 serum resulted in a higher signal than the pre-immune serum from the same rabbit, although undifferentiated N2A cells do not express detectable levels of endogenous MeCP2 protein ([11], and our own observations). Detection of the myc epitope using the 9E10 MAb (mouse anti-myc; ATCC) gave higher levels of staining than its isotype control on N2A control cells, presumably because of the binding of the antibody to the endogenous myc protein (Figure 5.2A, top left panel). Nevertheless, specific staining with anti-myc or anti-MeCP2 on N2A cells transfected with the MeCP2-myc-His vector resulted in 3- to 5-fold higher signal values relative to nontransfected N2A cells (Figure 5.2A). With the GFP 1-10 assay, no detectable difference was observed in fluorescence intensities between unstained and stained N2A control cells (Figure 5.2A, top right panel). In cells expressing MeCP2-GFP 11, fluorescence signal was clearly separated from the negative control, resulting in signal-to-noise ratios >60 (Figure 5.2B). Similar results were obtained after stable expression of the same constructs in HEK 293 cells (Figures 5.4 and 5.2B).

5.4.4 Validation of the GFP 1-10 staining assay for FACS measurements

To further document the versatility of this system, we fused the GFP 11 tag to the N terminus of the H-Ras oncogene protein [localized mostly at the plasma membrane [12]] and to the C terminus of the nucleocytosolic immunophilin FK506 binding protein 12 (FKBP) [13]. We established stable populations for these constructs in N2A and HEK cells and stained them using GFP 1-10 protein for FACS analysis. For both proteins tagged with GFP 11, although the levels of expression were considerably lower than for MeCP2, the very low levels of background fluorescence of GFP 1-10 on nontransfected cells resulted in well-separated peaks (Figure 5.2C). To verify that the split GFP method can be combined with antibody staining, we then performed double staining on N2A-MeCP2-GFP 11 and HEK 293-GFP

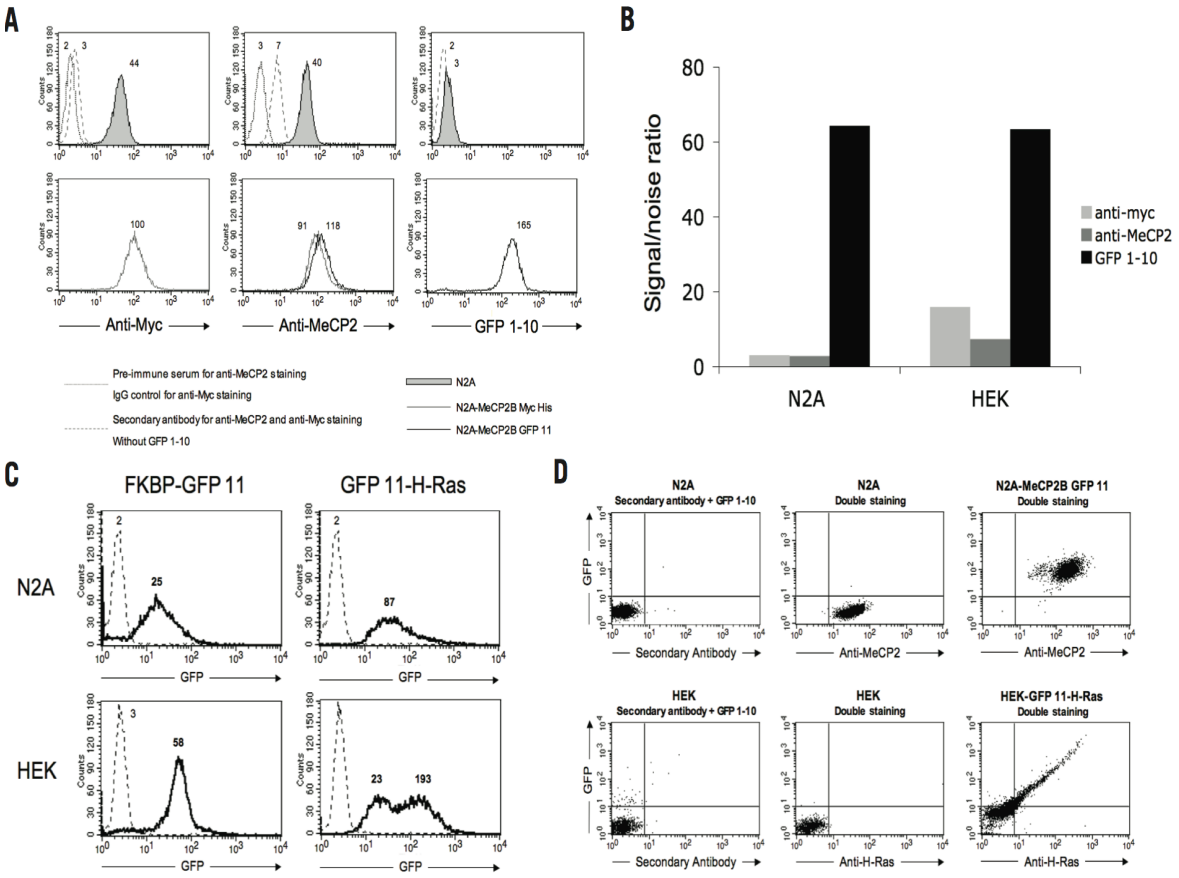

***Figure 5.2* — GFP 1-10 staining assay for FACS analysis.** (A) Comparison with MAb staining. FACS detection of MeCP2-myc-His and MeCP2-GFP 11 in N2A cells using anti-myc MAb (left), anti-MeCP2 polyclonal (middle), or recombinant GFP 1-10 (right). Negative controls are shown on the top row. Positive signals obtained from transfected N2A cells expressing MeCP2 are shown in the bottom row: MeCP2-myc-His (gray) or MeCP2-GFP 11 (black). (B) Signal-to-noise ratio for FACS detection of MeCP2 using staining with either anti-myc, anti-MeCP2 antibody, or recombinant GFP 1-10, in N2A and HEK cells. (C) FACS detection of FKBP-GFP 11 and GFP 11-H-Ras in N2A and HEK cells. Non-transfected N2A or HEK cells, dashed line; N2A or HEK cells expressing GFP 11-tagged proteins, black. (D) Double staining with antibodies (far red, FL4, x axis) and GFP1-10 (green, FL1, y axis). (Top row) N2A stably expressing MeCP2-GFP 11 or not. (Bottom row) HEK cells transiently transfected with GFP 11-H-Ras or not. Left panel, fluorescence of secondary antibodies on control cells; middle panel, anti-MeCP2 or anti-H-Ras signals on nontransfected control cells; right panel, double staining of transfectants.

11-H-Ras cells. The procedure involved a first step using the GFP 1-10 assay, followed by immunostaining using rhodamine-conjugated antibodies (see section 5.3). FACS analysis allowed the detection of both epitopes in the green (GFP) and red (anti-MeCP2 or anti-H-Ras) fluorescence (Figure 5.2D). Similar levels of detection were obtained for GFP 11 and MeCP2 (Figure 5.2D, top right graph), suggesting a good sensitivity of the split GFP method. Moreover, a clear correlation was observed between monoclonal anti-H-Ras Ab detection and GFP 1-10 staining for HEK cells transiently transfected with GFP 11-H-Ras, in which only

25% of the cell population expressed significant levels of the GFP 11-H-Ras protein (Figure 5.2D). We noticed that background on control cells with monoclonal anti-H-Ras antibody was very low (Figure 5.2D, middle panel). Even in these conditions, although the difference was less striking than for the anti-myc and anti-MeCP2 antibodies presented above, we found that GFP 1-10 staining of transiently transfected HEK cells still yielded better signal-to-noise ratios than antibody staining (50 versus 13) (Figure 5.6).

5.4.5 GFP 1-10 staining for microscopy

We next compared cellular localization of the three proteins tagged either with full-length GFP or with GFP 11 (Figure 5.3). In N2A cells stably expressing either MeCP2-GFP or MeCP2-GFP 11, fluorescence revealed a typical punctuated nuclear pattern seen in murine cells, due to the binding of MeCP2 to heterochromatin foci [14] (Figure 5.3A, top row). In HEK cells, heterochromatin is less condensed, and fluorescence was thus diffused throughout the nuclei [15] (Figure 5.3B, top row). The FKBP protein is generally distributed through the nucleus and the cytosol, but may be predominantly nuclear when it dimerizes [16]. In N2A and HEK cells, both FKBP-GFP and FKBP-GFP 11 fusions were found mostly localized in the perinuclear region (Figure 5.3, A and B, middle rows). Finally, both GFP-H-Ras and GFP 11-H-Ras fusions were found mostly associated with the plasma membrane. For GFP-H-Ras however, we noticed the presence of additional intracellular vesicular structures in both cell types [Figure 5.3, A and B (lower rows) and D]. This observation is reminiscent of previous reports showing that fusion of H-Ras to the whole GFP molecule resulted in its redistribution toward the ER and Golgi membrane, whereas unmodified H-Ras was found mostly at the plasma membrane [17]. Our results thereby suggest that the smaller size of the GFP 11 tag may alter the natural distribution of the tagged protein less than full-length GFP. To confirm that staining with split GFP is nonperturbing and correlates accurately with true protein localization, we performed double staining experiments, using specific antibodies against MeCP2 and H-Ras followed by rhodamine-coupled secondary antibody, for both GFP 11-tagged and GFP-tagged fusions of MeCP2 and H-Ras; this resulted in perfect co-localization of the red and green signals (Figure 5.3, C and D). Importantly, for both MeCP2 and H-Ras fusions, no background fluorescence was observed in the other channel when only one of the stainings was performed (Figures 5.7 and 5.8).

The split GFP detection system is particularly well-suited for protein tagging and detec-

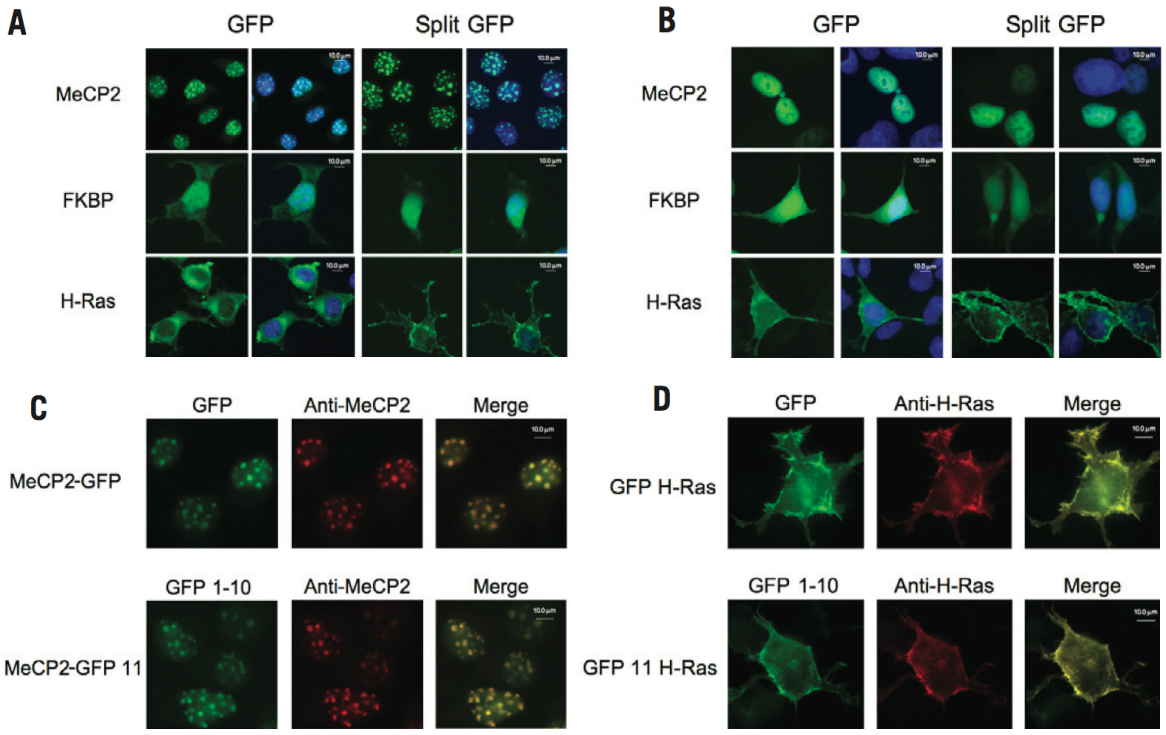

***Figure 5.3* — GFP 1-10 staining for studying protein localization by fluorescence microscopy.** Three proteins -MeCP2, FKBP, and H-Ras- were expressed in (A) N2A cells or (B) HEK 293 cells, as GFP fusions (left panels) or GFP 11 fusions (right panels). MeCP2-GFP 11, FKBP-GFP 11, and GFP 11-H-Ras were stained with recombinant GFP 1-10 reagent before mounting on microscope slides. Left image, green fluorescence at 488-nm excitation. Right image, overlay of green fluorescence and DAPI nuclear staining (blue). Scale bars, 10 μm. Double staining experiments are shown in panels C and D. Fluorescein isothiocyanate (FITC) emission channel at 530 nm with excitation at 488 nm (left), rhodamine emission channel detected at 590 nm with excitation at 545 nm (middle), superimposition of both images (right). (C) Anti-MeCP2 sera and GFP 1-10 staining were performed on N2A-MeCP2-GFP 11 cells and compared with N2A cells expressing MeCP2-GFP fusions. (D) Anti-H-Ras MAb and GFP 1-10 staining on HEK-GFP 11-H-Ras and GFP-H-Ras HEK cells.

tion in eukaryotic cells using multiple formats. Expression and localization can be simultaneously performed either in fixed models or in living cells with transient or stable expression of GFP 1-10 [18]. The main advantages over existing epitope tags [19, 20] are the high specificity and quantitative recognition between GFP 11 and GFP 1-10 fragments and the absence of fluorescence of the GFP 1-10 protein. This confers very low background signals and facilitates staining procedures, as it does not require extensive washing steps compared with classical immunostaining methods. The small size of the GFP 11 fragment (15 amino acids) should be less perturbing than the bulky GFP, and GFP 1-10 staining can be performed in combination with other immunostaining procedures as for GFP. The versatility of the system will be further enhanced by the possibilities of combining the split GFP method with chromatic variants of GFP, such as cyan and yellow 1-10. Engineering red autofluorescent

split proteins would expand the color repertoire of the split GFP system to perform simultaneous detections in vitro and ultimately in vivo, for example, in mice expressing the 1-10 fragment ubiquitously. Both possibilities are currently being pursued in our laboratories.

5.5 Acknowledgments

We are grateful to Evert Haanappel for his help with fitting kinetics curves, Christine Bordier for helping with fluorescence microscopy, and Denis Hudrisier and Jean Denis Pédelacq for helpful discussions. This work was supported by Association Française du Syndrome de Rett (AFSR) and Fondation pour la Recherche Medicale (FRM).

5.6 Competing interests

The split GFP and related intellectual properties are the subject of domestic and foreign patent applications by Los Alamos National Laboratories on behalf of the Department of Energy and LANS, L.L.C.

5.7 Correspondence

Address correspondence to Stéphanie Cabantous, INSERM U563, Département Innovation Thérapeutique et Oncologie Moléculaire, Institut Claudius Régaud, Université Paul Sabatier, 24 rue du Pont Saint-Pierre, 31052 Toulouse Cedex, France, e-mail: cabantous.stephanie@claudiusregaud.fr or Etienne Joly, CNRS, Institute of Pharmacology and Structural Biology (IPBS), 205 route de Narbonne, F-31077 Toulouse, France, e-mail: joly@ipbs.fr

Supplementary Materials For:

One-step split GFP staining for sensitive protein detection and localization in mammalian cells

Preparation of GFP 1-10 for in vitro assays

Bacterial cell culture

A solution of purified GFP 1-10 needs to be prepared to perform in vitro detection of GFP 11 fusion proteins. The engineered GFP 1-10 is 50% soluble, and the inclusion body fraction is processed to take advantage of the enrichment and partial purification afforded by using inclusion bodies. A 3-mL overnight culture is used to inoculate 500mL Luria-Bertani broth containing 35μg/mL kanamycin. GFP 1-10 expression is induced in the exponential phase (2h after inoculation) with 1 mM IPTG for 5h at 37°C (this forces the GFP 1-10 to aggregate into inclusion bodies). After centrifugation, cell culture pellets are resuspended in 15 mL 100 mM Tris-HCl, pH 7.4, 0.1 M NaCl, 10% glycerol (v/v, TNG buffer), sonicated, and centrifuged again to recover pellet cell debris containing crude inclusion bodies (discard supernatant).

Inclusion bodies purification

Ten milliliters protein extraction reagent (e.g., Bugbuster, Novagen, EMD Chemicals, Gibbstown, NJ, USA) are added to the pellet and sonicated to resuspend the crude inclusion bodies. After centrifugation at 8,000×g for 20 min, the supernatant is removed. Three of these Bugbuster washes are performed, followed by two washes with 10 mL TNG buffer (this step enables residual detergent from the pellet mass). The pellet is weighed and resuspended in appropriate TNG volume to obtain a concentration of 37.5 mg/mL washed pellet. Inclusion bodies are resuspended by sonication and dispensed into 1-mL aliquots in 1.7-mL microcentrifuge tubes. After centrifugation, the supernatant is removed. The pellet can be stored at -80°C for several months.

Preparation of GFP 1-10 reagent for assay

GFP 1-10 inclusion body pellet is dissolved by adding 1mL 9 M urea containing 5mM DTT and by incubating the tube in a 37°C water bath to help dissolution of the inclusion bodies. After complete dissolution, the microcentrifuge tube is centrifuged for 1min at 16,000×g to remove any aggregated material, and the supernatant is transferred into a 50-mL Falcon tube containing 25 mL TNG buffer. The solution is mixed gently by inversion and filtered through a 0.2-μm syringe filter. This solution is ready to use for in vitro protein quantification assays. The remaining solution may be stored up to 2 weeks at –20°C.

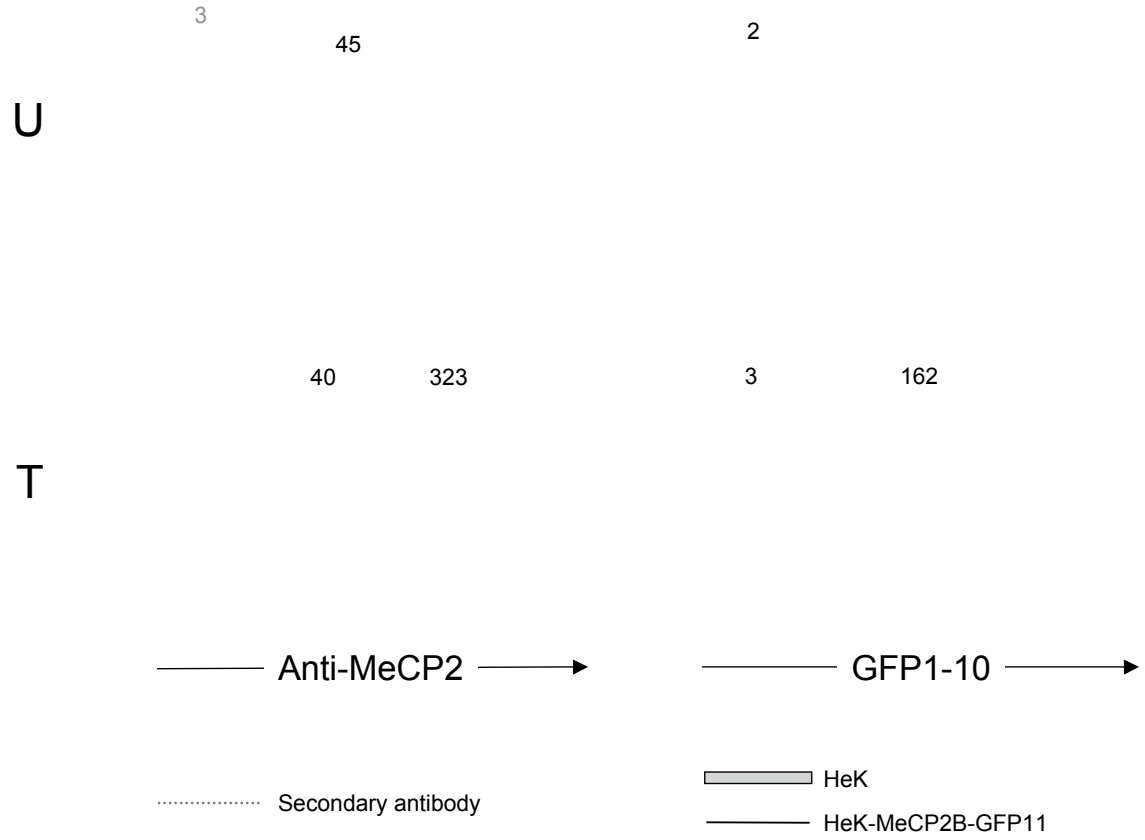

***Figure 5.4* — FACS detecting of MeCP2-GFP 11 in HEK cells.** Top panels represent staining of nontransfected HEK cells (U), and bottom panels represent staining of G418-resistant HEK cells after transfection with MeCP2-GFP 11(T), of which only around 15% are expressing detectable levels of the protein. (Left panels) Anti-MeCP2 immunostaining. Gray line in the upper left panel represents staining with secondary antibody only. (Right panels) Staining with GFP 1-10. The number adjacent to each peak corresponds to the mean fluorescence intensity of these peaks.

Supplementary Table S1. FACS fluorescence values of N2A cells after GFP 1-10 staining.

Time (h)	4°C			Room temperature			37°C		
	Mean fluorescence intensity of GFP			Mean fluorescence intensity of GFP			Mean fluorescence intensity of GFP		
	N2A	N2A MeCP2–GFP 11	Ratio	N2A	N2A MeCP2–GFP 11	Ratio	N2A	N2A MeCP2–GFP 11	Ratio
0	2.21	6.10	2.76	2.21	8.51	3.85	2.17	11.55	5.32
0.5	2.15	54.25	25.23	1.95	71.05	36.44	1.68	79.15	47.11
1	2.11	90.58	42.93	1.86	137	73.66	1.64	132.16	80.59
1.5	2.15	127.49	59.30	2.02	207.21	102.58	1.72	170.01	98.84
2	2.17	152.61	70.33	2.07	248.05	119.83	1.79	186.01	103.92
3	2.23	181.06	81.19	2.29	313.4	136.86	1.98	210.97	106.55
4	2.35	214.80	91.40	2.74	381.97	139.41	2.29	241.44	105.43
6.5	2.81	278.81	99.22	3.75	445.08	118.69	2.64	276.32	104.67
9.5	3.31	313.40	94.68	4.61	461.38	100.08	3.16	305.05	96.53
11.5	3.59	355.45	99.01	5.23	465.55	89.02	3.43	316.23	92.20
24	6.04	453.16	75.03	8.58	445.08	51.87	4.96	299.61	60.41

Fixed and permeabilized cells were incubated with GFP 1-10 at three temperatures: 4°C, RT, and 37°C. Fluorescence was measured by FACS at different time points (left column). Signal/noise ratio is indicated for each data set in a third column by dividing mean fluorescence intensities of transfected cells (N2A-MeCP2-GFP11) and control cells (N2A).

***Figure 5.5* — FACS fluorescence values of N2A cells after GFP 1-10 staining.**

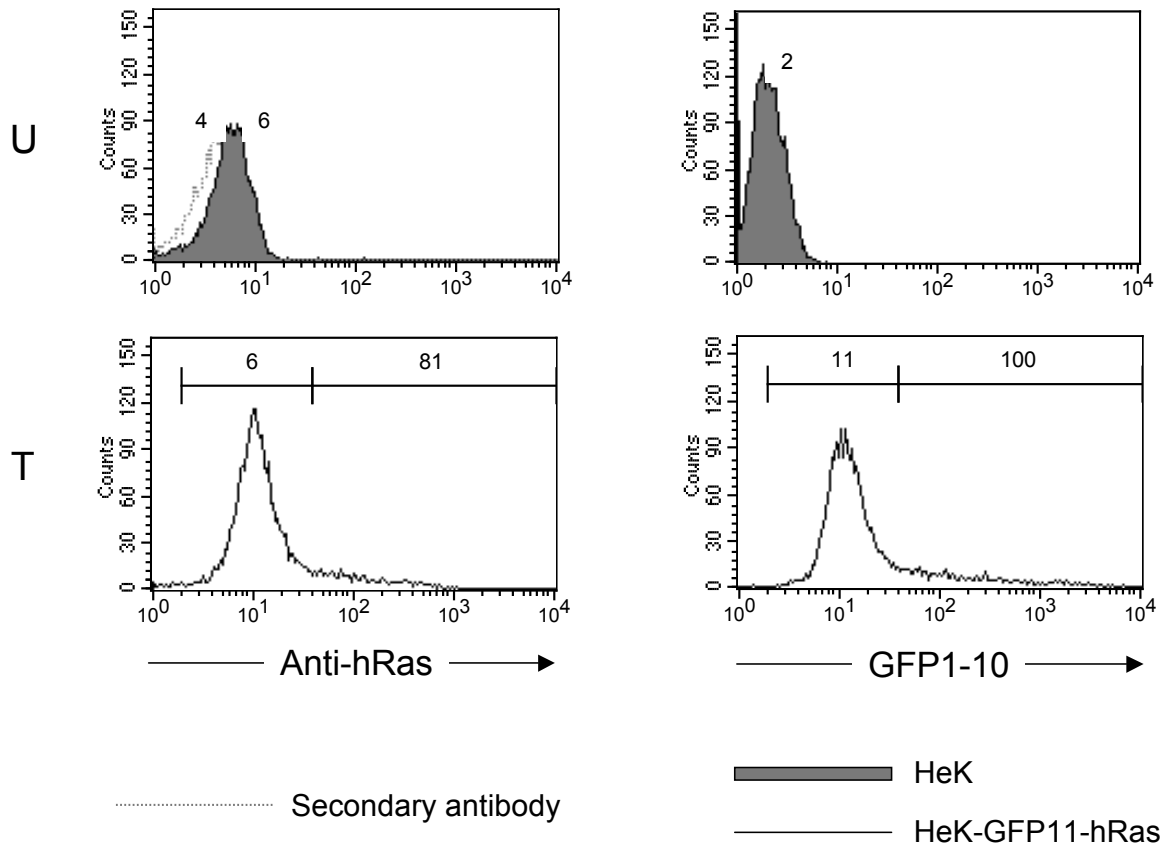

	HeK	HeK-GFP11-hRas	S/N
Anti-hRas	6	81	13,5
GFP1-10	2	100	50

Figure 5.6 — **FACS detection of GFP 11-H-Ras in HEK cells.** Top panels represent staining of nontransfected HEK cells (U), and bottom panels represent staining of HEK cells after transient transfection with GFP 11-H-Ras (T). (Left panels) Anti-H-Ras immunostaining with anti-H-Ras MAb (Pierce, Thermo Scientific). Gray line in the upper left panel represents staining with secondary antibody only. (Right panels) Staining with GFP 1-10. The number adjacent to each peak corresponds to the mean fluorescence intensity of these peaks. In transfected cells, these fluorescence intensities are indicated above for each cell population, for those expressing basal levels of H-Ras and transfected cells. The table summarizes these values. GFP 1-10 staining of transiently transfected HEK cells still yielded better signal-to-noise ratios than antibody staining (50 versus 13).

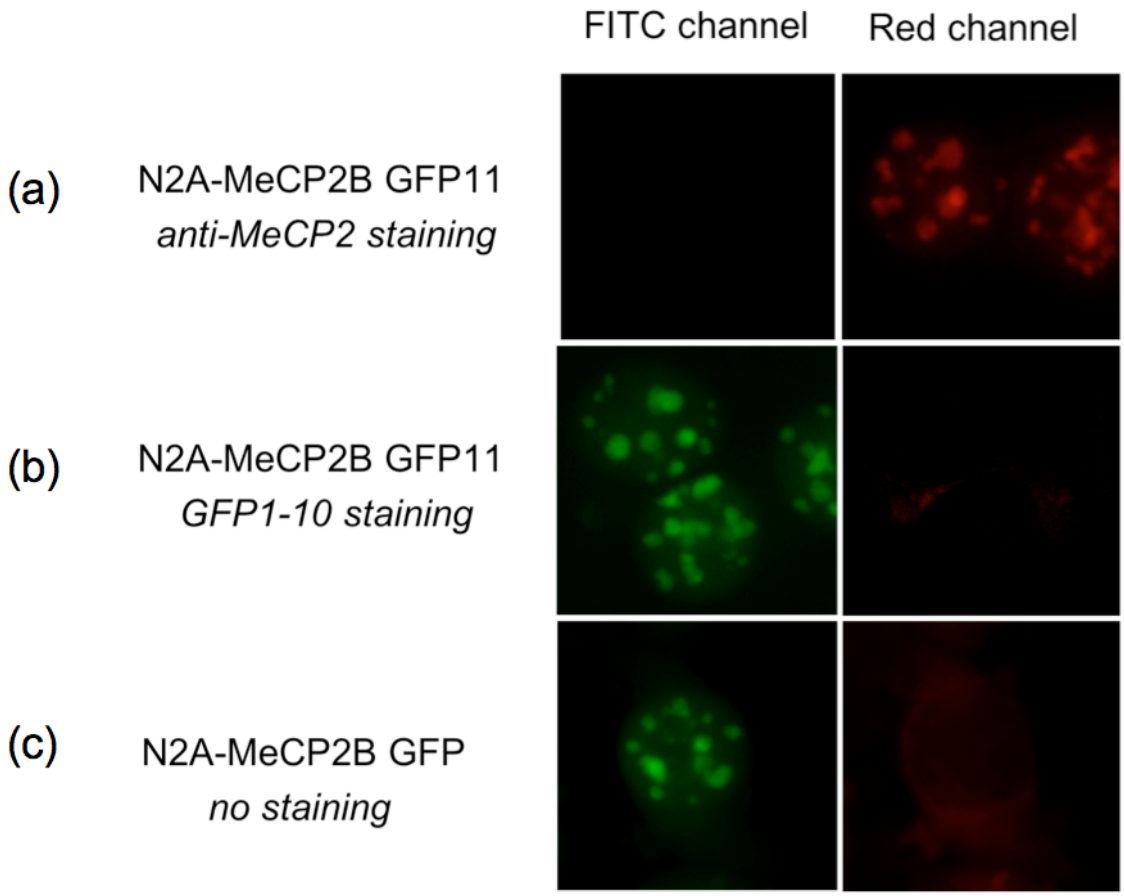

Figure 5.7 — **Absence of green and red channel interference for single staining of N2A MeCP2-GFP 11 cells with anti-MeCP2polyclonal antibody of GFP 1-10 reagent.** No green residual fluorescence is observed in the FITC channel when anti-MeCP2 rhodamine immunostaining is performed (A). Inversely, GFP 1-10 staining reveals only fluorescence in the FITC channel with no overlap in the red channel (B). Unstained N2A-MeCP2-GFP fusions display very slight red fluorescence, which is not correlated with MeCP2 localization but rather to background cell fluorescence (C).

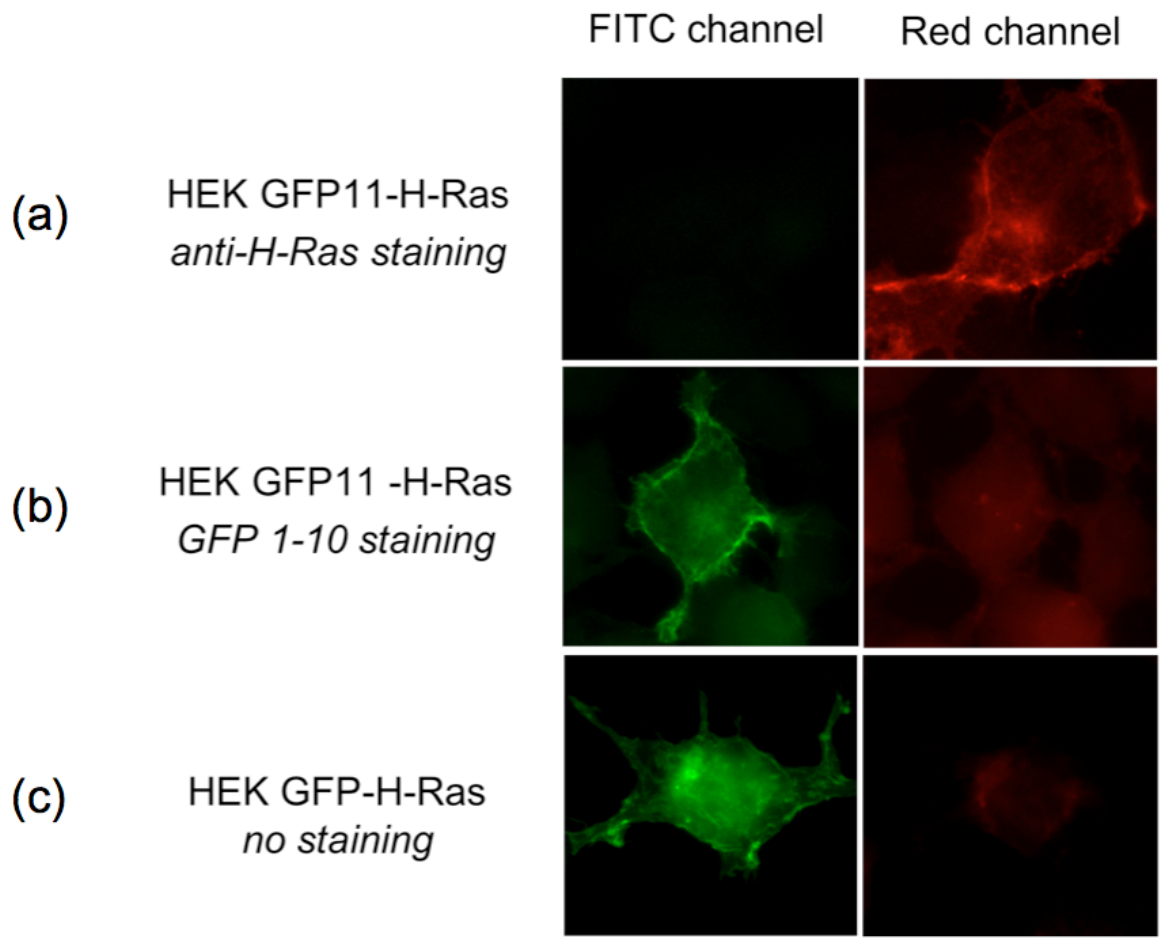

Figure 5.8 — **Absence of green and red channel interference for single staining of HEK cells expressing H-Ras using anti-H-Ras MAb of GFP 1-10 reagent.** Anti-H-Ras rhodamine immunostaining reveals membrane localization in the red channel for H-Ras-GFP 11 in HEK cells, while no green residual fluorescence is observed (A). With GFP 1-10 staining, clear membrane localization is revealed in the FITC channel with some background cell fluorescence in the red channel, which is not related to H-Ras localization (B). Similar effect is observed in HEK cells as in N2A cells for the GFP-H-Ras fusion protein, with some staining of interacellular membrane compartments not seen with the GFP 11-tagged form (C).

Bibliography

[1] R. Y. Tsien. The green fluorescent protein. *Annu Rev Biochem*, 67:509–44, 1998.

[2] D. A. Hanson and S. F. Ziegler. Fusion of green fluorescent protein to the C-terminus of Granulysin alters its intracellular localization in comparison to the native molecule. *J Negat Results Biomed*, 3:2, 2004.

[3] B. Brizzard. Epitope tagging. *Biotechniques*, 44(5):693–5, 2008.

[4] T. Krenacs, L. Krenacs, and M. Raffeld. Multiple antigen immunostaining procedures. *Methods Mol Biol*, 115:223–33, 1999.

[5] G. I. Evan, G. K. Lewis, G. Ramsay, and J. M. Bishop. Isolation of monoclonal antibodies specific for human c-myc proto-oncogene product. *Mol Cell Biol*, 5(12):3610–6, 1985.

[6] S. Cabantous, J. D. Pedelacq, B. L. Mark, C. Naranjo, T. C. Terwilliger, and G. S. Waldo. Recent advances in GFP folding reporter and split-GFP solubility reporter technologies: Application to improving the folding and solubility of recalcitrant proteins from Mycobacterium tuberculosis. *J Struct Funct Genomics*, 6(2-3):113–9, 2005.

[7] S. Cabantous and G. S. Waldo. In vivo and in vitro protein solubility assays using split GFP. *Nat Methods*, 3(10):845–54, 2006.

[8] G. N. Mnatzakanian, H. Lohi, I. Munteanu, S. E. Alfred, T. Yamada, P. J. MacLeod, J. R. Jones, S. W. Scherer, N. C. Schanen, M. J. Friez, J. B. Vincent, and B. A. Minassian. A previously unidentified MeCP2 open reading frame defines a new protein isoform relevant to Rett Syndrome. *Nat Genet*, 36(4):339–41, 2004.

[9] E. Choy, V. K. Chiu, J. Silletti, M. Feoktistov, T. Morimoto, D. Michaelson, I. E. Ivanov, and M. R. Philips. Endomembrane trafficking of Ras: the CAAX motif targets proteins to the ER and Golgi. *Cell*, 98(1):69–80, 1999.

[10] P. J. Skene, R. S. Illingworth, S. Webb, A. R. Kerr, K. D. James, D. J. Turner, R. Andrews, and A. P. Bird. Neuronal MeCP2 is expressed at near histone-octamer levels and globally alters the chromatin state. *Mol Cell*, 37(4):457–68, 2010.

[11] J. I. Young, E. P. Hong, J. C. Castle, J. Crespo-Barreto, A. B. Bowman, M. F. Rose, D. Kang, R. Richman, J. M. Johnson, S. Berget, and H. Y. Zoghbi. Regulation of RNA splicing by the methylation-dependent transcriptional repressor methyl-CpG binding protein 2. *Proc Natl Acad Sci U S A*, 102(49):17551–8, 2005.

[12] B. M. Willumsen, A. Christensen, N. L. Hubbert, A. G. Papageorge, and D. R. Lowy. The p21 Ras C-terminus is required for transformation and membrane association. *Nature*, 310(5978):583–6, 1984.

[13] T. Wang and P. K. Donahoe. The immunophilin FKBP12: a molecular guardian of the TGF-β family type I receptors. *Front Biosci*, 9:619–31, 2004.

[14] M. Marchi, A. Guarda, A. Bergo, N. Landsberger, C. Kilstrup-Nielsen, G. M. Ratto, and M. Costa. Spatio-temporal dynamics and localization of MeCP2 and pathological mutants in living cells. *Epigenetics*, 2(3):187–97, 2007.

[15] S. Akbarian, R. Z. Chen, J. Gribnau, T. P. Rasmussen, H. Fong, R. Jaenisch, and E. G. Jones. Expression pattern of the Rett Syndrome gene *mecp2* in primate prefrontal cortex. *Neurobiol Dis*, 8(5):784–91, 2001.

[16] D. A. De Angelis, G. Miesenbock, B. V. Zemelman, and J. E. Rothman. PRIM: proximity imaging of green fluorescent protein-tagged polypeptides. *Proc Natl Acad Sci U S A*, 95(21):12312–6, 1998.

[17] H. Zheng, J. McKay, and J. E. Buss. H-Ras does not need COP I- or COP II-dependent vesicular transport to reach the plasma membrane. *J Biol Chem*, 282(35):25760–8, 2007.

[18] S. B. Van Engelenburg and A. E. Palmer. Imaging type-III secretion reveals dynamics and spatial segregation of Salmonella effectors. *Nat Methods*, 7(4):325–30, 2010.

[19] E. Lobbestael, V. Reumers, A. Ibrahimi, K. Paesen, I. Thiry, R. Gijsbers, C. Van den Haute, Z. Debyser, V. Baekelandt, and J. M. Taymans. Immunohistochemical detection of transgene expression in the brain using small epitope tags. *BMC Biotechnol*, 10:16, 2010.

[20] Z. Shevtsova, J. M. Malik, U. Michel, U. Scholl, M. Bahr, and S. Kugler. Evaluation of epitope tags for protein detection after in vivo CNS gene transfer. *Eur J Neurosci*, 23(8):1961–9, 2006.

6 Generation and characterization of isoform-specific anti-MeCP2 antibodies

6.1 Abstract

Rett syndrome is a neurodevelopmental disorder caused by mutations in the MeCP2 gene. mRNA for MECP2 is alternatively spliced to generate two protein isoforms (MeCP2e1 and MeCP2e2) that differ at their N-termini. Whilst mRNAs for both forms are expressed ubiquitously, MeCP2e1 is more abundant than MeCP2e2 in the CNS. In transfected mouse cells both protein isoforms are nuclear and colocalize with densely methylated heterochromatic foci. To understand the contribution of each isoform in the pathogenesis of Rett syndrome, it would be very useful to have access to reagents that can distinguish between them, but until now, all antibodies directed against MeCP2 have been directed against regions of the protein present in the two isoforms. We have therefore attempted to generate isoform-specific anti-MeCP2 antibodies. To this end, we used peptides corresponding to the short amino-terminal portions that are different between the two isoforms to immunise rabbits. The polyclonal antibodies obtained detected their respective isoforms of MeCP2 specifically, both by Western Blot and immunofluorescence techniques. With those antibodies, we could easily detect specific signals for MeCP2e1 in mouse brain tissues, whilst, in our hands, MeCP2e2 remained below the level of detection.

6.2 Introduction

Rett syndrome is a dominant X-linked neurological disorder that affects girls during early childhood. It is a progressive disease with symptoms appearing around 6 to 18 months

after birth. After a normal developmental period, girls show growth retardation, microcephaly, stereotypic hand movement, motor abnormalities, mental retardation and communication dysfunction [1]. Most RTT cases are sporadic. However, using information from the rare familial cases, Amir *et al.* identified mutations in *MeCP2* gene as the origin of 95% of classic RTT cases [2]. MeCP2, methyl CpG binding protein 2, is an abundant nuclear protein identified in 1992 for its capacity to bind methylated DNA [3].

The *MeCP2* gene consists of four exons giving rise to two different isoforms of the protein due to alternative splicing of the mRNA. In addition, the MeCP2 mRNA has a long highly conserved 3'-UTR with three sites of polyadenylation generating three different transcripts for each isoform. The first isoform to be described, in 1992, was MeCP2e2 (also called MeCP2A or MeCP2β) which contains all four exons with the initiation site in exon 1 giving rise to a protein of 486 amino acids 5 [4]. The MeCP2e1 isoform (also called MeCP2B or MeCP2α) was identified eleven years later, in 2004, both in human [5] and mouse [6]. It lacks exon 2, and thus consists of exons 1, 3 and 4, and starting from the initiation site in exon 1, gives rise to a protein of 498 amino acids [4] and Figure 6.1A).

RT-PCR analyses have revealed the presence of two transcripts in all tissues in human and mouse, and also demonstrated that MeCP2e1 isoform is more abundant than MeCP2e2 in the brain, thymus and lung ([6, 5]). Many arguments suggest that the MeCP2e1 protein may be more physiologically relevant than MeCP2e2.

Firstly, in the MeCP2e2 mRNA, the ATG start codon present in exon 1 is followed by a very short open reading frame that terminates at the start of exon 2, and the initiation site for the translation of the whole length MeCP2e2 protein is then found further down in exon 2 (Figure 6.1A.). Kriaucionis and Bird actually demonstrated that the presence of this first ATG results in very inefficient translation of the MeCP2e2 protein.

Second, the ancestral form of MeCP2 inferred from sequence comparisons with non-mammalian vertebrates corresponds to MeCP2e1.

Third, until now, in the hundreds of sequences for MeCP2 genes obtained from patients affected by Rett syndrome, no mutation has yet been found in exon 2. On the other hand, work carried out between 2005 and 2009 has revealed the presence of 10 different mutations (deletions and missense) in exon 1 in patients with classical or atypical (mild and severe form) Rett syndrome [7].

Lastly, in 2 patients showing classical phenotype of Rett syndrome, but without seizures or microcephaly, Saunders *et al.* identified mutations affecting the initiation codon of MeCP2e1 [7], which would result in the lack of translation of the MeCP2e1 protein, but would be expected to somewhat 'restore' higher expression of MeCP2e2, similarly to what has been reported for the mouse cDNA [6].

On the other hand, the MeCP2e2 protein must be able to fulfill most functions of MecP2e1 since, in MeCP2 KO mice, the pathologic phenotype could be rescued by a tau-MeCP2e2 transgene [8]. It is also worthy of note that for historical reasons, many of the studies using on the expression of recombinant MeCP2 were based on cDNA constructs coding for the MeCP2e2 isoform.

To explore the expression of each isoform in vivo, and understand their respective contributions to Rett syndrome, it would be very valuable to have access antibodies to detect them separately. In this regard, however, all the described antibodies directed against MeCP2 were raised against portions common to the two isoforms, and thus recognize them both. With a view to obtain isoform-sepecific antibodies, we thus decided to immunize rabbits with peptides found only in one or the other of the isoforms, and to characterize those by western blot and immunofluorescence on both tissue culture cells and brain slices.

6.3 Material and methods

6.3.1 Rabbit immunization

For each antibody, two New Zealand white rabbits were immunized with a synthetic peptide corresponding to amino acids 1-12 of mouse MeCP2e2 (MVAGMLGLREEK-C), amino acids 19-29 of mouse MeCP2e1 (C-GGGEEERLEEK). The cysteine residues were added for conjugation with carrier proteins. Rabbit immunizations were carried out by Eurogentec France SASU, Angers, France. Four injections were performed on day 0, 21, 49, and 77 with thyroglobuline-conjugated peptides. Serums were harvested and then affinity purified on resins coupled to the respective peptides by Millegen (Labège, France). With the e2 peptide, the sera obtained from both rabbits gave comparable results. For the e1 peptide, however, only one rabbit responded satisfactorily.

The third antibody was raised against (C-PRPNREEPVDSRTP) corresponding to amino

acids 465-478 of both isoforms of mouse MeCP2 as described previously by others [9] and ourselves [10]. This polyclonal antibody was produced by Millegen (Labège, France). Rabbits received five injections on day 0, 12, 23, 44 and 57 with KLH-conjugated peptide. One of the two rabbits responded satisfactorily, and that serum was used directly without further affinity purification.

6.3.2 Cell culture and transfections

pcDNA3.1(A) vectors expressing Myc-tagged human MeCP2e1 and MeCP2e2 were provided by Dr. Berge A. Minassian of the Hospital for Sick Children, Toronto, Ontario, Canada [5].

N2A cells and G418-resistant stably transfected N2A cells expressing Myc-His-tagged human MeCP2e1 and MeCP2e2 were maintained in DMEM 10% FCS supplemented with 100 U/ml penicillin, 100 g/ml streptomycine, 0.1 mM Non-essential amino acids, 1 mM sodium pyruvate (+ 0,5 mg/ml G418 for the transfectants).

6.3.3 Immunofluorescence staining of tissue culture cells and microscopy

2.5×10^5 N2A cells were plated overnight on glass coverslips in 24-well plates. Cells were washed twice with PBS and fixed with PFA 3.7% in PBS for 30 min at room temperature. Cells were washed twice with PBS followed by microwave antigen retrieval step. For this cells were incubated in citrate buffer 0.1M (pH 6) and heated 4 × 30 seconds in microwave (750 watts). After two washes with PBS, cells were permeabilized in 0.3% Triton-X100 for 10 min at room temperature (RT). After 3 washes with PBS/FCS 2%, cells were incubated with Rabbit anti-MeCP2 serum (1:200 dilution in PBS/FCS 10%) for 45 min at RT. Cells were again washed 3 times before incubation with Alexa Fluor 488-labelled Goat anti-Rabbit, molecular probes Invitrogen (1:200 dilution in PBS/FCS 10%) for 30 min at RT. Cells were washed 3 times with PBS/FCS 2% and after a final wash with PBS, coverslips were mounted in DAPI-containing ProLong Gold antifading reagent (Molecular Probes). We used a LEICA DM-RB fluorescence microscope, with a 40X oil immersion objective to visualize the stained cells. Images were acquired with a Photometric CoolSNAP HQ camera and analyzed with Metamorph and/or ImageJ softwares.

6.3.4 Western Blot

Nuclear extract preparation of N2A cells or mouse tissues was carried out as described previously [11]. Various amounts of proteins from these nuclear extracts were loaded onto acrylamide gels. After separation, proteins were transferred to nitrocellulose membrane (0,45 μm BioRad). Membranes were blocked with TBS (Tris 10 mM, NaCL 0.15 M, pH 7.4) containing 3% skimmed powder milk (non-fat Régilait, France) and 0.1% Tween-20 overnight at 4°C. Before incubation, the TBS blocking buffer was always centrifuged (100000 g for 45 min) and filtered with 0,2 μm filters. Membranes were then incubated with rabbit anti-MeCP2 antibodies diluted in blocking buffer for 1h at RT. Anti-MCP2e1 was diluted to 1/2000, anti-MeCP2e2 to 1/5000 and anti-MeCP2 to 1/3000. After 4 × 10 min washes in PBS/ 0.1% Tween buffer, membrane were incubated with goat anti-rabbit HRP (BioRad, 1:10000 dilution in blocking buffer) for 1h at RT. Finally, the blots were washed 4 × 10 min in PBS/ 0.1% Tween buffer and revealed with an ECL kit (Pierce).

6.3.5 Brain tissue immunostaining

Mice were sacrificed with a lethal pentobarbitone injection (100 mg kg^{-1} i.p.) and transcardially perfused by PBS 0.1M containing 4% paraformaldehyde (10 min). Brainstem were postfixed 5 h in the same solution, placed in PBS 0.1 M containing 20% sucrose and frozen at -80 °C.

Brain sections (20 μm) were cut using a cryostat (Microm, France), permeabilized 15 min in PBS Triton 0.1%, blocked 45 min with 7% normal goat serum (NGS, Jackson Immuno)), and incubated overnight at RT with primary antibodies diluted 1/300 in PBS containing 3% NGS serum. The following day, sections were washed, incubated 2 h at RT with a secondary antibody (goat anti-rabbit alexa 546 (Invitrogen) diluted 1:400 in PBS containing 3% serum and re-washed. After 5 min incubation with DAPI (4',6-diamidino-2-phenylindole, dihydrochloride), slides were mounted in Shandon Immu-Mount (ThermoFisher). Immunostained slices were analyzed using a Leica DMR microscope (Leica Microsystems, Wetzlar, Germany) equipped with a CoolSNAP camera (PrincetonTrenton, NJ, USA). Pictures were then analyzed with ImageJ software.

6.4 Results and discussion

6.4.1 Peptide design and Rabbit immunization

A

B

Figure 6.1 — A.)Representation of the MECP2 gene and mRNA (adapted from [6] and [5]). Alternative splicing for the e1 (or B) isoform is shown above the gene and for the e2 (or A) isoform below the gene. B.) Alignment of mouse (m) and human (h) MeCP2e1 and MeCP2e2 N-termini show sequence similarities between the two species. Peptides sequences correspond to the region that differs between the two isoforms. Synthetic peptides was generated and conjugated to thyroglobulin before rabbit immunization.

6

MeCP2e1 and MeCP2e2 differ only by their N-terminal region. We designed and synthesized two peptides that would be isoform specific, but matched both the human and mouse sequences: the first corresponding to amino acids 19-29 of human MeCP2e1 (C-GGGEEERLEEK) and to amino acids 1-12 of human MeCP2e2 (MVAGMLGLREEK-C). Cysteine residues were added to the N terminus of the e1 and the C terminus of the e2 peptides for coupling with carrier proteins, for which we chosen thyroglobulin. Rabbits were immunized as described in materials and methods and serum was harvested 9 days after the final injection. Antibodies were affinity purified on columns coupled to peptide, and yielded a solution of 0,6 mg/ml for the MeCP2e1 antibody and 1 mg/ml for the MeCP2e2 antibody. Crude serum was used for the third antibody directed against both isoforms of MeCP2.

6.4.2 Antibodies characterization

6.4.2.1 Immunofluorescence and western blot

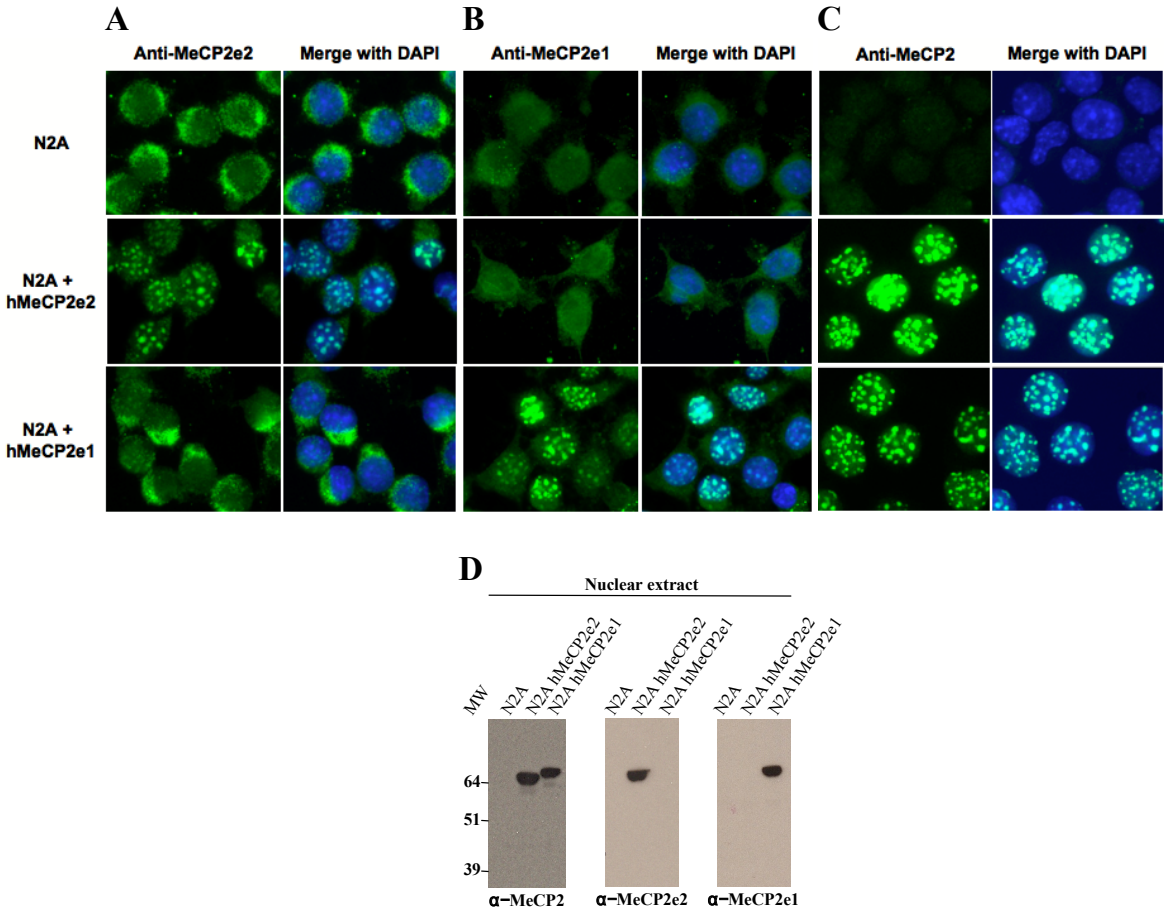

Figure 6.2 — **Antibodies characterization by immunofluorescence and western blot**: N2A cells stably expressing hMeCP2e1-myc-his and hMeCP2e2-myc-his were plated on coverslips and labeled with antibodies directed against MeCP2e1 (**A.**) or MeCP2e2 (**B.**) isoforms or with anti-MeCP2 (**C.**) directed against both isoforms. Nuclei were stained with DAPI. **D.**) Nuclear extracts of N2A cells expressing MeCP2 were separated by polyacrylamide gel electrophoresis, transferred to nitrocellulose and labeled with the different antibodies. Results show specific staining for each isoform.

To test the specificity of the antibodies, we used clones of the mouse neuroblastoma cell line Neuro2a (N2A) which stably express either MeCP2e1 or MeCP2e2. Despite the neuronal lineage of the N2A cells, it is worth underlining that undifferentiated N2A cells do not express any detectable level of MeCP2 [12]. As can be seen on figure 6.2(A-C) immunofluorescence staining with either of the isoform-specific antibodies led to nuclear labeling that co-localized with heterochromatin, as revealed by DAPI staining. For each of the two isoforms-specific antibodies generated, this staining was found to be specific since no cross-reaction was observed on the transfectants expressing the other isoform (Figure 6.2A.

and B.). Of note, for the MeCP2e1 antibody, microwave treatment of the samples before staining, which is commonly used for antigen retrieval, resulted in a noticeable improvement of the staining. This suggests that the N-terminal portion of the MeCP2e1 protein may not always be accessible, possibly because of interaction with other cellular components. This hypothesis is also supported by the observation that, even after antigen retrieval, the intensities attained were less intense than with the serum recognizing both forms of MeCP2 (Figure 6.2C). With the anti-MeCP2e2 antibody, no improvement of staining was obtained by microwaving. On the other hand, some noticeable staining was obtained in the cytoplasm, but this was clearly not specific for MeCP2 since similar levels of staining were also found in untransfected N2A cells (Figure 6.2A.). Quite remarkably, those levels of cytoplasmic staining appeared much more intense in cells that did not express MeCP2e2, which suggests that some antibodies that bind with high affinity to the N terminal portion of MeCP2 may actually cross react with some other cytoplasmic component(s), but with lower affinity. Blast searches of mammalian protein sequences with the sequence of the peptide used for immunizing the rabbits identified proteins of the plectin family as prime suspects since those have cytoplasmic distributions, and many start with MVAGML, the same six amino acids as found in MeCP2e2.

Western blot analysis of nuclear extracts prepared from the same cells confirmed the specific reactivity of both antibodies, with each revealing only the band corresponding to the MeCP2 isoform it was raised against, whilst the antibody raised against the 465-478 peptide recognised both isoforms, yielding band of similar intensities.

6.4.2.2 Immunostaining on brain sections of wildtype and MeCP2 KO mice

To verify if these antibodies are suitable to be used for histological staining, we prepared tissue sections from different regions of the brains of normal C57BL/6 and MeCP2 KO mice. Figure 6.3 shows the results obtained on cortex region. Using the MeCP2e1 antibody, staining of WT tissues revealed a specific nuclear punctuated labeling that colocalised perfectly with DAPI, whilst we did not detect any labeling on KO tissues. With the MeCP2e2 antibody, we did not detect any punctate nuclear signal which is so typical of MeCP2. Rather, we observed similar cytoplasmic labeling of cells in tissues obtained from both the WT and KO mice. This staining was thus non specific, and very similar to what we had observed on N2A cells.

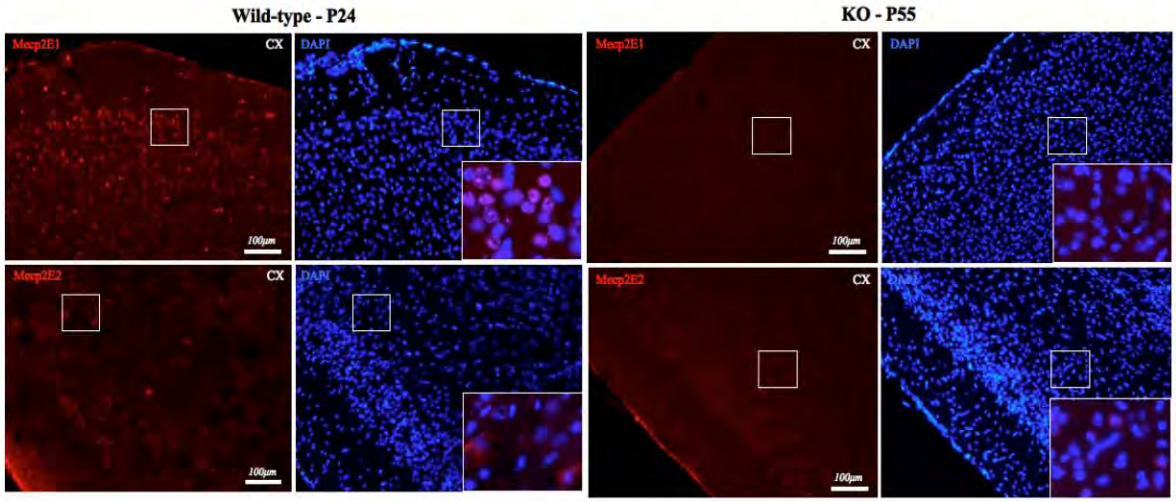

Figure 6.3 — **MeCP2e1 and MeCP2e2 expression in the cortex section of WT and MeCP2 KO mice**: staining with anti-MeCP2e1 antibody on WT mouse (left top panel) showed a specific nuclear staining characteristic of MeCP2. Magnified views reveal a punctate localization of MeCP2 that colocalises with DAPI in the nucleus. No labeling was observed with KO mice (right top panel). Staining with the anti-MeCP2e1 antibody showed similar cytoplasmic unspecific staining in WT (left bottom panel) and KO mice (right bottom panel).

Similar results were obtained with sections of other brain areas such as the hippocampus (Figure 6.4), the paraventricular nucleus and the arcuate nucleus at two different ages P24 (Figure 6.3) and P55 (figure 6.4).

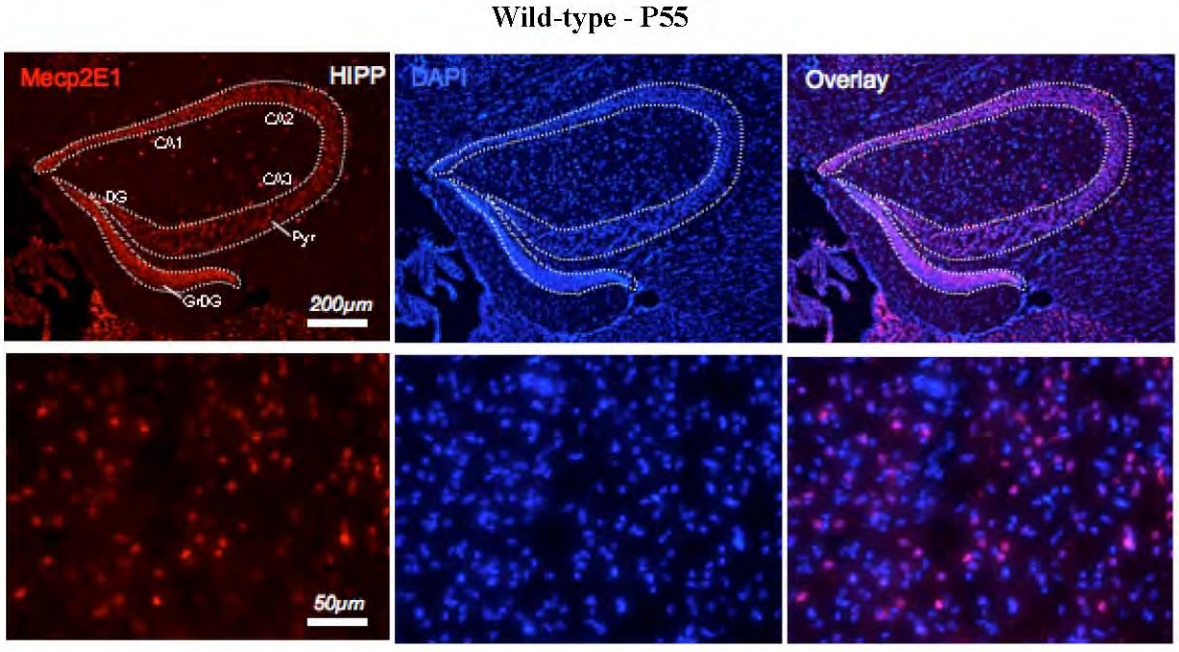

Figure 6.4 — **MeCP2e1 expression in the hippocampus section of WT P55 mice**: staining revealed specific nuclear labeling that colocalized with DAPI. For the MeCP2e2 antibody the same lack of specific staining was obtained as in the cortex (not shown).

Those two antibodies were then used to explore the expression of each isoform in different organs by western blot (Figure 6.5). For this we prepared nuclear extracts from brain (cortex and cerebellum), lung, heart, liver, thymus, spleen and kidney. As a positive control we used nuclear extracts from N2A cells transfected with either form of MeCP2, as described above (Figure 6.2D). Western blot analyses revealed the presence of MeCP2e1 protein at high levels in the CNS, and at lower levels in the lung and kidney. On the other hand, whilst the MeCP2e2 protein was readily and specifically detected in the transfectants, no band of the right size was obtained in any of the tissues. Several other bands of smaller sizes were, however, detected in all tissues, but those were clearly not due to MeCP2 since they were also seen in CNS extracts from an MeCP2 KO mouse.

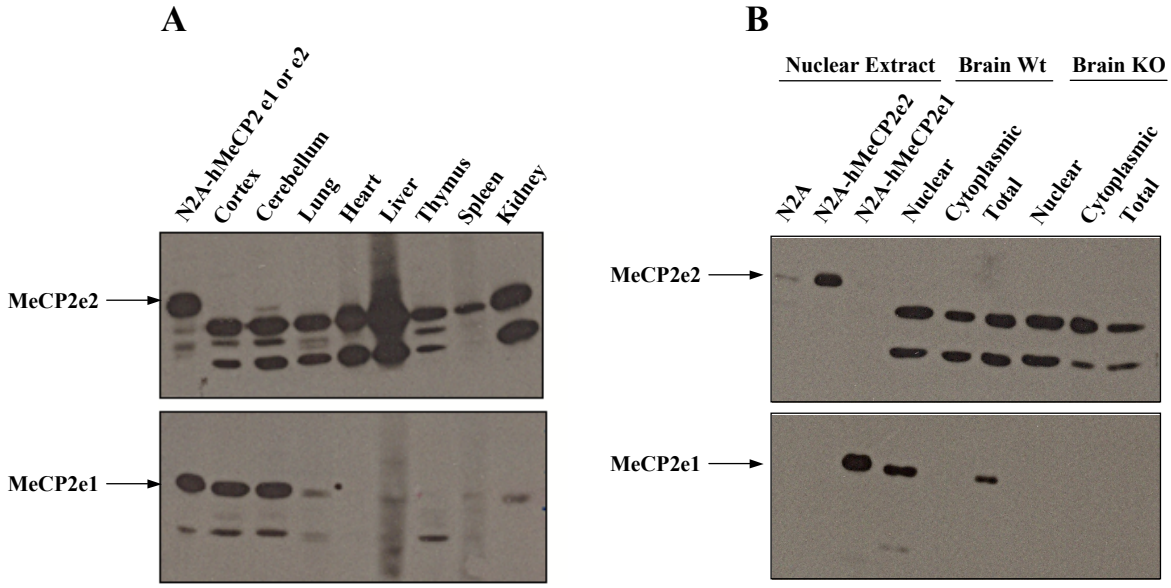

Figure 6.5 — **MeCP2e1 and MeCP2e2 expression in different organs of the mouse: A.)**: Western blot analysis revealed that MeCP2e1 isoform is expressed in the CNS, the lung and the kidney. No MeCP2e2 expression was detected in any tissue. **B.)** Western blot on KO brain revealed that the other bands on the gels correspond to non-specific proteins.

6.5 Conclusion

We have generated isoform-specific antibodies directed against each of the two MeCP2 isoforms: MeCP2e1 and MeCP2e2. Although the antibody directed against MeCP2e2 gives much higher background than that against MeCP2e1, both these antibodies are clearly specific of their respective isoform, and shown to be suitable for using by western blot and immunofluorescence.

We showed also that the MeCP2e1 isoform is expressed at high level in the brain and at low level in the lung and the kidney. On the other hand, we were unable to detect any expression of the MeCP2e2 protein in all the tissues analyzed, suggesting that, if the MeCP2 protein is expressed in the organism, it is at levels which are below the level of detection with our reagent.

Our data strongly support the already established view that the MeCP2e1 isoform is not only the most abundant isform in the organism, but also probably the only one with an important physiological role.

Bibliography

[1] M. Chahrour and H. Y. Zoghbi. The story of Rett Syndrome: from clinic to neurobiology. *Neuron*, 56(3):422–37, 2007.

[2] R. E. Amir, I. B. Van den Veyver, M. Wan, C. Q. Tran, U. Francke, and H. Y. Zoghbi. Rett Syndrome is caused by mutations in X-linked MECP2, encoding methyl-CpG-binding protein 2. *Nat Genet*, 23(2):185–8, 1999.

[3] J. D. Lewis, R. R. Meehan, W. J. Henzel, I. Maurer-Fogy, P. Jeppesen, F. Klein, and A. Bird. Purification, sequence, and cellular localization of a novel chromosomal protein that binds to methylated DNA. *Cell*, 69(6):905–14, 1992.

[4] T. Bienvenu and J. Chelly. Molecular genetics of Rett Syndrome: when DNA methylation goes unrecognized. *Nat Rev Genet*, 7(6):415–26, 2006.

[5] G. N. Mnatzakanian, H. Lohi, I. Munteanu, S. E. Alfred, T. Yamada, P. J. MacLeod, J. R. Jones, S. W. Scherer, N. C. Schanen, M. J. Friez, J. B. Vincent, and B. A. Minassian. A previously unidentified MeCP2 open reading frame defines a new protein isoform relevant to Rett Syndrome. *Nat Genet*, 36(4):339–41, 2004.

[6] S. Kriaucionis and A. Bird. The major form of MeCP2 has a novel N-terminus generated by alternative splicing. *Nucleic Acids Res*, 32(5):1818–23, 2004.

[7] C. J. Saunders, B. E. Minassian, E. W. Chow, W. Zhao, and J. B. Vincent. Novel exon 1 mutations in MeCP2 implicate isoform MeCP2_e1 in classical Rett Syndrome. *Am J Med Genet A*, 149A(5):1019–23, 2009.

[8] S. Luikenhuis, E. Giacometti, C. F. Beard, and R. Jaenisch. Expression of MeCP2 in postmitotic neurons rescues Rett Syndrome in mice. *Proc Natl Acad Sci U S A*, 101(16):6033–8, 2004.

[9] Z. Zhou, E. J. Hong, S. Cohen, W. N. Zhao, H. Y. Ho, L. Schmidt, W. G. Chen, Y. Lin, E. Savner, E. C. Griffith, L. Hu, J. A. Steen, C. J. Weitz, and M. E. Greenberg. Brain-specific phosphorylation of MeCP2 regulates activity-dependent BDNF transcription, dendritic growth, and spine maturation. *Neuron*, 52(2):255–69, 2006.

[10] L. Kaddoum, E. Magdeleine, G. Waldo, E. Joly, and S. Cabantous. One-step split GFP staining for sensitive protein detection and localization in mammalian cells. *Biotechniques*, 49(4):727–36, 2010.

[11] N. C. Andrews and D. V. Faller. A rapid micropreparation technique for extraction of DNA-binding proteins from limiting numbers of mammalian cells. *Nucleic Acids Res*, 19(9):2499, 1991.

[12] J. I. Young, E. P. Hong, J. C. Castle, J. Crespo-Barreto, A. B. Bowman, M. F. Rose, D. Kang, R. Richman, J. M. Johnson, S. Berget, and H. Y. Zoghbi. Regulation of RNA splicing by the methylation-dependent transcriptional repressor methyl-CpG binding protein 2. *Proc Natl Acad Sci U S A*, 102(49):17551–8, 2005.

7 MeCP2 Involvement in the DNA Damage Response

7.1 Introduction

The methyl CpG binding protein (MeCP2) is a transcription factor that binds to methylated DNA. When mutated, this protein is responsible for Rett syndrome, a neurodevelopmental X-linked disorder occurring in 1:10000 to 1:20000 female births [1, 2, 3].

The MeCP2 protein is encoded by a four-exon gene, giving rise to two different isoforms due to alternative splicing of the exon 2. The MeCP2 protein is highly expressed in mature neurons in the brain. It contains four functional domains: a methyl-CpG-binding domain (MBD), a transcriptional repression domain (TRD), a nuclear localization signal and a C-terminal region which facilitate its binding to the nucleosomes and is important for protein-protein interactions [4, 5].

Different functions have been described for MeCP2. It was initially thought that MeCP2 was a transcription repressor that binds to CpG methylated promoters and recruits histone deacetylase complex [6]. However, recently, 2 studies revealed that MeCP2 could act as a transcription activator suggesting that MeCP2 should be considered as a transcription modulator [7, 8]. Other studies revealed that MeCP2 has a role in maintaining the methylation profile of DNA by interacting with DNMT1 [9] and in modulating mRNA splicing by interacting with the Y box-binding protein 1 [10]. It was also shown that MeCP2 can have a role in regulating global chromatin architecture, suggesting that MeCP2 is a multifunctional nuclear protein [11, 12].

In vitro studies revealed that the binding of MeCP2 to chromatin is affected when the CpG sequence is altered. For example oxidative damage inhibits the binding of MeCP2 [13] whereas halogenated pyrimidine lesions enhance its binding capacity [14]. Recently, other

studies revealed that a decrease in MeCP2 expression is accompanied by an increase in damaged DNA [15]. Importantly, MeCP2 could enhance the number of UV lesions by enhancing photodimer formation but on the other side, it inhibits the deamination step required for the photoproduct to become mutagenic [16, 17].

All these studies suggest a potential role of MeCP2 in the DNA damage response. In this study we introduced different DNA lesions using multiphoton laser micro-irradiation and DNA intercalators with laser photo-activation and we showed that MeCP2 is recruited rapidly to the site of damage and that this recruitment depends on the C-terminal region of MeCP2. We showed also that MeCP2 accumulation is independent from GG-NER and TC-NER pathways and is independent from transcription.

7.2 Results

7.2.1 Expression and detection of MeCP2-GFP and mutants derivatives

In order to investigate the implication of MeCP2 in DNA damage response and to understand its role in this pathway, we stably expressed the human MeCP2 protein in fusion with the GFP protein (Figure 7.1A) in different cell lines. For this, we chose to study the e1 isoform since it is the major form expressed in the brain. We also elected to fuse the GFP fluorescent marker at the C-terminal region of MeCP2 in agreement with a previous study showing that a knock in mouse model expressing MeCP2-GFP protein are viable and behaves like a normal wild-type mouse, suggesting that this fusion construct does not significantly alter the most vital function(s) of MeCP2 [18]. To study the implication of each region of MeCP2 in the DNA damage response, we introduced different missense mutations: in the MBD (R133C) and the TRD (R306C) domains of MeCP2 and one nonsense mutation (Δ308) lacking the C-terminal region of MeCP2 [19]. These mutants were all fused to the GFP protein (Figure 7.1A). To verify the localization and the expression of the wild-type hMeCP2-GFP fusion protein, we performed immunofluorescence staining with anti-MeCP2 antibody on Human Embryonic Kidney (HEK) cells stably expressing the MeCP2-GFP protein (Figure 7.1B). Results showed a nuclear labeling with a perfect co-localization between the anti-MeCP2 and the GFP signals.

In order to exclude any degradation profile for MeCP2, we performed western blot analysis on nuclear extract from the HEK cells expressing or not the MeCP2-GFP protein (Figure

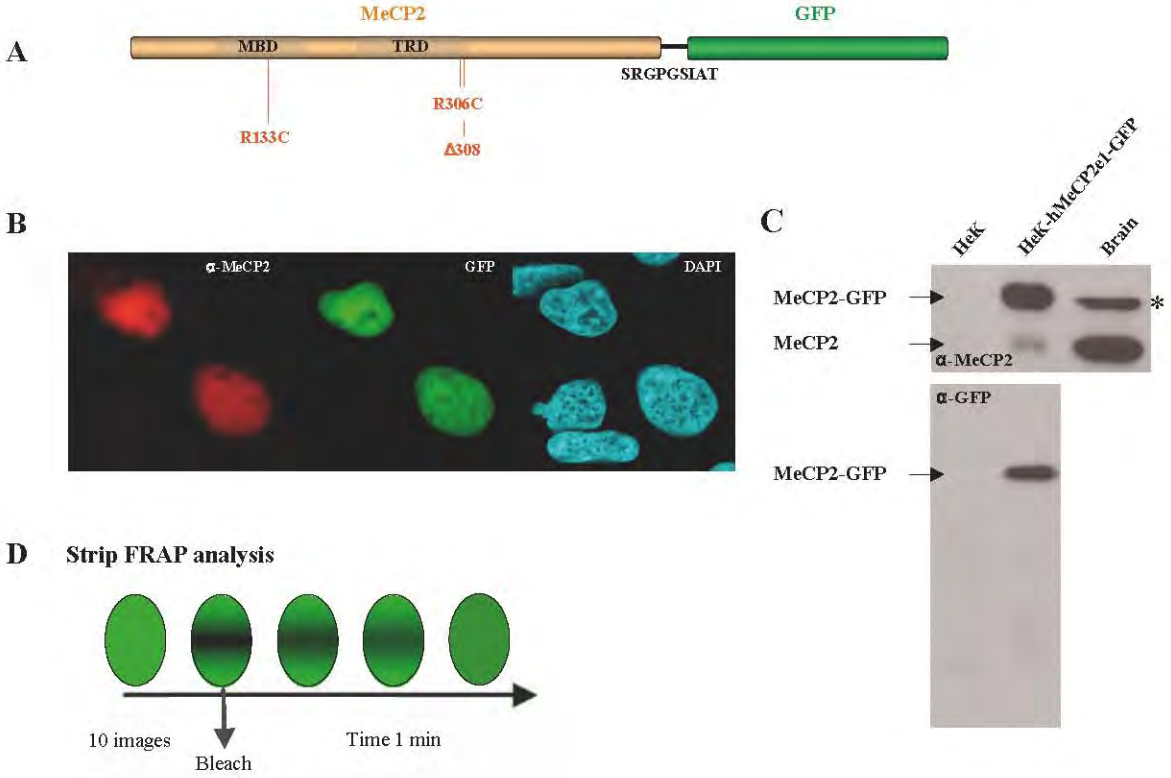

Figure 7.1 — Scheme of MeCP2 constructs used in this study: A) MeCP2 and its mutated forms were fused in the C-terminal region to the GFP protein. Western blot and immunofluorescence analyses were carried out to verify the expression and the localization of the protein. B) Immunofluorescence staining directed against MeCP2 revealed a co-localization with the GFP signal in the nucleus. C) Western blot analysis with anti-MeCP2 antibody revealed the presence of 2 bands in the nuclear extract from HEK-hMeCP2-GFP cells: the upper one corresponds to MeCP2-GFP protein and the lower one corresponds to endogenous protein at the same size of MeCP2 in the nuclear extract from the mouse brain. No expression of MeCP2 was detected in HEK cells. Asterisks correspond to a non specific bands also present in the nuclear extract from the brain of the MeCP2 KO mouse (Not shown). Western blot with anti-GFP antibody revealed the presence of MeCP2-GFP protein. In these cells we didn't detect any degradation products or free GFP. (D) Schematic representation of strip FRAP assay used in this study: Fluorescent molecules are bleached in a small strip in the middle of the nucleus, then the fluorescence recovery is monitored until one minute after bleach.

7.1C). Results obtained with anti-MeCP2 antibody showed two proteins in HEK-MeCP2-GFP cells, corresponding to the MeCP2-GFP fusion protein (also detected with the anti-GFP antibody), and the endogenous MeCP2. Western blots did not reveal any degradation product for MeCP2 or any free GFP molecules in HEK-MeCP2-GFP cells. As no endogenous expression of MeCP2 was detected in HEK cells, we suggest that it could be the expression of MeCP2-GFP which induces the expression of the endogenous protein. In conclusion, we established a human cell line stably expressing the hMeCP2-GFP protein and we were thus able to study the mobility of the MeCP2 protein in the nucleus, its dynamic interaction with the chromatin and its role in the DNA damage response in living cells using strip-FRAP

(Figure 7.1E) and laser micro-irradiation techniques.

7.2.2 MeCP2 localization on locally damaged DNA.

To verify whether MeCP2 is localized at DNA damage sites, we generated lesions in HEK cells expressing MeCP2-GFP, using microirradiation with a multiphoton laser, which induces different types of DNA damages (DSB, SSB, oxidative damage, etc.) [20]. After irradiation, we observed an accumulation of MeCP2 in the region of damage (Figure 7.2A). The accumulation of MeCP2 begins 30 seconds after irradiation, reaches its maximum 5 min after DNA damage and then gradually declines, to become barely detectable after 30 min. To characterize the type of lesions needed for the recruitment of MeCP2, we induced different types of DNA lesions separately and we detected in which conditions MeCP2 accumulates. After induction of cyclobutane pyrimidine dimer (CPD) or pyrimidine pyrimidone (6-4PP) photoproducts lesions by local UV irradiation through 5 μm filters using 60 J/m^2 UV light [21], no MeCP2 accumulation could be observed, either at 10 min or 30 min after UV damage (Figure 7.2B left panel). As a positive control, we used cells expressing the XPC-GFP protein, an essential protein whose role is to initiate GG-NER [22], and to recognize and repair UV lesions. Unlike MeCP2, the XPC-GFP protein shows an accumulation 10 min after irradiation (Figure 7.2B right panel).

Another way to induce DNA lesion is to use DNA intercalators with laser photoactivation. In this study we used the Actinomycin D, which is usually used as a transcription inhibitor, but also known to produce DNA lesions like single strand breaks, oxidative damage and bulky lesions when photo-activated with the 488 nm laser used in strip-FRAP techniques [23]. HEK-MeCP2-GFP cells treated with Actinomycin D (2 μg/ml, for 1h) showed an accumulation of MeCP2-GFP in the region of the 488 nm illumination (Figure 7.2C). This accumulation was also observed for other proteins implicated in DNA repair like XPC and XPB [24] or Ku80, CSB, Fen1 (Figure 7.3). Other proteins like XPA, TTDA [24] or CSA (Figure 7.3 do not accumulate on this DNA damage.

7.2.3 MeCP2 recruitment on local damage is transcription and CSB independent

In order to determine in which pathway MeCP2 is implicated, we expressed MeCP2-GFP in 2 different cell lines deficient in DNA repair: the XPC-/- cells deficient in GG-NER and the CSB-/- deficient in TC-NER. Initially, we studied the localization and the mobility of

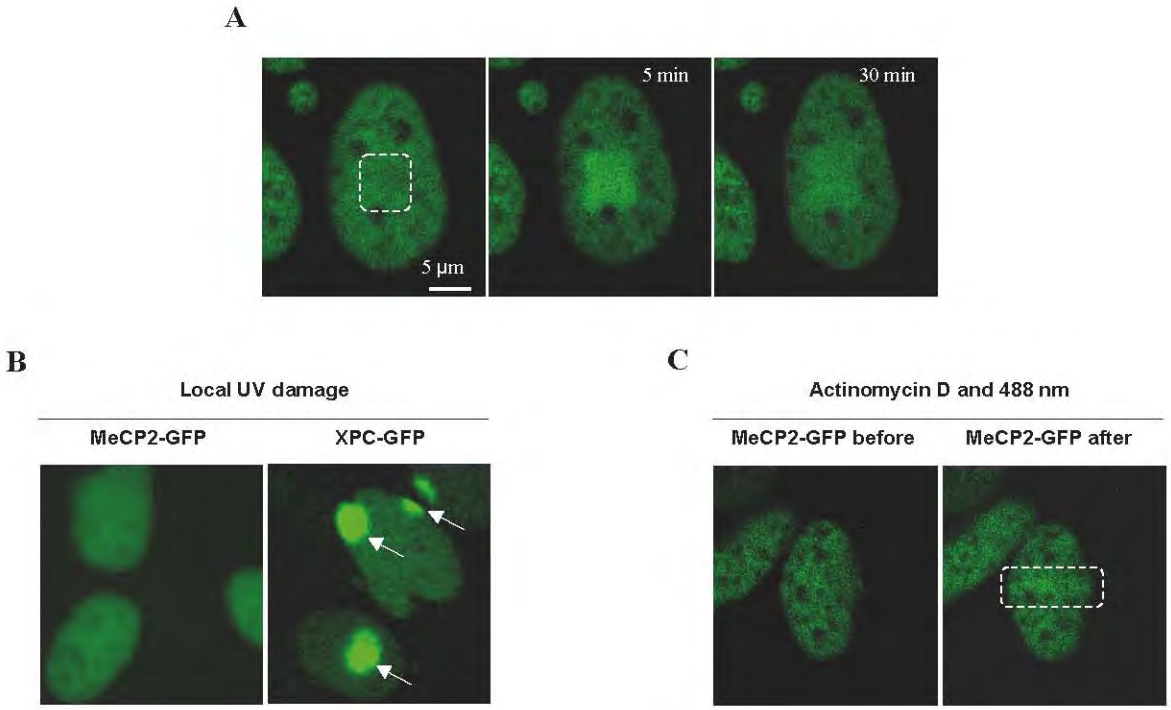

Figure 7.2 — Recruitment of MeCP2 on DNA damage. A) An example of MeCP2-GFP accumulation on DNA lesions induced by multiphoton laser micro-irradiation which produce different types of DNA damage. B) To identify the kind of lesions on which MeCP2 accumulates, we induced local UV damage through 5 μm filters. Results did not show any recruitment of MeCP2 on these lesions (left panel). As a positive control, (right panel) we used cells expressing XPC-GFP. Arrows show the accumulation of XPC on UV lesions. C) When we induced DNA damage, like SSB, oxidative damage and bulky lesions, via photo-activation of Actinomycin D, we observed accumulation of MeCP2-GFP in the photo-activated region.

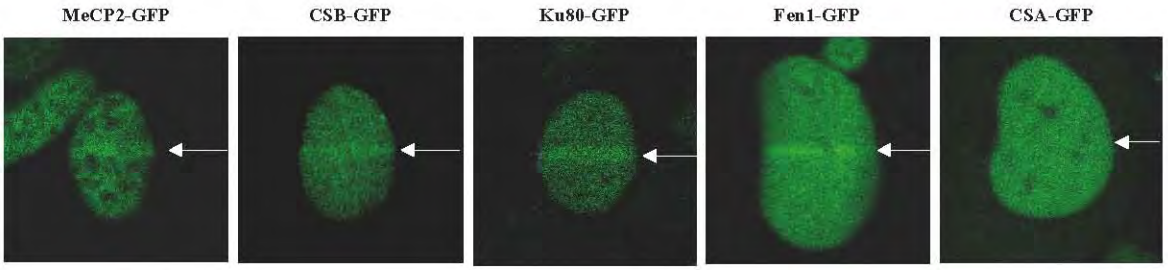

Figure 7.3 — Recruitment of GFP-tagged protein on DNA damage induced by photo-activated ActinomycinD. After strip-FRAP analysis MeCP2, CSB, Ku80 and Fen1, but not CSA, accumulates in the photo-activated region (white arrows).

the MeCP2 protein in these cell lines. In untreated cells (Figure 7.4A violet curves), MeCP2 shows a reduced mobility with a high immobile fraction in HEK and XPC-/- cells suggesting that in these cells MeCP2 binds strongly to the chromatin as was described earlier [25]. In the CSB-/- cells, MeCP2 shows a rapid kinetic with a reduced immobile fraction suggesting that in the absence of CSB, MeCP2 was unable to bind its substrate. To induce lesions to the DNA, we treated the cells with Actinomycin D for 1h and we performed strip-FRAP

analysis (488 nm repeated illuminations). For the three cell lines, FRAP curves (Figure 7.4A blue curves) show an increase signal after a certain number of 488 nm laser pulses illumination. This dynamic behavior is typically observed when proteins accumulate in the region of the photobleaching. We could verify that MeCP2 had indeed accumulated in this area by imaging the treated cells 5 min after the procedure, as shown in living images (Figure 7.4B) of HEK, XPC-/- and CSB-/- cells expressing MeCP2-GFP fusion protein. As previously shown, MeCP2 co-localizes with heterochromatin in HEK and XPC-/- cells. However, in CSB-/- cells this typical heterochromatin co-localization was replaced by a more diffuse nuclear localization. In conclusion, we found that MeCP2 is recruited on DNA lesions induced by Actinomycin D and 488nm photo-activation. This recruitment is independent of XPC and CSB suggesting that MeCP2 recognizes the damage before these two proteins or is implicated in other pathways. Finally, we showed that MeCP2 needs CSB to bind properly to the chromatin.

MeCP2 is a transcription modulator factor that tracks methylation genome wide. Chip-chip analysis in the brain showed that the binding profile of MeCP2 to the chromatin overlap the binding profile of the RNA polymerase II protein [8]. We thus wanted to verify if the recruitment of MeCP2 to the damage is transcription dependent.

For this we treated the HEK and the CSB-/- (deficient in TC-NER) cells with α-amanitin, a specific transcription inhibitor that binds the catalytic domain of RNA polymerase II (RNAP2) and impedes the binding of RNAP2 with the DNA. In HEK cells, treatment with α-amanitin provokes an increase in the immobile fraction of MeCP2, suggesting that after transcription inhibition, MeCP2 binds more to the chromatin either to induce its compaction (Figure 7.5 left panel), or in consequence of an increased number of methylated CpGs. Surprisingly, in CSB-/- cells no changes between treated and untreated cells could be observed, suggesting that the absence of CSB can hinder MeCP2 functions (Figure 7.5 right panel). However, after induction of damage in α-amanitin treated cells, we observed similar accumulation curves as in untreated cells in both HEK and CSB-/- cells, suggesting that MeCP2 accumulation to damaged areas is independent of transcription and of CSB presence.

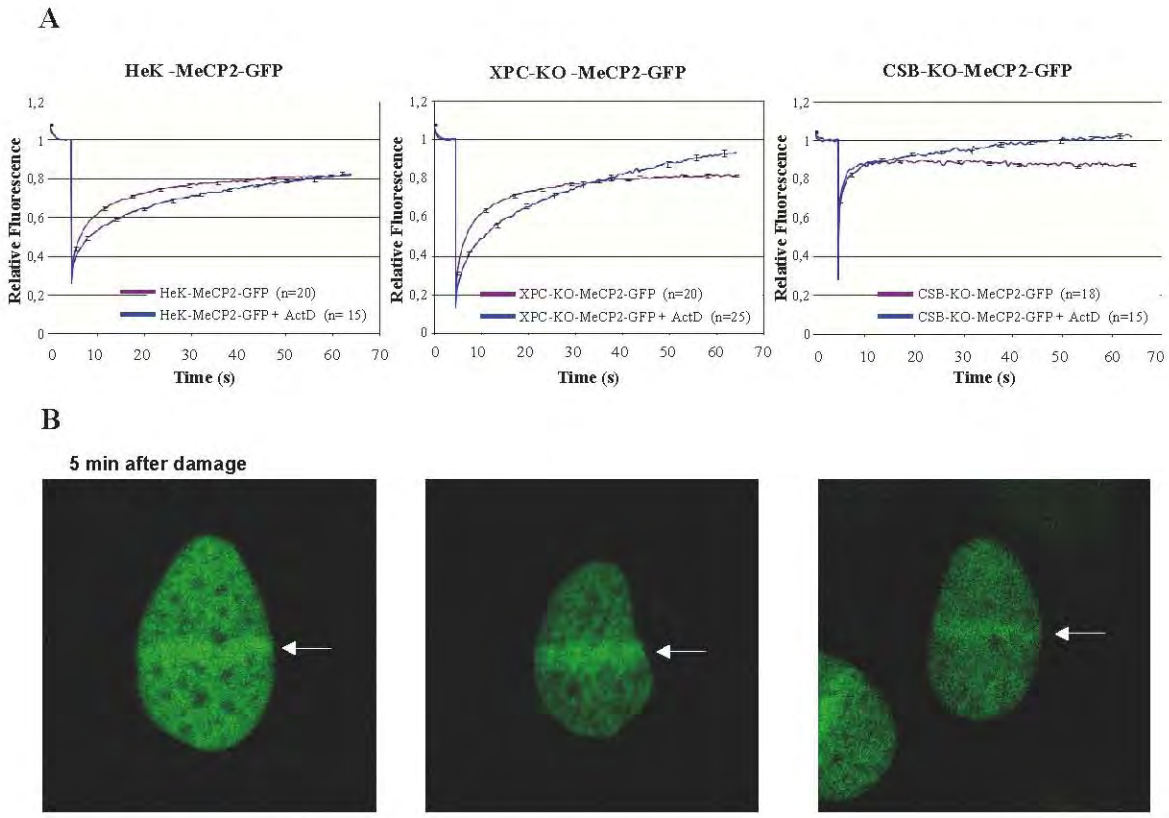

Figure 7.4 — FRAP analysis of MeCP2-GFP protein in untreated (Violet curves) and Actinomycin D (Blue curves) treated HEK, XPC-/- and CSB-/- cells: A) In untreated cells, MeCP2 showed the same reduced mobility in HEK and in XPC-/- cells with a high immobile fraction. In CSB-/- cells, the immobile fraction of MeCP2 decreases strongly. After treatment with Actinomycin D, FRAP kinetics (blue curves) and microscope images showed accumulation of MeCP2 in the region of the strip. We also noticed a difference in the localization pattern of MeCP2. In HEK and XPC-/- cells, MeCP2 is enriched at the heterochromatic regions, whereas in CSB-/- cells this enrichment is not very clear.

7.2.4 MeCP2 recruitment on Local Damage is dependant on protein/protein interaction but is DNA methylation independent.

The MeCP2 protein contains four functional domains. We wanted to know which domain is important for its recruitment on DNA lesions. To answer this question, we introduced two missense mutations in the MeCP2 DNA: 1) the R133C in the MBD, which abolishes the binding of MeCP2 to methylated DNA, 2) the R306C mutation in the TRD (a recurrent mutation found in patients with Rett syndrome) that does not affect binding or repression activity of MeCP2 and 3) the nonsense mutation R308X, resulting in MeCP2 lacking the C-terminal region which is essential for its non-methylated-dependent chromatin binding and for protein/protein interactions. All these constructs were fused to the GFP protein and stably expressed in HEK cell lines. Initially, we analyzed the mobility of both wild type

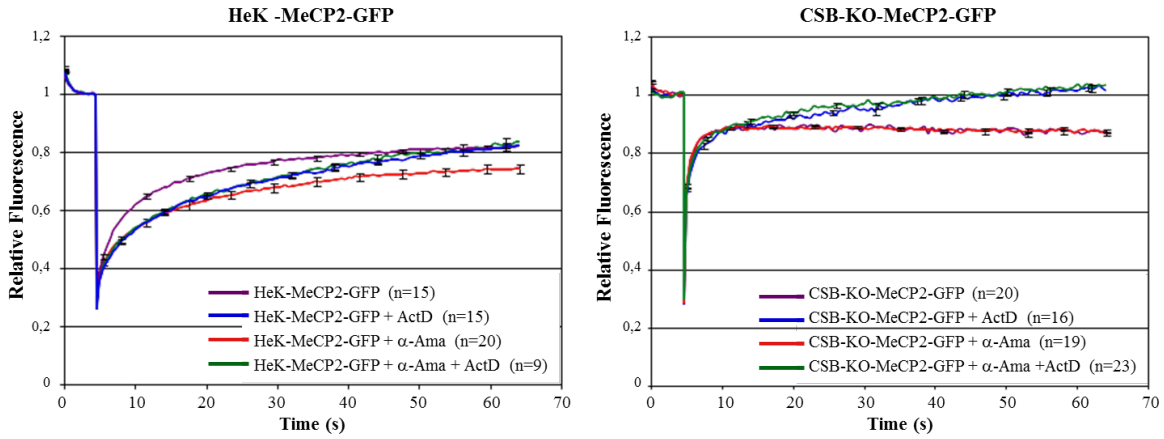

Figure 7.5 — Recruitement of MeCP2 on the lesions is independant from transcription: Representation of FRAP analysis of MeCP2-GFP protein in α-amanitin treated HEK and CSB-/- cells with (Red curves) and without (green curves) DNA damages. Blue and violet curves are the same as shown in Figure 3A. Transcription inhibition after treatment with α-amanitin increase the immobile fraction of MeCP2 in HEK cells in comparision with the untreated cells (violet curve). α-amnitin does not have any effect on the mobility of MeCP2 in CSB-/- cells. When we looked at the recruitment of MeCP2 on DNA lesions before (Blue curves) and after (green curves) treatment with α-amanitin, we did not notice any effect of transcription inhibition on MeCP2 accumulation.

and mutant proteins using strip-FRAP techniques. Wild-type MeCP2-GFP protein (Figure 7.6, left panel violet), showed a retarded fluorescence recovery with a relatively high immobile fraction, suggesting that MeCP2 binds strongly to the chromatin. Strip-FRAP curves for R306C (red) and Δ308 (blue) mutants showed a slight decrease in the immobile fraction. In contrast, the R133C mutant (green) showed a very fast recovery of fluorescence and an unusual mobile fraction, suggesting that the arginine at position 133 is important for the binding of MeCP2 on the chromatin. When we treated the cells with actinomycine D/488 nm (Figure 7.6, right panel violet), wild type MeCP2 and two mutants (R133C and R306C) showed accumulation in the region of damage. In contrast, the Δ308 mutant did not show any accumulation suggesting that the C-terminal region of the MeCP2 protein (responsible for its protein-protein interaction) is important for its recruitment to the damage. These results suggest that the accumulation of MeCP2 on the damaged DNA is independent from methylation but requires the interaction with other partners.

7.2.5 MeCP2 Binding to chromatin is altered in neuron from CSB-/- mice

The localization pattern and the FRAP curves of the MeCP2 protein in CSB-/- cells revealed that MeCP2 binds very weakly to chromatin. To confirm these results in living tissue, we decided to extract MeCP2 from the brain of WT and CSB-/- mouse models [26]. MeCP2

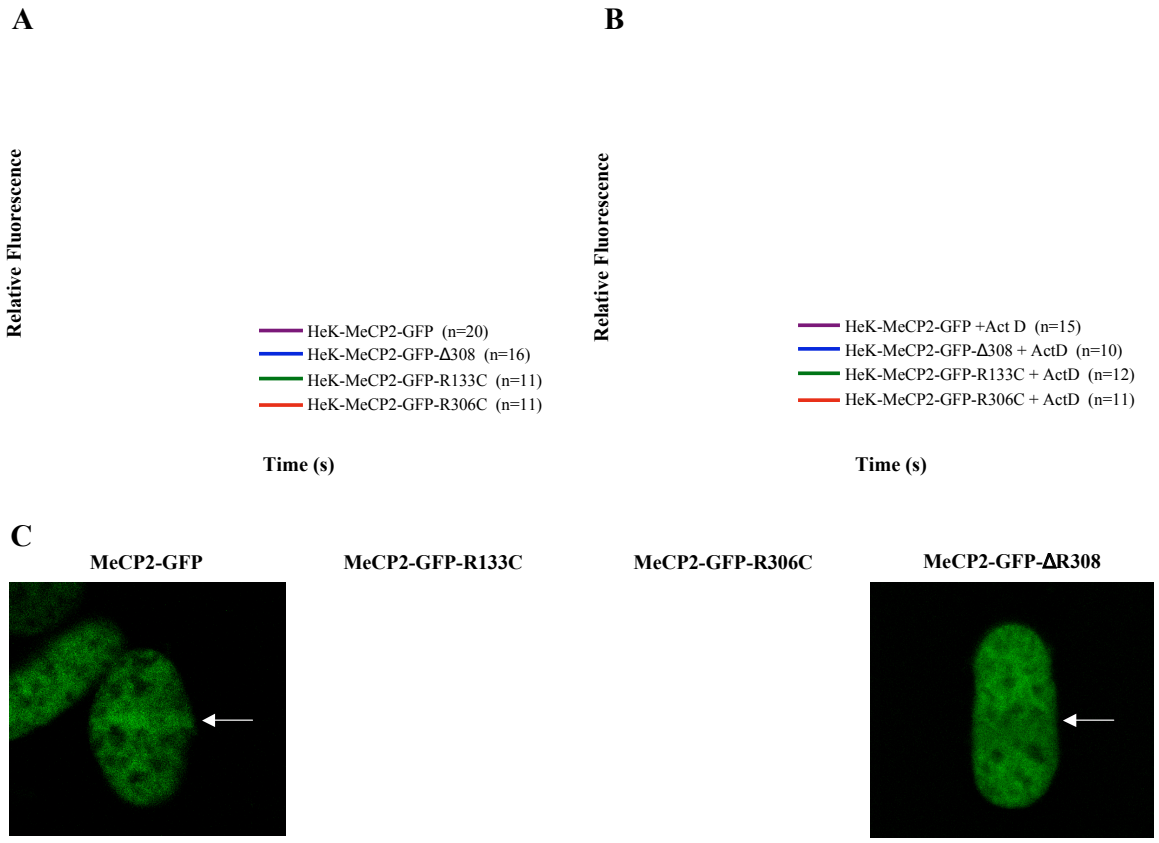

Figure 7.6 — The C-terminal region of MeCP2 is important for its function in the DNA damage response: A: FRAP kinetics of MeCP2 and its mutant forms showed slight decrease in the immobile fraction of the R306 and the Δ308 mutants in comparison with the WT form. In contrast, the R133C construct lacking its ability to bind methylated DNA showed a high increase in the mobility of the protein. B) After treatment with actinomycin D, FRAP curves revealed an increase in fluorescence characteristic of the recruitment of the GFP protein in the photo-bleached region as showed with microscope images (white arrows). We noticed that the accumulation of the mutant form lacking the C-terminal region of MeCP2 is delayed in comparison with other forms.

was eluted from the DNA and the different fractions were loaded on an acrylamide gel. Results of Western blot directed against MeCP2 (Figure 7.7) showed that when the brain was homogenized and incubated in a 450 mM NaCL buffer and sonicated two times, significant and equivalent quantities of MeCP2 were released from the chromatin from the two brains. In the brain from the WT mouse, however, a residual quantity of MeCP2 remained in the pellet (3 folds more than in the KO mouse) and needed 3 additional sonication cycles to be removed. These results suggest that in the WT brain MeCP2 bound more strongly to the chromatin in comparison with the CSB-/- brain.

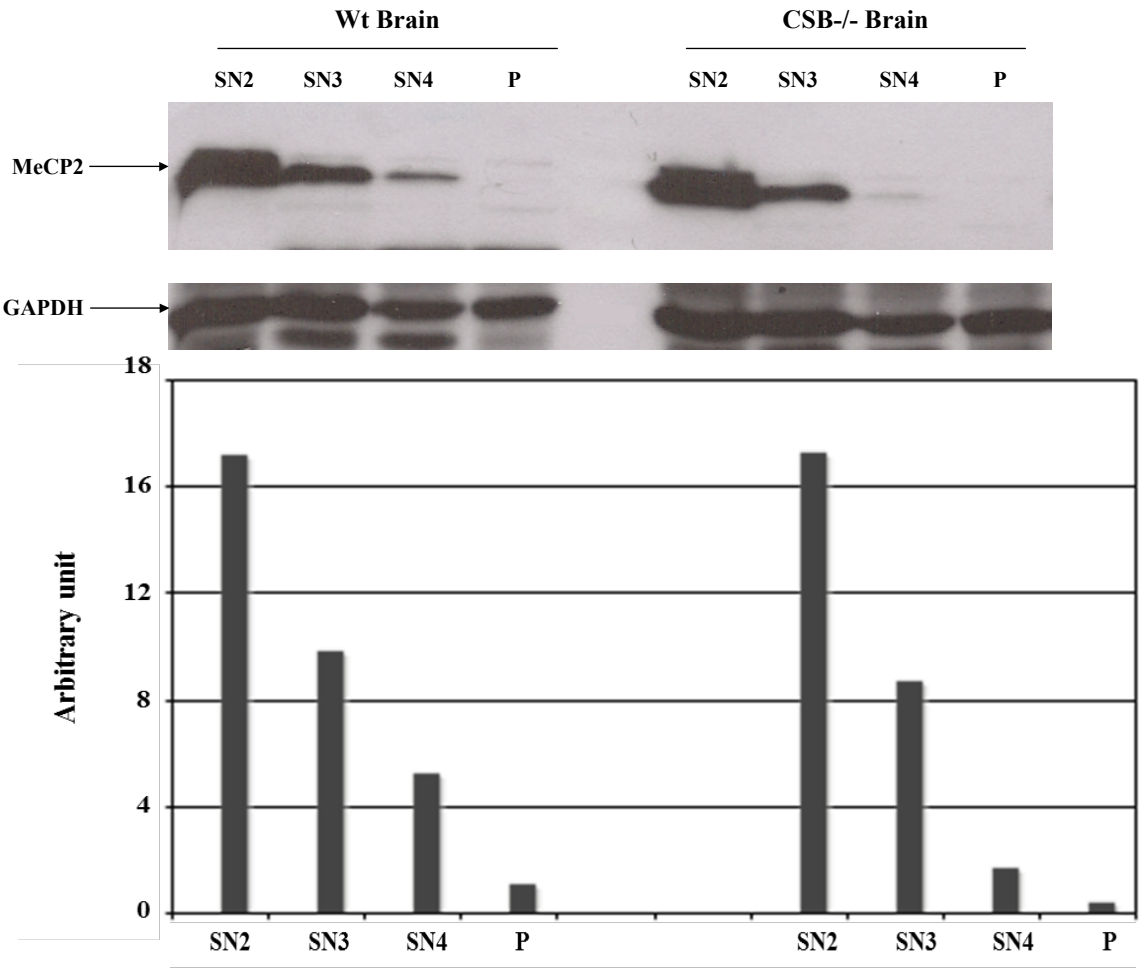

Figure 7.7 — MeCP2 binding to the chromatin is altered in CSB-/- brain tissue: Different fractions corresponding to the elution of MeCP2 from the WT *vs* the CSB KO mice were loaded on acrylamide gel. Western blot revealed the presence of MeCP2 in the first two fractions in similar quantities between the two brains. In the SN4 fraction, we detected the presence of MeCP2 protein in the WT brain 3 folds more than in CSB-/- cells suggesting that MeCP2 binds strongly to the chromatin in WT tissue and requires more steps to be eluted.

7.3 Discussion

MeCP2 is a highly abundant protein in mature neurons, with a number of molecules approaching the number of histone octamers. It is a nuclear protein playing different roles in transcription modulation, chromatin remodelling, mRNA splicing etc. In this study, we disclose a potential novel role for MeCP2 in the DNA damage response. We showed for the first time a recruitment of the MeCP2 protein on the DNA lesions induced by multiphoton laser micro-irradiation and by 488nm-photo-activated actinomycin D.

Multiphoton laser microirradiation induces different types of DNA damages such as

DSB, SSB, oxidative damage, etc. [20], whereas Actinomycin D, usually used as a transcription inhibitor, is known to induce single strand breaks, oxidative damage and bulky lesions when photo-activated with the 488 nm laser [23]. In order to determine in which DNA repair pathway MeCP2 is implicated, we stably expressed the hMeCP2-GFP fusion protein in XPC-/- cells deficient in GG-NER and in CSB-/- cells deficient for TC-NER. In these cells, we showed that MeCP2 is recruited to the DNA lesions independently from these two pathways, and that this accumulation is also independent of the transcription state of the cell, since α-amanitin (a specific RNAP2 inhibitor) did not have any detectable effect on the recruitment of MeCP2 to the lesions. These results suggest that MeCP2 either senses the damage before XPC and CSB or that MeCP2 is implicated in other pathways. Several other proteins implicated in DNA repair have been described to bind actinomycin D lesions, in earlier studies (XPB, XPC) or in this work (CSB, Ku80 and Fen1). Other experiments should be performed to determine if MeCP2 is implicated in NHEJ or in BER pathways or if this protein recognizes the damage before all other proteins and initiates a signaling cascade to allow the recruitment of the other proteins implicated in DNA repair.

The fact that the C-terminal region of MeCP2 is important for its recruitment to the damaged region suggests that other proteins can be needed for its accumulation on the lesion. It was shown that MeCP2 interacts with the Y box protein (Yb-1) in an RNA-dependent manner to regulate the mRNA splicing activity and that MeCP2 lacking the C-terminal region is responsible for 50 to 70% of this binding activity [10]. It was also demonstrated that the Yb-1 protein is implicated in the DNA damage response: it recognizes cisplatin modified base pairs, mispaired bases [27] and single stranded nucleic acid [28], it possesses 3' to 5' exonuclease activity [28] and interacts with different proteins implicated in DNA repair such as PCNA, MSH2, DNA polymerase delta, Ku80 and WRN proteins [27]. Other studies revealed that MeCP2 interacts with the YY1 protein via its TRD domain to repress the ANT1 gene encoding a mitochondrial adenine nucleotide translocase [29]. It was also shown that YY1 protein is essential for homologous recombination-based DNA repair (HRR) [30]. This lets us hypothesize that, in the context of DNA lesions, MeCP2 can be recruited by these proteins to the site of damage.

What is the role of MeCP2 on the DNA lesions? Different studies have previously revealed that in the region of a locally damaged DNA (UV lesions [22] or DSB lesions [31]), transcription is inhibited. Recently, Jackson's laboratory showed that the proteins of the his-

tone deacetylase complex HDAC1 and HDAC2 are recruited to DSB to promote NHEJ [32]. The transcription in the region where HDAC were recruited was also inhibited. Knowing that MeCP2 interacts with HDAC1 and 2. It is tempting to hypothesize that MeCP2 can recruit HDAC on DSB. Another study revealed that when a DSB occurs in a promoter region, SIRT1, EZH2, DNMTI, DNMT3B are recruited to the area around the break site. DNMT1 and DNMT3B can methylate the DNA [33]. It's known that DNMT1 can recruit MeCP2 to methylated DNA to repress transcription [9]. Further experiments should be performed to elucidate this question. For example, local damage can be induced in cells deficient or not for MeCP2. After BrU incorporation we can monitor transcription in the damaged region. We can also use a siRNA directed against DNMT1 to abolish the recruitment of MeCP2 on methylated DNA.

To verify if the damaged DNA is methylated, an immunofluorescence experiment using anti-methylcytosine antibody can be used.

Finally another important point of this study is the relation between the absence of CSB and MeCP2 mobility. CSB is a 168 kDa protein related to the family of the SWI/SNF family. It has an ATP-dependant chromatin remodeling activity [34]. It recognizes stalled RNAP2 on lesions and initiate transcription-coupled repair. It is important to know why MeCP2 binding to the chromatin is reduced in the absence of CSB. Does MeCP2 interact directly with CSB or it is in a complex containing the CSB protein. Previous studies have revealed that the transcription machinery is less tightly associated with chromatin and that the transcription is reduced in CSB-deficient cells compared to wild type [35, 36].

Mutations in the CSB gene cause Cockayne syndrome. Patients with Cockayne syndrome present a panel of neurological symptoms which are very similar to those found in Rett syndrome patients such as mental retardation, microcephaly, seizures or coordination problem [37]. The fact that the chromatin binding capacity of MeCP2 is altered in CSB deficient cells/mouse brain suggests that in the brain of Cockayne syndrome patients MeCP2 binding would also be altered, thus possibly explaining some neurological defects of CS patients.

C-terminal mutations in MeCP2 lack their capacity to accumulate on DNA lesions. These mutations can be found in Rett syndrome patients. The characterization of the role of MeCP2 in the DNA damage response will thus also be relevant for the pathogenesis of Rett syndrome.

7.4 Materials and Methods

7.4.1 Cell lines and cell culture

Human Embryonic Kidney (HEK) cells were maintained in DMEM supplemented with 10% FCS, 100 U/mL penicillin, 100 μg/mL streptomycin, 0.1 mM nonessential amino acids, and 1 mM sodium pyruvate.

XP4PASV (XPC-/-), CS1aSNV (CSB-/-), CS1aSNV+ GFP-CSB, XR-V15B eGFP-Ku-80, Mouse dermal fibroblast Fen1-YFP, CS3BESV+ CSA-GFP were maintained in DMEM/Ham F10 mixture (1:1) supplemented with 10% FCS, 100 U/mL penicillin and 100 μg/mL streptomycin.

Cells were treated with ActinomycinD 2 μg/ml for 1h at 37°C (2 mg/ml stock solution in Ethanol), α-amanitin 25 μg/ml for 10h at 37°C (1 mg/ml stock solution in Water).

7.4.2 DNA constructs and cell transfection

pcDNA3.1 vector expressing the Myc-His human MeCP2e1 were a gift from Dr. Berge Minassian (Hospital for sick children, Canada). Myc-His mutants forms (R133C, T158M, R306C and Δ308) were generated in the laboratory as described earlier [38]. To generate MeCP2e1-GFP (WT and mutants) constructs, the coding region was amplified from the pcDNA3.1 vector expressing MeCPe1 isoform and its mutants forms using the following primers:

- Forward: 5'-GATAAGATCTATGGCCGCCGCCGCCGCC-3'
- Reverse: 5'-ATAAGGGCCCCTAGAGCTAACTCTCT-3'
- Reverse for the Δ308: 5'-ATAAGGGCCCCTAGAGGTCTTGCGCT-3'

The amplified products were inserted in the eGFP-N3 plasmid using BglII and ApaI cloning sites.

7.4.3 Transfection and Generation of stable cell lines

Transfections were carried out using JetPEI (Polyplus Transfection, Illkirch, France) following the manufacturer's instructions (1 μg of DNA and 6 μl of JetPei). Stable clones were

selected using G418 (Invitrogen, Cergy Pontoise, France). At 0.5 mg/ml for HEK cells and 0.2 mg/ml for CSB and XPC cells.

7.4.4 Immunofluorescence staining

Cells (0,5 × 106) were plated overnight on 24 mm coverslips in 6-wells plate. Cells were washed twice with PBS and then fixed with paraformaldehyde (PFA) solution (2% in PBS) for 15 min at room temperature. After 3 shorts washes with PBS-Triton X100 0,1% solution, cells were permeabilized 2×10 min at RT in the same solution. After 2 washes with PBS+ solution (100 ml PBS, BSA, Glycine), cells were incubated 1h at RT or overnight at 4°C in PBS+. Incubation with the primary antibody (Home made rabbit anti-MeCP2 diluted to 1/300 in PBS+) were performed for 1 h at RT. After 3 short and 2×10 min washes with PBS-Triton X100, cells were incubated with secondary antibody (anti-rabbit IgG, Alexa633, Invitrogen diluted to 1/400 in PBS+) for 1 h at RT. Cells were washed again in PBS-Triton X100 and after a final wash with PBS, coveslips were mounted in Vectashield mounting medium with DAPI (Vector).

Images were captured using LSM 710 inverted confocal microscope and analyzed using Image J software.

7.4.5 Western blot analysis

Nuclear extract preparation of HEK cells was carried out as described previously [39]. Briefly cells were collected and washed with PBS. Cytoplasmic fraction was preparaed by incubating the cells for 10 min on ice in cytoplasmic buffer (Hepes-KOH 10 mM pH 7.9, KCl 10 mM, MgCl2 1.5 mM, DTT 0.5 mM and PMSF 0.2 mM). After incubation cells were vortexed for 10 sec and centrifuged at 14000 rpm for 10 seconds. The supernatant corresponds to the cytoplasmic extract. Pellets were washed twice with cytoplasmic buffer and then incubated with the nuclear buffer (Hepes 20 mM pH 7.9, NaCl 420 mM, MgCl2 1.5 mM, EDTA 0,2 mM, glycérol 25% , DTT 0.5 mM and PMSF 0.2 mM) for 20 min on ice. Nuclear extract were collected after centrifugation (14000 rpm for 2 min).

Around 25 μg of proteins from these nuclear extracts were loaded onto acrylamide gels. After separation, proteins were transferred to nitrocellulose membrane (0,45 μm BioRad). Membranes were blocked with TBS (Tris 10 mM, NaCL 0.15 M, pH 7.4) containing 3%

skimmed powder milk (non-fat Regilait, France) and 0.1% Tween-20 overnight at 4°C. Before incubation, the TBS blocking buffer was centrifuged (100000 g for 45 min) and filtered with 0,2 μm filters. Membranes were then incubated with rabbit anti-MeCP2 antibodies diluted in blocking buffer for 1h at RT. Anti-MCP2e1 was diluted to 1/2000, anti-MeCP2 to 1/3000 (home made antibody cf. chapter 6). After 4 × 10 min washes in PBS/ 0.1% Tween buffer, membrane strips were incubated with goat anti-rabbit HRP (BioRad, 1:10000 dilution in blocking buffer) for 1h at RT. Finally, the blots were washed 4 × 10 min in PBS/ 0.1% Tween buffer and revealed with an ECL kit (Pierce).

For anti-GFP staining, membranes were blocked in PBS with 5% skimmed powder milk (non-fat Regilait, France) and 0.1% Tween-20 for 1h at RT, incubated with monoclonal mouse anti-GFP antibody (Euromedex, diluted to 1/5000 in blocking buffer) for 2h at RT followed by 1h at RT in anti-Mouse HRP (Biorad, diluted to 1/4000 in blocking buffer).

7.4.6 MeCP2 extraction from Brain

Brains from WT and CSB-/- 3 months mice were collected and submitted to 25 passages through a Dounce homogenizer in 3 ml of Buffer A (Tris 50 mM pH=7.9, NaCL 150 mM, Glycerol 20%, NP40 0,1% and B-mercaptoethanol 5mM complemented at the last minute with protease inhibitor Complete C Roche and PMSF 1mM). After Dounce homogenization with A and B Douncers, 1ml of this mixture was centrifuged at 13200 rpm for 15 min at 4°C and the pellet was resuspended in 1 ml of Buffer B (Buffer A with NaCl adjusted to 450 mM) and incubated for 20 min on ice. After centrifugation (13200 rpm for 15 min at 4°C), the supernatant was removed (SN2) and the pellet was resuspended in 250 μl of Buffer B and sonicated 2×15 min. After another centrifugation the supernatant (SN3 fraction) was collected and the pellet resuspended in 100 μl of Buffer B. After 3 × 15 min sonication and a final centrifugation the supernatant was collected as SN4 fraction and the residual pellet (P) resuspended in laemmli buffer 6X. Quantification of MeCP2 in each fraction was normalized using GAPDH signal.

For anti-GAPDH staining, membrane were stripped after anti-MeCP2 staining and blocked in TBS with 3% BSA and 0.1% Tween-20 for 1h at RT. Membranes were incubated with monoclonal mouse anti-GAPDH antibody (Abcam, diluted to 1/2000 in blocking buffer) for 2h at RT followed by 1h at RT in anti-Mouse HRP (Biorad, diluted to 1/5000 in blocking buffer).

7.4.7 Strip-FRAP experiments

Cells were grown on coverslips. The FRAP experiments were performed on a Zeiss LSM 710 inverted confocal microscope, using a 40x/1.3 objective and under a controlled environment (37°C, 5% CO2). All recordings were made using the 488nm line of a 25 mW argon laser.

Briefly, a strip region of interest (10 pixels high) was measured at 500 ms intervals for 5 seconds (at 1% output power, pixel dwell time 3.2 μs and Zoom 6), and then the region was photobleached using 3 iterations at 100% output. Immediately after, fluorescence recovery was monitored within the strip region for 60 seconds (500 ms intervals). Error bars represent the standard error off the mean.

7.4.8 UV treatment

Cells were grown on 24 mm coverslips 2 days before experiments. The coverslips were washed twice in PBS and irradiated with 60 J/m^2 UVC (254 nm) through a 5 μm pore polycarbonate filter (Millipore). After irradiation, cells were incubated in their media for 10 and 30 min. Cells were then fixed and immunofluorescence was performed as described before.

7.4.9 Laser micro-irradiation

Laser-induced DNA damage was conducted as previously described [20]. Briefly, a Titanium TI: Sapphire laser system (Chameleon Ultra II coherent) was directly coupled to a LSM 510NLO microscope (Zeiss) to obtain an 800 nm pulsed output (200 fs pulse width at 76 MHz, 10 mW output at the sample). Single nuclei targeted with the multiphoton laser received an approximately 250 ms exposure restricted to a 1 μm wide strip.

Bibliography

[1] R. E. Amir, I. B. Van den Veyver, M. Wan, C. Q. Tran, U. Francke, and H. Y. Zoghbi. Rett Syndrome is caused by mutations in X-linked MECP2, encoding methyl-CpG-binding protein 2. *Nat Genet*, 23(2):185–8, 1999.

[2] B. Hagberg, J. Aicardi, K. Dias, and O. Ramos. A progressive syndrome of autism, dementia, ataxia, and loss of purposeful hand use in girls: Rett's Syndrome: report of 35 cases. *Ann Neurol*, 14(4):471–9, 1983.

[3] S. L. Williamson and J. Christodoulou. Rett Syndrome: new clinical and molecular insights. *Eur J Hum Genet*, 14(8):896–903, 2006.

[4] T. Bienvenu and J. Chelly. Molecular genetics of Rett Syndrome: when DNA methylation goes unrecognized. *Nat Rev Genet*, 7(6):415–26, 2006.

[5] M. Chahrour and H. Y. Zoghbi. The story of Rett Syndrome: from clinic to neurobiology. *Neuron*, 56(3):422–37, 2007.

[6] X. Nan, H. H. Ng, C. A. Johnson, C. D. Laherty, B. M. Turner, R. N. Eisenman, and A. Bird. Transcriptional repression by the methyl-CpG-binding protein MeCP2 involves a histone deacetylase complex. *Nature*, 393(6683):386–9, 1998.

[7] M. Chahrour, S. Y. Jung, C. Shaw, X. Zhou, S. T. Wong, J. Qin, and H. Y. Zoghbi. MeCP2, a key contributor to neurological disease, activates and represses transcription. *Science*, 320(5880):1224–9, 2008.

[8] D. H. Yasui, S. Peddada, M. C. Bieda, R. O. Vallero, A. Hogart, R. P. Nagarajan, K. N. Thatcher, P. J. Farnham, and J. M. Lasalle. Integrated epigenomic analyses of neuronal MeCP2 reveal a role for long-range interaction with active genes. *Proc Natl Acad Sci U S A*, 104(49):19416–21, 2007.

[9] H. Kimura and K. Shiota. Methyl-CpG-binding protein, MeCP2, is a target molecule for maintenance DNA methyltransferase, Dnmt1. *J Biol Chem*, 278(7):4806–12, 2003.

[10] J. I. Young, E. P. Hong, J. C. Castle, J. Crespo-Barreto, A. B. Bowman, M. F. Rose, D. Kang, R. Richman, J. M. Johnson, S. Berget, and H. Y. Zoghbi. Regulation of RNA splicing by the methylation-dependent transcriptional repressor methyl-CpG binding protein 2. *Proc Natl Acad Sci U S A*, 102(49):17551–8, 2005.

[11] T. Nikitina, R. P. Ghosh, R. A. Horowitz-Scherer, J. C. Hansen, S. A. Grigoryev, and C. L. Woodcock. MeCP2-chromatin interactions include the formation of chromatosome-like structures and are altered in mutations causing Rett Syndrome. *J Biol Chem*, 282(38):28237–45, 2007.

[12] T. Nikitina, X. Shi, R. P. Ghosh, R. A. Horowitz-Scherer, J. C. Hansen, and C. L. Woodcock. Multiple modes of interaction between the methylated DNA binding protein MeCP2 and chromatin. *Mol Cell Biol*, 27(3):864–77, 2007.

[13] V. Valinluck, H. H. Tsai, D. K. Rogstad, A. Burdzy, A. Bird, and L. C. Sowers. Oxidative damage to methyl-CpG sequences inhibits the binding of the methyl-CpG binding domain (MBD) of methyl-CpG binding protein 2 (MeCP2). *Nucleic Acids Res*, 32(14):4100–8, 2004.

[14] V. Valinluck, P. Liu, Jr. Kang, J. I., A. Burdzy, and L. C. Sowers. 5-halogenated pyrimidine lesions within a CpG sequence context mimic 5-methylcytosine by enhancing the binding of the methyl-CpG-binding domain of methyl-CpG-binding protein 2 (MeCP2). *Nucleic Acids Res*, 33(9):3057–64, 2005.

[15] T. Squillaro, N. Alessio, M. Cipollaro, A. Renieri, A. Giordano, and U. Galderisi. Partial silencing of methyl cytosine protein binding 2 (MeCP2) in mesenchymal stem cells induces senescence with an increase in damaged DNA. *Faseb J*, 24(5):1593–603, 2010.

[16] V. J. Cannistraro and J. S. Taylor. Methyl CpG binding protein 2 (MeCP2) enhances photodimer formation at methyl-CpG sites but suppresses dimer deamination. *Nucleic Acids Res*, 2010.

[17] G. Giglia, N. Dumaz, C. Drougard, M. F. Avril, L. Daya-Grosjean, and A. Sarasin. p53 mutations in skin and internal tumors of xeroderma pigmentosum patients belonging to the complementation group C. *Cancer Res*, 58(19):4402–9, 1998.

[18] R. S. Schmid, N. Tsujimoto, Q. Qu, H. Lei, E. Li, T. Chen, and C. S. Blaustein. A methyl-CpG-binding protein 2-enhanced green fluorescent protein reporter mouse model provides a new tool for studying the neuronal basis of Rett Syndrome. *Neuroreport*, 19(4):393–8, 2008.

[19] T. M. Yusufzai and A. P. Wolffe. Functional consequences of Rett Syndrome mutations on human MeCP2. *Nucleic Acids Res*, 28(21):4172–9, 2000.

[20] P. O. Mari, B. I. Florea, S. P. Persengiev, N. S. Verkaik, H. T. Bruggenwirth, M. Modesti, G. Giglia-Mari, K. Bezstarosti, J. A. Demmers, T. M. Luider, A. B. Houtsmuller, and D. C. van Gent. Dynamic assembly of end-joining complexes requires interaction between Ku70/80 and XRCC4. *Proc Natl Acad Sci U S A*, 103(49):18597–602, 2006.

[21] M. J. Mone, M. Volker, O. Nikaido, L. H. Mullenders, A. A. van Zeeland, P. J. Verschure, E. M. Manders, and R. van Driel. Local UV-induced DNA damage in cell nuclei results in local transcription inhibition. *EMBO Rep*, 2(11):1013–7, 2001.

[22] M. Volker, M. J. Mone, P. Karmakar, A. van Hoffen, W. Schul, W. Vermeulen, J. H. Hoeijmakers, R. van Driel, A. A. van Zeeland, and L. H. Mullenders. Sequential assembly of the nucleotide excision repair factors in vivo. *Mol Cell*, 8(1):213–24, 2001.

[23] J. X. Pan, Y. Liu, S. P. Zhang, T. C. Tu, S. D. Yao, and N. Y. Lin. Photodynamic action of actinomycin D: an EPR spin trapping study. *Biochim Biophys Acta*, 1527(1-2):1–3, 2001.

[24] G. Giglia-Mari, C. Miquel, A. F. Theil, P. O. Mari, D. Hoogstraten, J. M. Ng, C. Dinant, J. H. Hoeijmakers, and W. Vermeulen. Dynamic interaction of TTDA with TFIIH is stabilized by nucleotide excision repair in living cells. *PLoS Biol*, 4(6):e156, 2006.

[25] M. Marchi, A. Guarda, A. Bergo, N. Landsberger, C. Kilstrup-Nielsen, G. M. Ratto, and M. Costa. Spatio-temporal dynamics and localization of MeCP2 and pathological mutants in living cells. *Epigenetics*, 2(3):187–97, 2007.

[26] G. T. van der Horst, H. van Steeg, R. J. Berg, A. J. van Gool, J. de Wit, G. Weeda, H. Morreau, R. B. Beems, C. F. van Kreijl, F. R. de Gruijl, D. Bootsma, and J. H. Hoeijmakers. Defective transcription-coupled repair in Cockayne Syndrome B mice is associated with skin cancer predisposition. *Cell*, 89(3):425–35, 1997.

[27] I. Gaudreault, D. Guay, and M. Lebel. YB-1 promotes strand separation in vitro of duplex DNA containing either mispaired bases or cisplatin modifications, exhibits endonucleolytic activities and binds several DNA repair proteins. *Nucleic Acids Res*, 32(1):316–27, 2004.

[28] H. Izumi, T. Imamura, G. Nagatani, T. Ise, T. Murakami, H. Uramoto, T. Torigoe, H. Ishiguchi, Y. Yoshida, M. Nomoto, T. Okamoto, T. Uchiumi, M. Kuwano, K. Funa, and K. Kohno. Y box-binding protein-1 binds preferentially to single-stranded nucleic acids and exhibits 3'–>5' exonuclease activity. *Nucleic Acids Res*, 29(5):1200–7, 2001.

[29] G. Forlani, E. Giarda, U. Ala, F. Di Cunto, M. Salani, R. Tupler, C. Kilstrup-Nielsen, and N. Landsberger. The MeCP2/YY1 interaction regulates ANT1 expression at 4q35: novel hints for Rett Syndrome pathogenesis. *Hum Mol Genet*, 19(16):3114–23, 2010.

[30] S. Wu, Y. Shi, P. Mulligan, F. Gay, J. Landry, H. Liu, J. Lu, H. H. Qi, W. Wang, J. A. Nickoloff, C. Wu, and Y. Shi. A YY1-INO80 complex regulates genomic stability through homologous recombination-based repair. *Nat Struct Mol Biol*, 14(12):1165–72, 2007.

[31] L. V. Solovjeva, M. P. Svetlova, V. O. Chagin, and N. V. Tomilin. Inhibition of transcription at radiation-induced nuclear foci of phosphorylated histone H2AX in mammalian cells. *Chromosome Res*, 15(6):787–97, 2007.

[32] K. M. Miller, J. V. Tjeertes, J. Coates, G. Legube, S. E. Polo, S. Britton, and S. P. Jackson. Human HDAC1 and HDAC2 function in the DNA-damage response to promote DNA NonHomologous End-Joining. *Nat Struct Mol Biol*, 17(9):1144–51, 2010.

[33] H. M. O'Hagan, H. P. Mohammad, and S. B. Baylin. Double strand breaks can initiate gene silencing and SIRT1-dependent onset of DNA methylation in an exogenous promoter CpG island. *PLoS Genet*, 4(8):e1000155, 2008.

[34] E. Citterio, V. Van Den Boom, G. Schnitzler, R. Kanaar, E. Bonte, R. E. Kingston, J. H. Hoeijmakers, and W. Vermeulen. ATP-dependent chromatin remodeling by the Cockayne Syndrome B DNA repair-transcription-coupling factor. *Mol Cell Biol*, 20(20):7643–53, 2000.

[35] A. S. Balajee, A. May, G. L. Dianov, E. C. Friedberg, and V. A. Bohr. Reduced RNA polymerase II transcription in intact and permeabilized Cockayne Syndrome group B cells. *Proc Natl Acad Sci U S A*, 94(9):4306–11, 1997.

[36] C. P. Selby and A. Sancar. Cockayne Syndrome group B protein enhances elongation by RNA polymerase II. *Proc Natl Acad Sci U S A*, 94(21):11205–9, 1997.

[37] J. de Boer and J. H. Hoeijmakers. Nucleotide excision repair and human syndromes. *Carcinogenesis*, 21(3):453–60, 2000.

[38] J. Miralves, E. Magdeleine, L. Kaddoum, H. Brun, S. Peries, and E. Joly. High levels of MeCP2 depress MHC class I expression in neuronal cells. *PLoS One*, 2(12):e1354, 2007.

[39] N. C. Andrews and D. V. Faller. A rapid micropreparation technique for extraction of DNA-binding proteins from limiting numbers of mammalian cells. *Nucleic Acids Res*, 19(9):2499, 1991.

Conclusion

In 1999, Dr Zoghbi's group revealed for the first time that mutations in the MeCP2 gene are the cause of Rett syndrome. From 1999 until now, several milestone progresses have been made to understand and identify the function of MeCP2 in the cell. It is quite clear now that MeCP2 is a complex multifunctional protein controlling the genomic integrity at different level. It has a role in chromatin remodeling, transcription, mRNA splicing and the maintenance of the DNA methylation profile. This can explain the large variety of symptoms observed in Rett patients.

Our work allowed us to establish new tools to detect the protein and to suggest a potential new role of MeCP2 in the DNA damage response.

The first part of my thesis was dedicated to develop new antibodies specific to each isoform of MeCP2 and to explore the expression of each isoform in vivo. It is hoped that this will ultimately help to understand their respective contributions to Rett syndrome. We showed that antibodies we generated can be used to perform Western blot, Immunofluorescence and Immunohistochemistry experiments. Recent results in our laboratory have shown that these antibodies can be also used for immunoprecipitation of native chromatin (NChIP). In order to study the expression of each isoform in vivo, we performed immunohistochemistry study on brain tissue of P24 and P55 Wt and MeCP2 KO mice. Results showed the expression of the MeCP2e1 isoform in different structures of the brain such as the hippocampus, the paraventricular nucleus and the arcuate nucleus. In this study we were unable to detect any expression of MeCP2e2 isoform. These results were confirmed by western blot techniques performed on brain tissue but also on other organs like lung, heart, liver, thymus, spleen and kidney. Western blot analyses revealed the presence of MeCP2e1 protein at high levels in the CNS, and a little in the lung and kidney.

Consequently we suggest that the MeCP2e1 isoform is the most abundant form in the or-

ganism, whilst the MeCP2e2 isoform is expressed at such low levels that it was not detected in our experiments.

The second part of my project was to understand the role of the MeCP2 protein in the DNA damage response. Indeed we showed that MeCP2 accumulate on the damaged DNA. We also demonstrated that the recruitment of MeCP2 to the lesions was independent from transcription, GG-NER and TC-NER pathways but depends on the C-terminal region of MeCP2. This region is important for the binding of MECP2 on the unmethylated DNA and for its protein / protein interactions.

My results revealed also that in the absence of the Cockayne syndrome protein, CSB, MeCP2 were unable to bind tightly to the chromatin.

It is important now to understand the function of MeCP2 in the DNA damage response: Does the protein act directly in the repair pathway? Does it recognize the damage and constitute a platform to recruit all other proteins implicated directly in the repair? Does MeCP2, as a chromatin remodeler, modify the chromatin in the damaged region to allow the recruitment of proteins implicated in DNA repair? Does MeCP2 have a role in reconstituting chromatin after DNA damage?

To determine in which pathway MeCP2 could be involved, the MeCP2-GFP construct can be expressed in other DNA repair deficient cell lines (Ku80-/-, BRCA1-/-, OGG1-/- or PARP-1-/-, etc.). The recruitment will be monitored after damage induction with laser micro-irradiation or photo-activated actinomycin D. We can also identify the type of lesions recognized by MeCP2 by using different damaging agents (UV, Ionizing Radiation, Paraquat, Mitomycin-C, MMS, etc.).

It is known that transcription is inhibited at the site of damaged area. Does MeCP2 act as a transcription repressor at the lesion sites? To answer this question, transcription activity can be measured in locally damaged region after BrU incorporation in MeCP2-/- cells *vs* Wt.

It is interesting also to understand the relationship between MeCP2 and CSB. Does MeCP2 interact directly with CSB? Can MeCP2 be found in the same complex with CSB? Immunoprecipitation or ChiP experiments with or without DNA damage followed by Mass Spectrometry analysis can be performed to answer this question.

All these results increase the complexity to understand the real function of MeCP2 in the cell. The fact that the C-terminal region of MeCP2 is important for it's binding to damaged

DNA, and that this kind of mutations is found in Rett patients suggest that this novel role for MeCP2 should be considered in the pathogenesis of Rett syndrome.

On the other hand we observed that Cockayne syndrome patients present clinical symptoms very similar to those observed in Rett patients. The fact that the binding of MeCP2 to the chromatin is altered in the absence of CSB can explain the neurological problems observed in patients with Cockayne syndrome.

It is hoped that the results obtained in the course of this research project will pave the way towards a better understanding of MeCP2's many function, and ultimately helps to designing therapies for Rett syndrome patients.

Studying the MeCP2 protein:
Exploring its involvement in the DNA Damage Response, and developing new tools for its detection.

Appendix

A Appendix

High Levels of MeCP2 Depress MHC Class I Expression in Neuronal Cells

Julie Miralvès[1], Eddy *Magdeleine*[1], Lara *Kaddoum*[1], Hélène *Brun*[2], Sophie *Peries*[1], Etienne *Joly*[1]

[1]Institut de Pharmacologie et Biologie Structurale, Centre National de la Recherche Scientifique (CNRS), Toulouse, France

[2] Centre de Physiopathologie Toulouse-Purpan, INSERM, Toulouse, France

Adapted from **PLoS One. 2007 Dec 26;2(12):e1354**

A

A.1 Abstract

Background. The expression of MHC class I genes is repressed in mature neurons. The molecular basis of this regulation is poorly understood, but the genes are particularly rich in CpG islands. MeCP2 is a transcriptional repressor that binds to methylated CpG dinucleotides; mutations in this protein also cause the neurodevelopmental disease called Rett syndrome. Because MHC class I molecules play a role in neuronal connectivity, we hypothesised that MeCP2 might repress MHC class I expression in the CNS and that this might play a role in the pathology of Rett syndrome. **Methodology.**We show here that transiently transfected cells expressing high levels of MeCP2 specifically downregulate cell-surface expression of MHC class I molecules in the neuronal cell line N2A and they prevent the induction of MHC class I expression in response to interferon in these cells, supporting our first hypothesis. Surprisingly, however, overexpression of the mutated forms of MeCP2 that cause Rett syndrome had a similar effect on MHC class I expression as the wild-type protein. Immunohistological analyses of brain slices from *MECP2* knockout mice (the $MeCP2^{tm1.1Bird}$ strain) demonstrated a small but reproducible increase in MHC class I when compared to their wild-type littermates, but we found no difference in MHC class I expression in primary cultures of mixed glial cells (mainly neurons and astrocytes) from the knockout and wild-type mice. **Conclusion.**These data suggest that high levels of MeCP2, such as those found in mature neurons, may contribute to the repression of MHC expression, but we find no evidence that MeCP2 regulation of MHC class I is important for the pathogenesis of Rett syndrome.

A.2 Introduction

Mutations in the X-linked gene *MECP2* cause Rett syndrome (RTT) [1, 2, 3], a progressive neurodevelopmental disorder that affects around 1 in 10,000 female births [4]. Girls with RTT develop normally until 6-18 months old, when they begin to regress, losing the speech and hand skills they had acquired. Most patients develop severe mental retardation, seizures, repetitive hand movements, irregular breathing and motor-control problems [5, 6, 7]. *MECP2* encodes the methyl-CpG-binding protein 2 (MeCP2) [8, 9], which is thought to regulate gene expression, but we do not yet understand how mutations in this protein produce the pathological features of RTT.

MECP2 knockout mice [10, 11, 12] and mice expressing a truncated form of MeCP2 [13] display a RTT-like phenotype, demonstrating that MeCP2 deficiency is sufficient to induce the syndrome. Moreover, mice in which *MECP2* was conditionally deleted in neurons had a similar phenotype to RTT patients [10, 14], and MeCP2-deficient mice were cured by expression of a transgenic *MECP2* gene specifically in post-mitotic neurons [15]. These findings indicate that the pathology of RTT is due to the lack of MeCP2 in the mature central nervous system (CNS). Two recent studies have shown that the neurological defects in mutant mice are reversed by restoration of MeCP2 expression in neurons, even at late postnatal stages [16, 17], suggesting that gene therapy may be feasible.

The *MECP2* mRNA is alternatively spliced to generate two protein isoforms (MeCP2*A* and MeCP2*B*) that differ at their N-termini. Both forms are expressed ubiquitously, but MeCP2*B* is more abundant than MeCP2*A* in the CNS [18, 19]. MeCP2 represses transcription [20] by binding through its methyl-CpG-binding domain (MBD) [21] to methylated CpG nucleotides [22, 23] and recruiting co-repressors that bind to its transcription repression domain (TRD) [24, 25, 26, 27]. Other studies, however, indicate that MeCP2 is a multifunctional protein that affects gene regulation at many levels: MeCP2 interacts with an RNA-binding protein called Y box-binding protein 1 to regulate splicing of target RNAs [28, 29]; two studies suggest that MeCP2 influences gene expression by participating in chromatin architecture, independently of its capacity to bind methylated DNA [30, 31]; moreover, MeCP2 associates with the DNA methyltransferase Dnmt1 bound to hemi-methylated DNA and may thus participate in maintaining the methylation state of newly synthesised DNA [32, 33].

Our knowledge of the activities of MeCP2 suggests that the pathologies associated with *MECP2* mutations are most likely due to the misregulation of neuronal genes. Several studies have identified possible target genes that are controlled by MeCP2, including the gene encoding brain-derived neurotrophic factor (BDNF) [34, 35, 36], genes encoding inhibitors of differentiation [37], and genes regulated by glucocorticoids [38]; their expression is altered in *MECP2* knockout mice, but whether this is responsible for the neuropathology seen in RTT remains questionable.

We hypothesised that genes encoding MHC class I molecules (MHC class I) might be amongst those that MeCP2 regulates in the CNS because these genes have a particularly high CG content [39]. Two studies have demonstrated that expression of MHC class I is dynamically regulated during the post-natal development of the CNS and that MHC class I ex-

pression is necessary for the activity-dependent synaptic rearrangements that occur during normal brain development and for normal synaptic plasticity in the mature hippocampus [40, 41]. If MHC class I expression was regulated by MeCP2, defects in these developmental functions of MHC class I might contribute to the symptoms of RTT.

MHC class I is generally not expressed in adult brain except in response to cytokines (i.e. inflammation) or injury [42]. This is believed to protect nervous tissue, which regenerates poorly, from cytotoxic attack by the immune system. Several lines of evidence, however, suggest that MHC class I is expressed in specific areas of the mature brain, as well as during brain development, and they evoke a function for MHC class I molecules in neuronal signalling [41, 43, 44, 45, 46]. This suggests that, rather than being simply shut down, MHC class I genes must be very finely regulated throughout the CNS by activators and inhibitors that, on the one hand, allow their function during development and, on the other hand, ensure their silencing in the majority of neurons in which their expression could be detrimental.

We reasoned that misregulated expression of MHC class I in the brain due to mutations in MeCP2 might disturb the establishment and maintenance of neuronal connections and remodelling in the hippocampus during early child development and thus account for the neurodevelopmental disorders of RTT. We therefore investigated whether MHC class I gene expression is under the control of MeCP2 in neuronal cell lines in culture and whether MHC class I gene expression is affected in *MECP2* knockout mice.

A.3 Results

A.3.1 Overexpression of MeCP2 downregulates basal MHC class I

To investigate whether MeCP2 represses MHC class I expression, we transfected the murine neuronal cell line N2A with pCMX plasmids that transiently express either human or murine MeCP2*A*. Forty-eight hours after transfection, we evaluated by flow cytometry the cell surface levels of K^k, L^d and D^d (the three 'classical' MHC class I molecule heavy chains expressed by N2A), β-2-microglobulin (the light chain subunit of MHC class I) and, as control, the transferrin receptor, a cell surface glycoprotein of similar size and half-life to MHC molecules (Figure A.1). The expression of MeCP2 in transfected cells was detected by a rabbit anti-MeCP2 polyclonal antibody on cells fixed and permeabilised after they had

been stained for MHC class I cell surface expression. Dot plot representative examples of these analyses are shown on Figure A.1A, where each dot represents an individual cell, and an decrease in MHC staining results in a shift to the left, and an increase in MeCP2 in an upward shift. Because these are transient transfections, MeCP2 overexpression is detected in only a certain percentage (typically 20-30%) of the cells. As can be seen for all MHC class I molecules (K^k, L^d, D^d) and β-2-microglobulin, in the cloud of cells overexpressing MeCP2, we detected a clear shift to the left compared to the lower cloud of untransfected cells and to mock-transfected cells, indicating a reduction of the cell surface expression of all these molecules in the cells that overexpress MeCP2. This effect appears to be specific for these molecules since the level of transferrin receptor was basically unaffected by MeCP2 overexpression. The reproducibility and statistical significance of these observations was ascertained by repeating this experiment many times, which also allowed us to conclude that MeCP2 overexpression results in a similar 40% decrease of all three MHC class I molecules and of β-2-microglobulin (Figure A.1B). In the experiment shown, the mock-transfected cells were simply treated with the transfection reagent, but similar results were obtained when the negative control consisted of empty plasmids, or plasmids expressing other proteins such as GFP (not shown).

No functional difference has been described between the two isoforms of MeCP2, MeCP2*A* and MeCP2*B*. We therefore explored whether these two isoforms had the same effect on MHC class I molecules and whether their effects might differ according to the cell type in which they are expressed. We transfected vectors encoding the Myc-tagged version of human MeCP2*A* or MeCP2*B* into either N2A or the mouse fibroblast cell line NIH 3T3. In this experiment, we detected MeCP2 expression by using an anti-Myc9E10 monoclonal antibody because it produced a much stronger signal than the anti-MeCP2 antibody. The level of MHC class I was evaluated at the same time by using a rat anti-pan-MHC antibody, M1/42. The double staining in mock-transfected and transfected cells was analysed by flow cytometry. MeCP2 overexpression induced a similar extent of repression of MHC class I irrespective of the isoform or cell type in which it was expressed (Figure A.1C): the cell surface level of MHC class I decreased by approximately 35% when compared to the basal level (p<0.01 in N2A; p<0.001 in NIH 3T3) when either MeCP2*A* or MeCP2*B* were overexpressed in N2A or in NIH 3T3 cells.

We noted a correlation in these experiments between the repressive effect exerted by

A

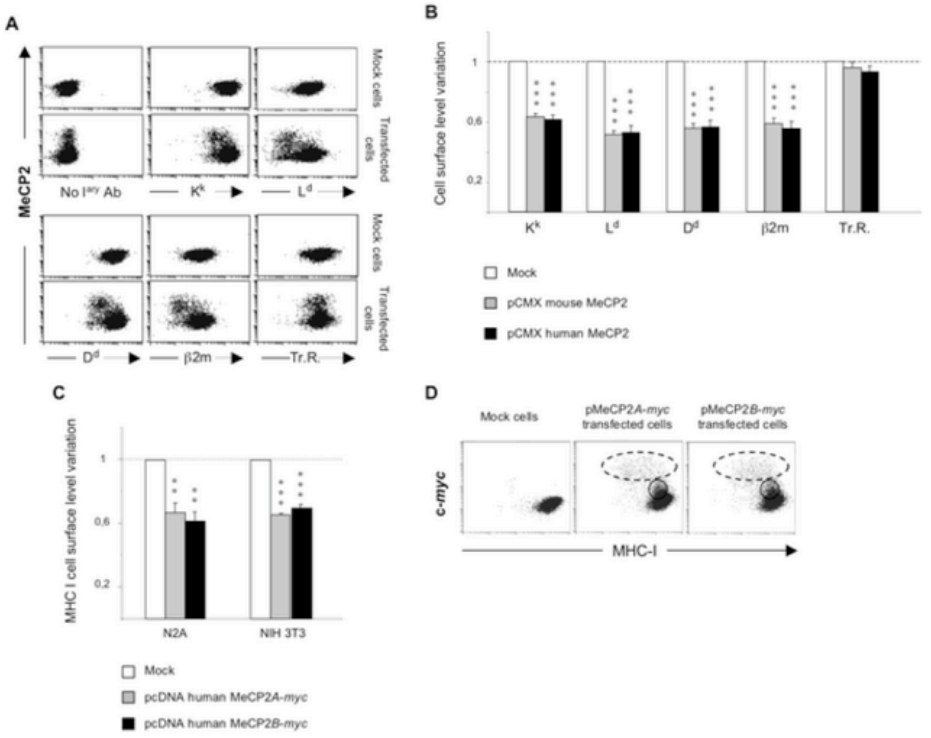

Figure A.1 — MeCP2 overexpression diminishes MHC class I expression. N2A cells transfected with pCMX vectors expressing either murine or human MeCP2 were immunostained for one of the three MHC class I molecules (K^k, L^d or D^d), β2-microglobulin or the transferrin receptor on the cell surface as well as for intracellular MeCP2. The level of staining was then analysed by fluorescence-activated cell sorting. Panel A: Dot plots of the amount of surface antigen (x-axis) against the amount of intracellular MeCP2 (y-axis) in cells transiently transfected with pCMX expressing human MeCP2 and analysed 48 hrs later. Panel B: For each kind of staining, the variation in expression level was calculated as the ratio of MFI of MeCP2 overexpressing cells over MFI of mock-transfected cells. The histograms summarise the mean (±SEM) of the variation in cell surface levels from 15 independent transfections with vectors expressing mouse MeCP2A (grey fill) and 12 independent transfections with vectors expressing human MeCP2*A* (black fill). Panel C: N2A and NIH3T3 cells were transfected with empty pcDNA3.1(+) (mock cells) or expressing Myc-tagged human MeCP2*A* or *B* isoforms. 48 h after transfection, cells were subjected to double staining against cell surface MHC class I molecules and intracellular Myc-tagged MeCP2, then analyzed by flow cytometry. The variation in expression level of MHC class I molecules was calculated as the ratio of MFI of MeCP2 over-expressing cells over the MFI of mock cells. The histograms represent the mean (±SEM) of the cell surface level variation from 4 independent transfections with each of the vectors. Panel D: A representative example of dot-plots obtained for double immunostaining of transiently transfected N2A cells with anti-Myc 9E10 and rat-anti-mouse-MHC I M1/42 monoclonal antibodies. Dotted and continuous circles indicate the different populations expressing high and intermediate levels of MeCP2, respectively. Statistical significance of difference between groups was analysed by using an unpaired t-test ($**$, p<0.01; $***$, p<0.001).

MeCP2 on MHC class I and β-2-microglobulin and the quantity of MeCP2 expressed by the transfected cells: cells expressing high levels of MeCP2 (dotted circle, Figure A.1D) had less MHC class I on their surface than cells expressing MeCP2 at lower levels (continuous circle), which expressed levels of MHC class I similar to those in cells in which no MeCP2 staining

was detected and to those in mock-transfected cells. Repression of MHC class I expression by MeCP2 therefore appears to require very high levels of MeCP2. We generated stably transfected lines of N2A expressing either MeCP2*A* or MeCP2*B* but the levels of protein expressed by these cells was relatively low (at best comparable to those in the continuous circle in Figure A.1D). It is therefore of little surprise that the levels of MHC class I expressed by those cells was not discernibly different from that of untransfected cells (not shown). Evaluation by quantitative western blot of the levels of MeCP2 protein expressed in these various transfected cells revealed bands of comparable intensities in stable transfectants and in brain extracts, and bands that were two to five fold more intense in transiently transfected populations (not shown). Since mature neurons represent approximately 15% of all cells in the brain parenchyma, we can further estimate that our stable transfectants express levels of MeCP2 which are roughly one sixth of those found in mature neurons. Conversely, since the efficiency of the transient transfections in this experiment was approximately 10%, we estimate that the levels of MeCP2 attained in high expressors after transient transfections are 20 to 50 fold higher than the levels in stable transfectants (and therefore three to eight fold higher than in intra-cerebral neurons).

A.3.2 Overexpression of MeCP2 markedly reduces MHC class I upregulation by IFN-γ

The cytokine IFN-γ transactivates MHC class I expression predominantly by binding to IFN regulatory factor-1, which binds, in turn, to the interferon-stimulated response element, ISRE, a GC-rich region and therefore a potential binding site also for MeCP2 [47]. Since MeCP2 appeared to act as a repressor of MHC class I expression (Figure A.1), we wanted to test whether it would interfere with transactivation of MHC class I expression by IFN-γ. To do so, we transfected N2A cells with pCMX vectors driving the expression of either murine or human forms of MeCP2*A*. The following day, these transiently transfected cells were divided into two flasks that were either treated or not with IFN-γ for 48hrs. The levels of cell-surface MHC class I, β-2-microglobulin and transferrin receptor, and intracellular MeCP2, were evaluated by flow cytometry as in the previous experiments (Figure A.2). As can be seen by the shift of the clouds between the higher and the lower panels, treatment with IFN-γ resulted in a two- to four-fold induction of MHC class I and β2-microglobulin in both mock-transfected populations and transfected populations (Figure A.2A). Individ-

A

ual transfected cells expressing MeCP2 at high levels, however, had little more L^d and β2-microglobulin when treated with IFN-? than untreated MeCP2-expressing cells (compare the populations encircled in Figure A.2A IFN-γ with those without IFN-γ). Cells overexpressing MeCP2 therefore appear to respond to IFN-γ by upregulating MHC class I to a much lesser extent than do cells not expressing MeCP2.

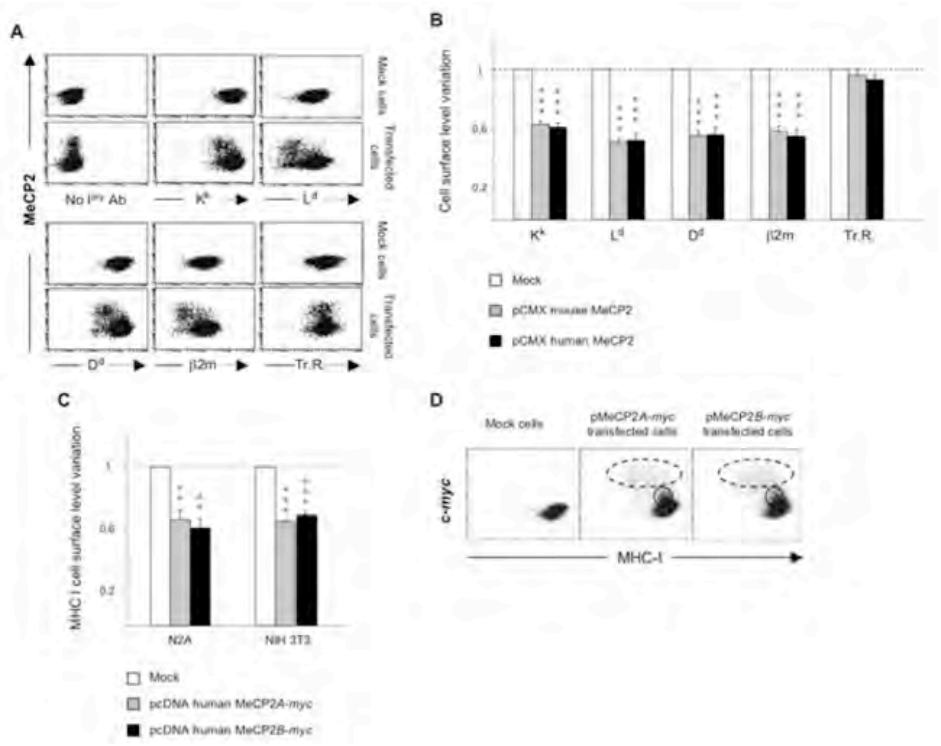

Figure A.2 — Transient overexpression of MeCP2 inhibits MHC class I induction by IFN-γ. N2A cells transfected with pCMX vectors expressing murine or human MeCP2 were treated or not with IFN-γ for 48 hrs and then double immunostained for cell surface β2-microglobulin, transferrin receptor or MHC class I and intracellular MeCP2. Panel A: Dot-plots of transfected cells analysed by flow cytometry showing the cell surface level of the MHC class I molecule L^d or β2-microglobulin (x-axis) plotted against the level of intracellular MeCP2 (y-axis). Panel B: The induction factor was calculated as the ratio of MFI of treated cells (over-expressing MeCP2 or untransfected cells) on MFI of untreated N2A cells. Values used for the histogram are the mean (±SEM) of induction factors obtained in seven independent transfection experiments. Statistical significance of difference between groups was analysed by using an unpaired t-test ($*$, p<0.05; $**$, p<0.01; $***$, p<0.001).

The statistical significance of the differences in response to IFN-γ was confirmed for all three MHC class I molecules expressed by the N2A cell line (K^k, L^d, D^d) and for β-2-microglobulin in six independent experiments (Figure A.2B), whereas the levels of transferrin receptor were not significantly affected. This effect was also observed in other cell lines such as NIH 3T3 fibroblasts and human HEK 293 cells (not shown).

A.3.3 MeCP2 mutants retain their repressive effect on MHC class I expression

Many disease-causing mutations of *MECP2* have been described [48]. Among them, some occur more frequently than others, and/or have been more thoroughly characterised. To investigate the effect of these *MECP2* mutations on MHC class I expression, we transiently transfected the N2A cell line with plasmids expressing well-characterised mutants of both the A and B isoforms of MeCP2 (T158M, R133C, R306C and R308$*$). The point mutations T158M, R133C and R306C are located in the functional MBD and TRD domains of the protein (Figure A.3A). The mutant form that is truncated after the R308 residue corresponds to the form of MeCP2 found in the mouse model of RTT generated by Dr. Zoghbi's group [13]. We performed mutagenesis on vectors expressing either the A or B form of Myc-tagged MeCP2. All the mutated plasmids were sequenced and checked for functional expression and intracellular localisation of the wild-type and mutated MeCP2 proteins by anti-Myc immunofluorescence on transiently transfected N2A cells (Figure A.3B). All the mutant forms of Myc-taged MeCP2 were located in intranuclear punctate structures typical of the wild-type protein, which forms foci on heterochromatin [49, 23] (data is shown for the R133C MeCP2*A*-Myc mutant and the wild-type pMeCP2*A*-Myc protein only). Subsequently, we evaluated the cell-surface expression level of MHC class I in the transiently transfected N2A cells by flow cytometry using the rat anti-pan-MHC I antibody M1/42, as before. The intracellular MeCP2 level was evaluated based on the intensity of immunostaining for the Myc tag, and was found to be similar to the wild-type for both the A and B forms of the four mutants. The R133C MeCP2*A*-Myc mutant had the same effect as its wild-type counterpart on the cell-surface level of MHC class I (Figure A.3C), whereas neither mutant nor wild-type had a significant effect on expression of the transferrin receptor (not shown). Similar effects were found for both A and B isoforms of all four mutants tested (Data for T158M R306C and R308$*$ are not shown). Thus, these mutations responsible for RTT do not abolish the repressive effect of MeCP2 on MHC class I in cells in culture. These results strongly suggest that the repressive function of MeCP2 on the levels of MHC molecules expressed by transiently transfected cells in vitro is unlikely to be directly related to the pathogenesis of Rett syndrome.

A

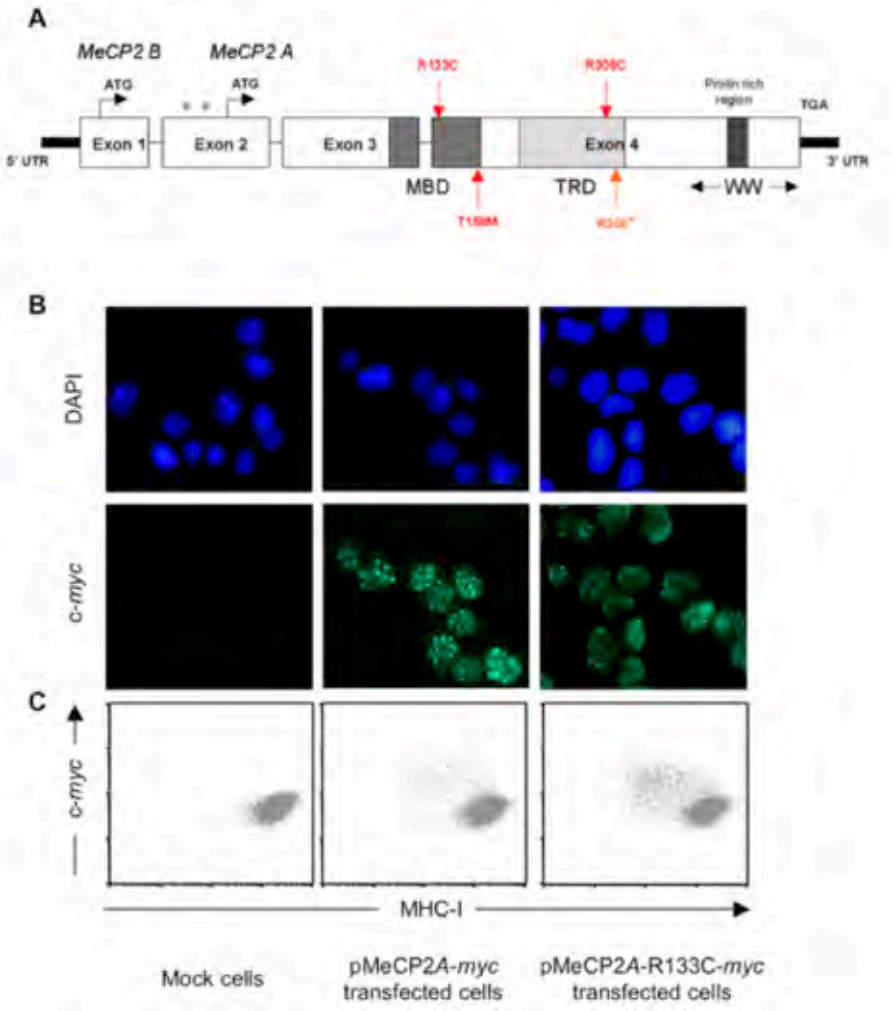

Figure A.3 — TMutant forms of MeCP2 that cause RTT retain their repressive effect on MHC class I expression. Panel A: Schematic representation of the MeCP2 protein. Red and orange arrows indicate the positions of the mutations introduced in MeCP2 by site-directed mutagenesis (MBD: methyl-CpG binding domain, TRD: transcription repression domain, WW: group II WW-domain-binding region). Panel B: N2A cells transfected with empty pcDNA3.1 (mock cells), with pcDNA3.1 expressing Myc-tagged MeCP2*A* (pMeCP2*A*-*myc*) or with pcDNA3.1 expressing Myc-tagged MeCP2*A* with the R133C point mutation (pMeCP2*A*-R133C-*myc*) were stained with mouse anti-Myc 9E10 monoclonal antibody, and FITC-labelled anti-mouse IgG antibody. Coverslips were mounted in DAPI-containing ProLong Gold antifade reagent (Molecular Probes) before observation by fluorescence microscopy. Panel C: N2A cells transfected as in panel B were double immunostained for cell surface MHC class I and intracellular Myc-tagged MeCP2, then analysed by flow cytometry. Similar data were obtained for all four mutated forms of MeCP2*A* and MeCP2*B* (not shown), and these observations were reproduced in three independent transfection experiments.

A.3.4 Expression of MHC class I in cells from MeCP2-knockout mice is no different to that in cells from wild-type mice

Our data from experiments with cells in culture (above) suggest that the genes encoding MHC class I and β2-microglobulin are controlled by MeCP2; overexpression of normal

MeCP2 downregulates their expression. To find out whether this is the case in vivo, we investigated whether neuronal cells from MeCP2 knockout mice ($MeCP2^{tm1.1Bird}$) contained elevated levels of MHC class I by performing immunohistochemistry on frozen brain sections of MECP2 knockout hemizygous male (-/y) mice and of their wild-type littermates using two different rat monoclonal antibodies directed against mouse MHC class I molecules. The results we obtained suggest that there are slightly higher levels of MHC class I expression in some regions of the brains of MeCP2 knockout mice than in the same regions of the wild-type control brains (Figure A.4). Although these differences were not always seen for all brain areas of MECP2 knockout mice compared to their control littermates, when a difference was seen, it was always for higher expression in MECP2 knockout animals.

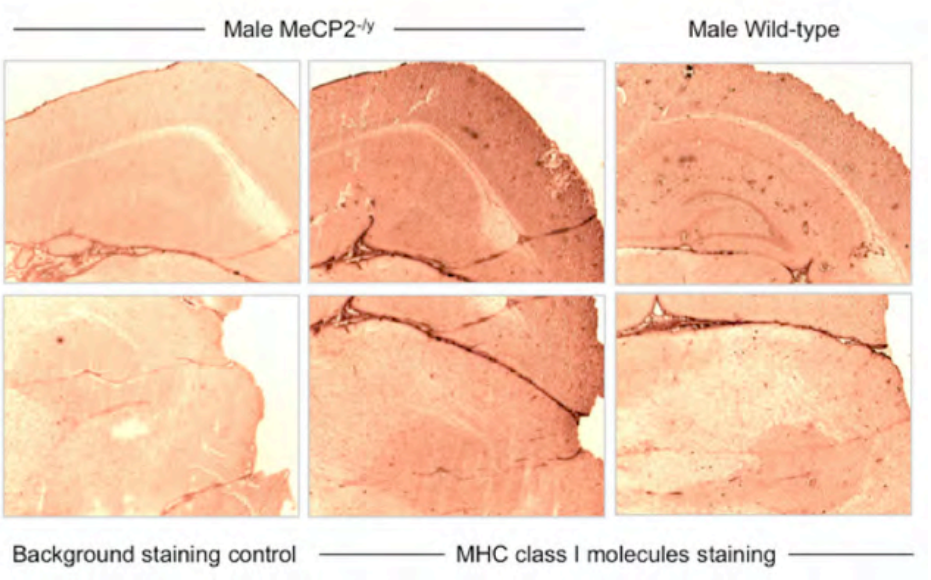

Figure A.4 — Evaluation of MHC class I expression in adult mouse brain slices. Serial frozen sections of adult male wild-type and $MeCP2^{-/y}$ littermates were analysed for expression of MHC class I by immunohistochemistry using the rat R1-21.2 monoclonal antibody and EnVision detection technology (Dako). For the negative control, the same staining process was used omitting the primary antibody. Similar results were obtained with the M1/42 monoclonal antibody. Similar results were obtained in independent experiments on brains from three different pairs of mice.

The immunohistochemistry approach did not allow us to quantify the small variations we observed in MHC class I expression between MeCP2 knockout and wild-type mice or to identify the cell types that expressed MHC class I in the absence of MeCP2 (neurons, astrocytes, oligodendrocytes or endothelial cells). We therefore decided to look at primary cultures of brain cells (called mixed glial cells; MGCs) and fibroblasts from spleen taken from individual 2-day-old mice born from crossing a heterozygous female ($MeCP2^{tm1.1Bird+/-}$) with a wild-type male. The tail DNA from each newborn mouse used to prepare the cell

lines was analysed to establish the genotype of each culture. On the second day of culture, the MGCs were treated with IFN-γ or not and then analysed two days later for expression of MHC class I on the cell surface by flow cytometry (Figure A.5). The fibroblast cultures, which took a few more days to establish, were similarly treated with IFN-γ after five days and analysed on the seventh day. Figure A.5A shows typical examples of histograms obtained with wild-type and $MeCP2^{tm1.1Bird-/y}$ male littermates. Similar data were obtained for all four genotypes: wild-type female (+/+) and male (+/y), heterozygous mutant female ($MeCP2^{tm1.1Bird-/+}$) and hemizygous mutant male ($MeCP2^{tm1.1Bird-/y}$).

Neurons, which we identified by their expression of βIII-tubulin and their smaller size (see population R2, inset Figure A.5A), had no detectable MHC class I (grey-filled curves) when compared to background (white-filled curves), and treatment with IFN-γ induced a small amount of MHC class I in cells from both the wild-type and knockout animals. Astrocytes, which comprise the majority of the population of large cells [50] (population R1, inset Figure A.5A), spontaneously expressed more MHC class I, which was highly induced by IFN-γ but no significant differences were seen between the two genotypes. Although the populations in the cultures of spleen-derived fibroblasts were much more heterogeneous, similar levels of MHC class I were found in the cells from the wild-type and knockout animals. These measurements were performed on cell cultures derived from 24 newborn animals from nine independent litters, with very similar results.

To compare data obtained in independent experiments, we plotted the fold-induction of MHC class I expression after treatment with IFN-γ compared to untreated cells. Figure A.5B displays the fold-induction of MHC class I by IFN-γ in each cell culture derived from an individual mouse as well as the mean for cell cultures of each genotype. No significant differences were found between wild-type and MeCP2-knockout cells. The deficiency in MeCP2 thus affects neither the basal nor the inducible MHC class I expression level in primary MGC cultures.

A.4 Discussion

Reports by Shatz and colleagues [40, 51, 41] have demonstrated clearly that tight regulation of MHC class I genes in the CNS contributes to the establishment and maintenance of neuronal connections during development, as well as to plastic remodelling in the hip-

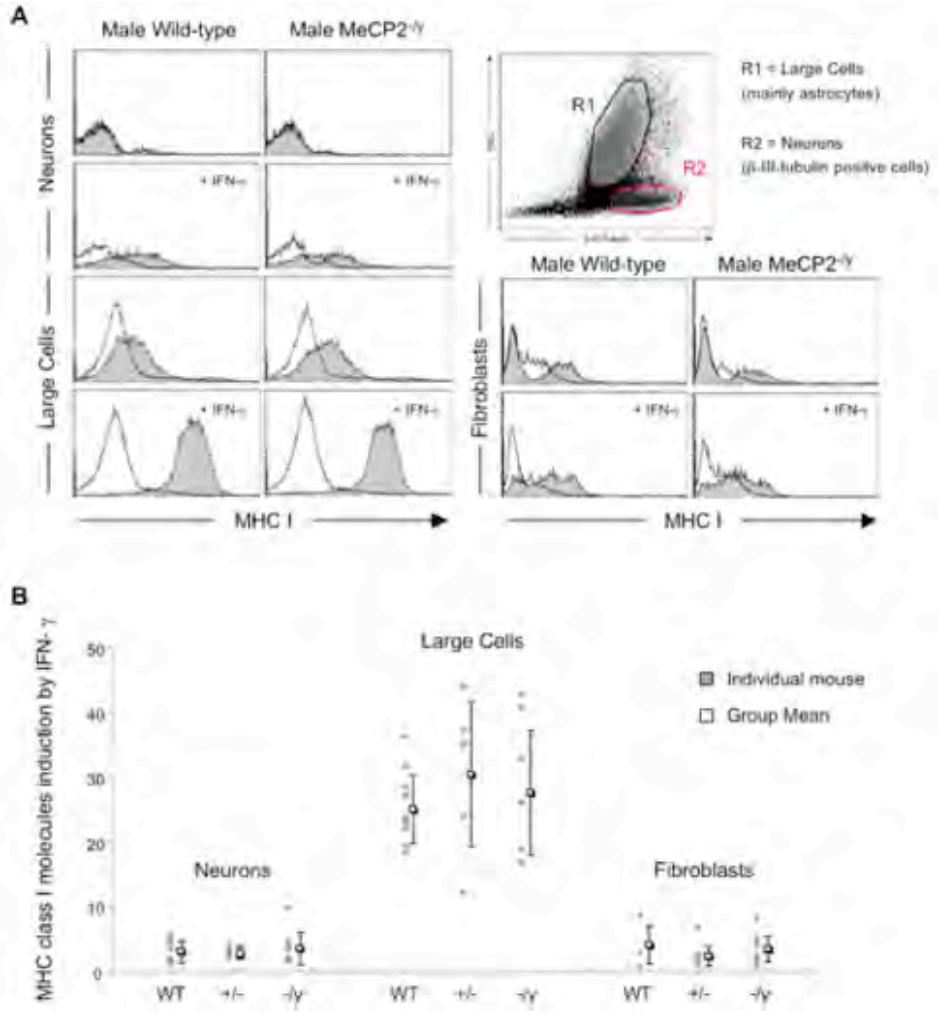

Figure A.5 — Deletion of MECP2 does not affect basal or IFN-γ -induced MHC class I expression in primary cultures of mixed glial cells. Mixed glial cell cultures established from two-day old wild-type, $MeCP2^{+/-}$ and $MeCP2^{-/y}$ mice (10, 6 and 8 animals per group, respectively) were treated or not with IFN-γ on the second day of culture and analysed two days later by flow cytometry for MHC class I expression. Neurons were identified by their intracellular staining with an anti-β-III-tubulin antibody (inset). Large cells, containing mainly astrocytes, were analysed separately by an appropriate forward/side scatter gate. Primary spleen fibroblasts from the same mice were also subjected or not to IFN-γ treatment and stained for their MHC class I expression. Panel A: Representative histograms showing cell surface staining (x axis) against cell number (y axis), obtained with cells from wild-type and $MeCP2^{-/y}$ male littermates. White-filled curves represent background staining, gray-filled curves represent MHC I-specific staining. Panel B: MHC class I fold-induction in response to IFN-γ was calculated as the ratio of MFI of treated cells (induced MHC I level) on MFI of untreated cells (basal MHC I level). Grey-filled squares show MHC class I fold-induction for individual mice and for each cell type. White-filled squares represent the group's mean of fold-inductions (±SD).

pocampus and to neuronal signalling in specific areas of the brain [40, 51, 41]. We reasoned that the transcriptional repressor MeCP2 might be involved in regulating MHC class I expression in the CNS for three main reasons. Firstly, expression of MeCP2 is strictly regulated during development [52, 53, 54] and specifically in various cell types [55] and is highest

in mature neurons [56, 57], which do not express MHC class I. Secondly, MeCP2 binds to methylated cytidine residues on CpG dinucleotides [21] and the genes for MHC class I are particularly rich in C/G residues [39]. Thirdly, mutations in the *MECP2* gene are responsible for the neurodevelopmental disorder RTT. We hypothesised that MeCP2 represses expression of MHC class I and that mutations responsible for RTT might cause the loss of this activity.

In support of the first part of this hypothesis, we showed clearly that overexpression of either of the two isoforms of MeCP2 by transient transfection of neuronal and fibroblastic cell lines results in reduced levels of MHC class I and β2-microglobulin at the cell surface. Furthermore, overexpression of MeCP2 blocked induction of MHC class I in these cells in response to IFN-γ. We could not determine whether this decreased expression of MHC class I and β2-microglobulin in response to MeCP2 overexpression was due to reduced transcription, translation or transport to the cell surface because the cells were transiently transfected; only cells that expressed high levels of MeCP2 showed reduced levels of MHC class I on their surface, so we could not quantify the levels of mRNA by RT-PCR or northern blot.

The fact that we observed very similar extents of repression of all three MHC class I forms (K^k, L^d and D^d) as well as of β2-microglobulin suggests that MeCP2 probably does not act directly on the promoters of the various loci encoding MHC class I, which are not identical. These considerations lead us to think that the effect of MeCP2 may be a more 'global', indirect mechanism than transcriptional repression by binding to methyl cytosine in the promoters.

The global decrease in cell surface MHC class I in MeCP2-expressing cells might be due to an effect on chromatin architecture encompassing the whole MHC region, which includes, in addition to the MHC class I loci, other genes involved in the assembly and transport of MHC molecules [58, 59] that might contribute to a global effect. If MeCP2 condenses the chromatin in the MHC region, this might block access of transcription factors and regulatory factors to the genes, as suggested by the work of Georgel and colleagues [30]. Such chromatin condensation would also explain the failure of IFN-γ to induce MHC class I in cells overexpressing MeCP2 if it prevented IFN regulatory factors from binding to their response element.

Our findings that the MeCP2 forms mutated either in the MBD or TRD domains conserve their repressive effect on MHC class I expression strengthen this interpretation that

MeCP2 has an indirect effect on transcription through its effect on chromatin architecture. These mutations affect only transcriptional repression by MeCP2, preventing it from binding to methylated DNA and from recruiting repressor partners, but the other functions of the protein are not affected, particularly its capacity to silence gene expression by driving chromatin condensation [30, 60] and stabilising large silencing chromatin loops [31]. The ability of MeCP2 to condense chromatin by methylation-independent DNA binding relies on regions within the N-terminal 294 residues, distinct from the MBD [30, 61].

MeCP2 induces chromatin condensation in three successive steps: first, it binds to the linker DNA between nucleosomes; second, it brings the nucleosomes together in a 'stem conformation' through DNA-protein interactions, and third, it binds to the nucleosomes themselves to produce full chromatin compaction [60]. Whereas the C-terminal region of MeCP2 is dispensable for the two first steps, it is apparently required for maximal compaction of the chromatin since the R294X mutation abolishes bridging between nucleosomes [61, 60]. By contrast, the R133C mutation, which abolishes the selective recognition of methylated DNA, retains the chromatin compaction properties of the wild-type protein [30]. The two other point mutations we tested in this study, T158M and R306C, like R133C, may retain their compaction properties and thus their repressive effect on MHC genes. Our findings with the truncated form R308$*$, which also retains the same repressive effect on MHC class I expression as the wild-type protein, indicate that the repression of MHC genes by MeCP2 does not involve the C-terminal portion of the protein. The effects of MeCP2 on MHC expression therefore probably does not involve the third step of MeCP2-induced chromatin condensation (above) but may involve a conformational change in the 'stem organization' of the chromatin around the MHC region [61, 60].

If MeCP2 represses MHC class I expression, we expected to see elevated levels of MHC class I in the brains of *MECP2* knockout mice (strain $MeCP2^{tm1.1Bird}$) when compared to mice with fully functional *MECP2* [11]. When we stained brain slices immunohistochemically with two different antibodies, we saw a small but reproducible increase in MHC class I expression in the brains of three knockout male mice when compared to those of their wild-type littermates, but these results were purely qualitative, and it was not possible to quantify these differences by immunohistochemistry. We decided, therefore, to produce primary cultures of MGCs from knockout mice in order to quantify MHC class I expression by flow cytometry. This approach also allowed us to distinguish a neuronal population, comprised

of small cells expressing βIII-tubulin, and a population of large cells comprised mostly of astrocytes. This quantitative analysis detected no difference between MHC class I levels on the surface of cells derived from animals carrying an inactivated *MECP2* gene and those from their wild-type littermates whether for the basal level of MHC class I expression or for the level induced by IFN-γ. This was true for the neuronal population and the astrocyte population, as well as for primary cultures of spleen fibroblasts.

We conclude from these studies that there may be a small quantitative increase in MHC class I in the brains of *MECP2* knockout mice when compared to the wild-type but this increase is not seen in isolated primary MGCs containing mostly neurons and astrocytes. The possibility remains that the levels of MeCP2 in these primary cell cultures were insufficient to see a difference. Indeed, our experiments with N2A cells showed that relatively high levels of MeCP2 are necessary to observe its repressive effect on MHC class I expression. Several studies have shown a direct correlation between age and MeCP2 expression, with maximal levels of expression in post-mitotic mature and differentiated neurons [62, 52, 53, 56, 57, 55]. Although the neuronal populations in our MGCs expressed βIII-tubulin, a marker of neuronal differentiation, they were very probably far from being fully mature. In support of this, we were unable to detect MeCP2 expression in neonatal MGCs by flow cytometry (not shown). The neurons that we analysed in neonate MGC might therefore have been too immature to demonstrate a defect in MHC regulation due to MeCP2 deficiency. It was, however, not feasible to obtain brain tissue from adult *MECP2* knockout animals for these studies because the mice die at around eight weeks old.

Three groups have performed transcriptome analyses on microarrays of cDNA prepared from post-mortem brain tissue of girls with RTT and from the brains of *MECP2* knockout mice [63, 64, 65]. At least one of these studies supports the idea that MeCP2 may influence MHC expression in the CNS: *Colantuoni et al.* [63] found a 5.8-fold increase in expression of the mRNA for the MHC class I molecule HLA-A in a RTT syndrome patient relative to matched controls. This small increase in MHC class I expression in the absence of MeCP2 is consistent with our hypothesis and further suggests that such subtle disregulation might be detectable only in older mice than those we used in our study.

We found that the forms of MeCP2 carrying RTT-causing mutations retained their repressive function on MHC expression in transiently transfected cells. Although this observation does not go against our findings that MeCP2 can down-regulate MHC expression in

cells where it is expressed at high levels, these results lead us to conclude that repression of MHC class I expression by MeCP2 is very probably not directly relevant to the pathogenesis of RTT. Mutations in the *MECP2* gene are also suspected to be at the origin of a large panel of other neurological diseases such as autism [66, 67], Angelman syndrome [68], X-linked mental retardation [69, 70], and severe neonatal encephalopathy [71, 72]. It may therefore be that those types of mutations responsible for other diseases could be related to the MHC-regulating activity of MeCP2. Additionally, the majority of *MECP2* mutations in RTT are loss-of-function mutations, but overexpression of *MECP2* by gene duplication in a mouse model [73], as well as in human clinical cases [74, 75, 76, 77], also causes mental retardation and progressive neurological diseases. Since high levels of MeCP2 can repress cell surface expression of MHC class I, at least in neuronal cell lines, MeCP2 overexpression might result in an overrepression of MHC gene expression in the CNS, which may contribute to certain pathologies by preventing MHC molecules from fulfilling their roles during CNS development and in synaptic plasticity [51]. Inappropriate temporal and spatial repression of MHC genes by overexpressed MeCP2 might induce defects in neuronal functions similar to those observed in β2m/TAP1 deficient mice [41]. Further experiments will be required to explore this eventuality.

This leaves us with the important conclusion that high levels of MeCP2, like those found in mature neurons, repress expression of MHC class I molecules and this may be an important physiological factor contributing to the repression of MHC class I in the CNS.

A.5 Materials and Methods

A.5.1 Mice

The *MEPC2* knockout mice ($MeCP2^{tm1.1Bird}$) were obtained from the *Institute for Stem Cell Research*, Edinburgh, UK. These mice have a RTT-like progressive neurodevelopmental disease very similar to that seen in patients; the males (-/y) suffer from a much more severe form of the disease than the heterozygous (+/-) females, and are sterile. $MeCP2^{+/-}$ female mice were mated with C57BL/6 male mice purchased from the Centre de Recherche et d'Élevage, Janvier, France. The litters obtained were genotyped initially as recommended by the Jackson Laboratory, and later with an optimised set of primers [78]. All experiments involving animals were performed in compliance with the relevant laws and institutional

guidelines.

A

A.5.2 Cell lines

The N2A and NIH 3T3 cell lines were maintained in DMEM with 10% foetal calf serum (FCS) and antibiotics. For the origin and description of these cell lines see ATCC.

A.5.3 Antibodies

Polyclonal primary antibodies: rabbit anti-MeCP2 polyclonal IgG (Upstate), mouse anti-C terminal peptide of MeCP2 (Sigma) and rabbit anti-beta III-tubulin polyclonal IgG (Abcam).

Hybridoma supernatants from clones (obtained from ATCC): 9E10 (mouse anti-myc IgG1), M1/42 (rat anti-H2 IgG_{2a}), R1-21.2 (rat anti-mouse H2 IgG_{2b}), HB25 (mouse anti-H2 K^k IgG_{2a}), 28.14.8 (mouse anti-H2 D^b, L^d and D^q IgG_{2a}), 30.5.7 (mouse anti-H2 L^d, D^q and L^q IgG_{2a}), 34.4.20 (mouse anti-H2 D^d IgG_{2a}), Y-3 (mouse anti-H2 K^b IgG_{2b}), S19.8 (mouse anti-beta 2 microglobulin b and c IgG_{2b}), R17.217 (rat anti-mouse transferrin receptor IgG_{2a}).

Secondary fluorescent antibodies: FITC goat anti-mouse IgG (Dako), fluorescein goat anti-rabbit IgG (H+L) (Molecular Probes, Invitrogen), AlexaFluor 647 goat anti-rat IgG (H+L) (Molecular Probes, Invitrogen), AlexaFluor 647 and 680 goat anti-mouse IgG (H+L) (Molecular Probes, Invitrogen).

A.5.4 Plasmids

pCMX vectors expressing mouse MeCP2α, MeCP2β and human MeCP2*A* were described previously [79, 18]. pcDNA3.1(A) vectors expressing Myc-tagged human MeCP2*A* and MeCP2*B* [19] were provided by Dr. Berge A. Minassian of the Hospital for Sick Children, Toronto, Ontario, Canada.

A.5.5 Mutagenesis

Site-directed mutagenesis of pcDNA3.1(A) vectors driving expression of Myc-tagged human MeCP2*A* and MeCP2*B* was carried out as described previously [80]. Briefly, during a first PCR reaction typically [9× (95°C for 30 s, 55°C for 1 min, 68°C for 1 min)] using

high-fidelity Taq polymerase (Invitrogen), a DNA template was generated between a forward T7 oligonucleotide (5′-GTAATACGACTCACTATAG-3′) annealing to pcDNA3.1 (A) upstream of the multiple cloning site and a reverse oligonucleotide annealing to the MeCP2 sequence and carrying the chosen mutations:

- R133C: 5′-aatcaactccactttactgcagaaggcttttccctg-3′
- T158M: 5′-ccctctcccagttaccatgaagtcaaaatcatt-3′
- R306C: 5′-gatgctgaccgtctcacgcgtcttgcacttcttgatggggag-3′

These primers were designed to produce or remove a restriction enzyme site allowing simple screening of the recovered plasmids (gain of an PstI site for R133C; gain of an NlaIII site for T158M, and loss of an SmaI site for R306C). During a second PCR reaction [9× (95°C for 30 s, 68°C for 6 min)], the newly amplified DNA fragments served as megaprimers to complete the synthesis of the remainder of the plasmids. The extension time of the last cycle was 16 min, followed by digestion with 10 U *Dpn*I at 37°C for 1 hr to destroy the original methylated plasmids. The mutated plasmids were recovered by transforming competent DH5α bacteria and they were screened by restriction digest. The sequence of the inserts corresponding to the MeCP2 open reading frame was then checked by direct sequencing.

To generate pcDNA3.1 plasmids expressing the R308$*$ truncated forms of Myc-tagged MeCP2*A* and MeCP2*B*, a PCR reaction [12× (94°C, 45 s; 50°C, 45 s; 68°C, 2 min 30 s), 12× (94°C, 45 s; 68°C, 2 min 30 s)] using high-fidelity Taq polymerase (Invitrogen), was carried out on pcDNA3.1-MeCP2A using the following oligonucleotides:

- Forward T7 primer: 5′-GTAATACGACTCACTATAG-3′
- Reverse primer: 5′-gcgtctagagagggtggacaccagca-3′

The reverse common primer, annealing in the *MECP2* sequence, was designed to include an XbaI restriction site immediately following residue 308 of MeCP2, which is also located upstream of the sequence encoding the Myc tag in the original pcDNA3.1 Myc plasmid. The amplified MeCP2(1-308) sequence was digested with XcmI and XbaI and ligated, using T4 DNA ligase (NEB), into pcDNA3.1 human MeCP2*A* or *B* myc-tagged plasmids digested with the same enzymes. The plasmids expressing truncated Myc-tagged MeCP2*A* and *B* forms were recovered by transforming competent DH5α bacteria and they were screened

by restriction digest. The sequence of the inserts corresponding to the MeCP2(R308$*$) open reading frame was then checked by direct sequencing.

A.5.6 Transfection

Transfections were carried out using FuGENE 6 (Roche Applied Bioscience), following the manufacturer's instructions (using 2 μg of plasmid and 6 μl of transfection reagent). Briefly, N2A or NIH 3T3 cells were plated in 25 cm^2 flasks at least 12 hrs before transfection. Stable N2A transfectants expressing Myc-tagged wild-type and mutated MeCP2*A* and MeCP2*B* were selected by adding 0.5 mg/ml of G418 three days after transfection, and the populations obtained were subsequently maintained in this selecting medium.

A.5.7 Quantitative Western Blot

Whole cellular extracts from adult mouse brain, and from transiently and stably transfected N2A cells were prepared, and blotted on nitrocellulose after separation by 4-12% SDS-PAGE (50 μg of cellular extract per sample). Levels of MeCP2 were then measured on an Odyssey infrared scanner (Li-Cor) after staining with a mouse anti-MeCP2 polyclonal antibody (C terminal portion, Sigma), followed by an Alexa 680 anti-mouse secondary antibody. Normalisation between samples was carried out using a mouse monoclonal against GAPDH (ab9484, abcam) and the same secondary reagent on the lower part of the same blot.

A.5.8 Cells staining and cytometry

For immunochemical staining of the cell surface for MHC class I, β-2-microglobulin or transferrin receptor, cells were harvested by trypsinisation and washed once with medium to obtain a single-cell suspension. The resuspended cells were then incubated on ice with a saturating concentration of the appropriate hybridoma supernatant. Thirty minutes later, cells were washed three times in phosphate-buffered saline (PBS) containing 2% FCS, then incubated for thirty minutes on ice with the suitable secondary reagent and washed three times before fixation in PBS containing 1% paraformaldehyde. When intracellular MeCP2 or β-III-tubulin was also analysed, further staining steps were performed as described above, but adding 0.3% saponin in all buffers. Labelled cells were analysed using a FACScalibur

cytometer and CellQuest software (BD Biosciences). Dead cells were excluded using appropriate forward/side scatter gates.

A.5.9 Immunohistochemistry of brain slices

Brains from adult $MeCP2^{-/y}$ and wild-type mice were embedded in Tissue-Tek OCT compound (Sakura) and frozen in dry ice-cold isopentane. Serial coronal sections of 10 μm were cut with a cryostat at ?20°C, placed on Super Frost Plus slides (Menzel-Gläser), air dried overnight at room temperature and fixed in acetone and air dried rapidly. The tissue sections were then rehydrated in PBS containing 3% bovine serum albumin (BSA) and endogenous peroxidase activity was quenched by incubating with peroxydase block reagent (Dako). Following washes in PBS containing 1% BSA, the specimens were incubated with saturating concentrations of rat hybridoma supernatant for 1 hr and then rinsed in PBS containing 1% BSA before incubation with the rabbit anti-rat Ig antibody Z0494 (Dako). The sections were then treated with EnVision as instructed by the manufacturer (Dako) using a labelled polymer-HRP goat anti-rabbit Ig. Finally, slides were mounted in Mowiol. Observation and image acquisitions were carried out on a Leica RM-IRB microscope using the 10× objective. Pictures were taken with a COHU CCD camera.

A.5.10 Immunofluorescence staining

N2A cells growing on coverslips were transfected with empty pcDNA3.1(+), with pcDNA3.1 expressing Myc-tagged wild-type MeCP2*A* or *B*, or pcDNA3.1 expressing Myc-tagged mutated MeCP2*A* or *B* containing the T158M, R133C, R306C or R308$*$ mutations. Cells were fixed with acetone and incubated with mouse anti-Myc monoclonal antibody (9E10) followed by FITC-labelled anti-mouse IgG antibody for 30 min at room temperature. After the final wash, the coverslips were mounted in DAPI-containing ProLong Gold antifading reagent (Molecular Probes). Observation and image acquisition were carried out on a Leica RM-IRB microscope using 40× or 20× objectives. Pictures were taken with a COHU CCD camera and acquired as TIFF stacks of images with Q-Fluoro software, after integration of the signal for 1 sec for in the case of FITC labelling (no integration of the signal was necessary for DAPI labelling).

A.5.11 Primary cultures

Brains removed from two-day old mice were cut in small pieces in ice-cold PBS containing glucose, then centrifuged at 80 *g* for 5 min at 4°C and digested with trypsin (Gibco) for 40 min at 37°C. The trypsin was blocked by adding DMEM supplemented with 10% FCS for 5 min at room temperature. The digested brain material was then washed twice with DMEM containing 10% FCS and once in neurobasal medium (Gibco) supplemented with B27 and 2% FCS, and recovered between washes by centrifugation at 80 *g* for 5 min at 4°C. During the final wash, mechanical dissociation of the cells into a single-cell suspension was achieved by pipetting up and down several times. Brain cell suspensions were plated on six-well plates coated at least 12 hrs before with poly-D-ornithine (SIGMA) and maintained in neurobasal medium containing B27 and 2% FCS.

For cultures of splenic fibroblasts, spleens were cut into small pieces in PBS/glucose, digested in trypsin and washed, as above, and finally plated on six-well plates and maintained in RPMI containing 10% FCS.

A.6 Acknowledgments

We would like to thank Dr. Brian Hendrich for his gift of reagents and helpful discussions, Drs Berge Minassian, and Adrian Bird for their gifts of plasmids, Denis Hudrisier and Jean Charles Guéry for helpful suggestions and discussions, and Carol Featherstone for her help with the manuscript.

A.7 Author Contributions

Conceived and designed the experiments: EJ JM. Performed the experiments: EM JM LK SP HB. Analyzed the data: EJ JM LK SP. Wrote the paper: EJ JM

Bibliography

[1] R. E. Amir, I. B. Van den Veyver, M. Wan, C. Q. Tran, U. Francke, and H. Y. Zoghbi. Rett Syndrome is caused by mutations in X-linked MECP2, encoding methyl-CpG-binding protein 2. *Nat Genet*, 23(2):185–8, 1999.

[2] T. Bienvenu, A. Carrie, N. de Roux, M. C. Vinet, P. Jonveaux, P. Couvert, L. Villard, A. Arzimanoglou, C. Beldjord, M. Fontes, M. Tardieu, and J. Chelly. MeCP2 mutations account for most cases of typical forms of Rett Syndrome. *Hum Mol Genet*, 9(9):1377–84, 2000.

[3] N. Sirianni, S. Naidu, J. Pereira, R. F. Pillotto, and E. P. Hoffman. Rett Syndrome: confirmation of X-linked dominant inheritance, and localization of the gene to Xq28. *Am J Hum Genet*, 63(5):1552–8, 1998.

[4] A. K. Percy. Rett Syndrome. Current status and new vistas. *Neurol Clin*, 20(4):1125–41, 2002.

[5] B. Hagberg, J. Aicardi, K. Dias, and O. Ramos. A progressive syndrome of autism, dementia, ataxia, and loss of purposeful hand use in girls: Rett's Syndrome: report of 35 cases. *Ann Neurol*, 14(4):471–9, 1983.

[6] J. L. Neul and H. Y. Zoghbi. Rett Syndrome: a prototypical neurodevelopmental disorder. *Neuroscientist*, 10(2):118–28, 2004.

[7] H. Y. Zoghbi. MeCP2 dysfunction in humans and mice. *J Child Neurol*, 20(9):736–40, 2005.

[8] M. D'Esposito, N. A. Quaderi, A. Ciccodicola, P. Bruni, T. Esposito, M. D'Urso, and S. D. Brown. Isolation, physical mapping, and northern analysis of the X-linked human gene encoding methyl CpG-binding protein, MECP2. *Mamm Genome*, 7(7):533–5, 1996.

[9] N. A. Quaderi, R. R. Meehan, P. H. Tate, S. H. Cross, A. P. Bird, A. Chatterjee, G. E. Herman, and S. D. Brown. Genetic and physical mapping of a gene encoding a methyl CpG binding protein, MeCP2, to the mouse X chromosome. *Genomics*, 22(3):648–51, 1994.

[10] R. Z. Chen, S. Akbarian, M. Tudor, and R. Jaenisch. Deficiency of methyl-CpG binding protein-2 in CNS neurons results in a Rett-like phenotype in mice. *Nat Genet*, 27(3):327–31, 2001.

[11] J. Guy, B. Hendrich, M. Holmes, J. E. Martin, and A. Bird. A mouse MeCP2-null mutation causes neurological symptoms that mimic Rett Syndrome. *Nat Genet*, 27(3):322–6, 2001.

[12] G. J. Pelka, C. M. Watson, T. Radziewic, M. Hayward, H. Lahooti, J. Christodoulou, and P. P. Tam. MeCP2 deficiency is associated with learning and cognitive deficits and altered gene activity in the hippocampal region of mice. *Brain*, 129(Pt 4):887–98, 2006.

[13] M. Shahbazian, J. Young, L. Yuva-Paylor, C. Spencer, B. Antalffy, J. Noebels, D. Armstrong, R. Paylor, and H. Zoghbi. Mice with truncated MeCP2 recapitulate many Rett Syndrome features and display hyperacetylation of histone H3. *Neuron*, 35(2):243–54, 2002.

[14] T. Gemelli, O. Berton, E. D. Nelson, L. I. Perrotti, R. Jaenisch, and L. M. Monteggia. Postnatal loss of methyl-CpG binding protein 2 in the forebrain is sufficient to mediate behavioral aspects of Rett Syndrome in mice. *Biol Psychiatry*, 59(5):468–76, 2006.

[15] S. Luikenhuis, E. Giacometti, C. F. Beard, and R. Jaenisch. Expression of MeCP2 in postmitotic neurons rescues Rett Syndrome in mice. *Proc Natl Acad Sci U S A*, 101(16):6033–8, 2004.

A

[16] E. Giacometti, S. Luikenhuis, C. Beard, and R. Jaenisch. Partial rescue of MeCP2 deficiency by postnatal activation of MeCP2. *Proc Natl Acad Sci U S A*, 104(6):1931–6, 2007.

[17] J. Guy, J. Gan, J. Selfridge, S. Cobb, and A. Bird. Reversal of neurological defects in a mouse model of Rett Syndrome. *Science*, 315(5815):1143–7, 2007.

[18] S. Kriaucionis and A. Bird. The major form of MeCP2 has a novel N-terminus generated by alternative splicing. *Nucleic Acids Res*, 32(5):1818–23, 2004.

[19] G. N. Mnatzakanian, H. Lohi, I. Munteanu, S. E. Alfred, T. Yamada, P. J. MacLeod, J. R. Jones, S. W. Scherer, N. C. Schanen, M. J. Friez, J. B. Vincent, and B. A. Minassian. A previously unidentified MeCP2 open reading frame defines a new protein isoform relevant to Rett Syndrome. *Nat Genet*, 36(4):339–41, 2004.

[20] X. Nan, F. J. Campoy, and A. Bird. MeCP2 is a transcriptional repressor with abundant binding sites in genomic chromatin. *Cell*, 88(4):471–81, 1997.

[21] X. Nan, R. R. Meehan, and A. Bird. Dissection of the methyl-CpG binding domain from the chromosomal protein MeCP2. *Nucleic Acids Res*, 21(21):4886–92, 1993.

[22] R. J. Klose, S. A. Sarraf, L. Schmiedeberg, S. M. McDermott, I. Stancheva, and A. P. Bird. DNA binding selectivity of MeCP2 due to a requirement for A/T sequences adjacent to methyl-CpG. *Mol Cell*, 19(5):667–78, 2005.

[23] X. Nan, P. Tate, E. Li, and A. Bird. DNA methylation specifies chromosomal localization of MeCP2. *Mol Cell Biol*, 16(1):414–21, 1996.

[24] P. L. Jones, G. J. Veenstra, P. A. Wade, D. Vermaak, S. U. Kass, N. Landsberger, J. Strouboulis, and A. P. Wolffe. Methylated DNA and MeCP2 recruit histone deacetylase to repress transcription. *Nat Genet*, 19(2):187–91, 1998.

[25] N. K. Kaludov and A. P. Wolffe. MeCP2 driven transcriptional repression in vitro: selectivity for methylated DNA, action at a distance and contacts with the basal transcription machinery. *Nucleic Acids Res*, 28(9):1921–8, 2000.

[26] K. Kokura, S. C. Kaul, R. Wadhwa, T. Nomura, M. M. Khan, T. Shinagawa, T. Yasukawa, C. Colmenares, and S. Ishii. The Ski protein family is required for MeCP2-mediated transcriptional repression. *J Biol Chem*, 276(36):34115–21, 2001.

[27] X. Nan, H. H. Ng, C. A. Johnson, C. D. Laherty, B. M. Turner, R. N. Eisenman, and A. Bird. Transcriptional repression by the methyl-CpG-binding protein MeCP2 involves a histone deacetylase complex. *Nature*, 393(6683):386–9, 1998.

[28] L. Jeffery and S. Nakielny. Components of the DNA methylation system of chromatin control are RNA-binding proteins. *J Biol Chem*, 279(47):49479–87, 2004.

[29] J. I. Young, E. P. Hong, J. C. Castle, J. Crespo-Barreto, A. B. Bowman, M. F. Rose, D. Kang, R. Richman, J. M. Johnson, S. Berget, and H. Y. Zoghbi. Regulation of RNA splicing by the methylation-dependent transcriptional repressor methyl-CpG binding protein 2. *Proc Natl Acad Sci U S A*, 102(49):17551–8, 2005.

[30] P. T. Georgel, R. A. Horowitz-Scherer, N. Adkins, C. L. Woodcock, P. A. Wade, and J. C. Hansen. Chromatin compaction by human MeCP2. Assembly of novel secondary chromatin structures in the absence of DNA methylation. *J Biol Chem*, 278(34):32181–8, 2003.

[31] S. Horike, S. Cai, M. Miyano, J. F. Cheng, and T. Kohwi-Shigematsu. Loss of silent-chromatin looping and impaired imprinting of DLX5 in Rett Syndrome. *Nat Genet*, 37(1):31–40, 2005.

[32] F. Fuks, P. J. Hurd, D. Wolf, X. Nan, A. P. Bird, and T. Kouzarides. The methyl-CpG-binding protein MeCP2 links DNA methylation to histone methylation. *J Biol Chem*, 278(6):4035–40, 2003.

[33] H. Kimura and K. Shiota. Methyl-CpG-binding protein, MeCP2, is a target molecule for maintenance DNA methyltransferase, Dnmt1. *J Biol Chem*, 278(7):4806–12, 2003.

[34] Q. Chang, G. Khare, V. Dani, S. Nelson, and R. Jaenisch. The disease progression of MeCP2 mutant mice is affected by the level of BDNF expression. *Neuron*, 49(3):341–8, 2006.

[35] W. G. Chen, Q. Chang, Y. Lin, A. Meissner, A. E. West, E. C. Griffith, R. Jaenisch, and M. E. Greenberg. Derepression of BDNF transcription involves calcium-dependent phosphorylation of MeCP2. *Science*, 302(5646):885–9, 2003.

[36] K. Martinowich, D. Hattori, H. Wu, S. Fouse, F. He, Y. Hu, G. Fan, and Y. E. Sun. DNA methylation-related chromatin remodeling in activity-dependent BDNF gene regulation. *Science*, 302(5646):890–3, 2003.

[37] S. Peddada, D. H. Yasui, and J. M. LaSalle. Inhibitors of differentiation (ID1, ID2, ID3 and ID4) genes are neuronal targets of MeCP2 that are elevated in Rett Syndrome. *Hum Mol Genet*, 15(12):2003–14, 2006.

[38] U. A. Nuber, S. Kriaucionis, T. C. Roloff, J. Guy, J. Selfridge, C. Steinhoff, R. Schulz, B. Lipkowitz, H. H. Ropers, M. C. Holmes, and A. Bird. Up-regulation of glucocorticoid-regulated genes in a mouse model of Rett Syndrome. *Hum Mol Genet*, 14(15):2247–56, 2005.

[39] M. L. Tykocinski and E. E. Max. CG dinucleotide clusters in MHC genes and in 5′ demethylated genes. *Nucleic Acids Res*, 12(10):4385–96, 1984.

[40] R. A. Corriveau, G. S. Huh, and C. J. Shatz. Regulation of class I MHC gene expression in the developing and mature CNS by neural activity. *Neuron*, 21(3):505–20, 1998.

[41] G. S. Huh, L. M. Boulanger, H. Du, P. A. Riquelme, T. M. Brotz, and C. J. Shatz. Functional requirement for class I MHC in CNS development and plasticity. *Science*, 290(5499):2155–9, 2000.

[42] H. Neumann, A. Cavalie, D. E. Jenne, and H. Wekerle. Induction of MHC class I genes in neurons. *Science*, 269(5223):549–52, 1995.

[43] T. Ishii, J. Hirota, and P. Mombaerts. Combinatorial coexpression of neural and immune multigene families in mouse vomeronasal sensory neurons. *Curr Biol*, 13(5):394–400, 2003.

[44] T. Leinders-Zufall, P. Brennan, P. Widmayer, P. C. S, A. Maul-Pavicic, M. Jager, X. H. Li, H. Breer, F. Zufall, and T. Boehm. MHC class I peptides as chemosensory signals in the vomeronasal organ. *Science*, 306(5698):1033–7, 2004.

[45] J. Loconto, F. Papes, E. Chang, L. Stowers, E. P. Jones, T. Takada, A. Kumanovics, K. Fischer Lindahl, and C. Dulac. Functional expression of murine V2R pheromone receptors involves selective association with the M10 and M1 families of MHC class Ib molecules. *Cell*, 112(5):607–18, 2003.

[46] J. Syken and C. J. Shatz. Expression of T cell receptor beta locus in central nervous system neurons. *Proc Natl Acad Sci U S A*, 100(22):13048–53, 2003.

[47] S. J. Gobin, M. van Zutphen, A. M. Woltman, and P. J. van den Elsen. Transactivation of classical and nonclassical HLA class I genes through the IFN-stimulated response element. *J Immunol*, 163(3):1428–34, 1999.

A

[48] M. D. Shahbazian and H. Y. Zoghbi. Molecular genetics of Rett Syndrome and clinical spectrum of MeCP2 mutations. *Curr Opin Neurol*, 14(2):171–6, 2001.

[49] J. D. Lewis, R. R. Meehan, W. J. Henzel, I. Maurer-Fogy, P. Jeppesen, F. Klein, and A. Bird. Purification, sequence, and cellular localization of a novel chromosomal protein that binds to methylated DNA. *Cell*, 69(6):905–14, 1992.

[50] F. H. McLaren, C. N. Svendsen, P. Van der Meide, and E. Joly. Analysis of neural stem cells by flow cytometry: cellular differentiation modifies patterns of MHC expression. *J Neuroimmunol*, 112(1-2):35–46, 2001.

[51] C. A. Goddard, D. A. Butts, and C. J. Shatz. Regulation of CNS synapses by neuronal MHC class I. *Proc Natl Acad Sci U S A*, 104(16):6828–33, 2007.

[52] D. R. Cohen, V. Matarazzo, A. M. Palmer, Y. Tu, O. H. Jeon, J. Pevsner, and G. V. Ronnett. Expression of MeCP2 in olfactory receptor neurons is developmentally regulated and occurs before synaptogenesis. *Mol Cell Neurosci*, 22(4):417–29, 2003.

[53] B. P. Jung, D. G. Jugloff, G. Zhang, R. Logan, S. Brown, and J. H. Eubanks. The expression of methyl CpG binding factor MeCP2 correlates with cellular differentiation in the developing rat brain and in cultured cells. *J Neurobiol*, 55(1):86–96, 2003.

[54] B. C. Mullaney, M. V. Johnston, and M. E. Blue. Developmental expression of methyl-CpG binding protein 2 is dynamically regulated in the rodent brain. *Neuroscience*, 123(4):939–49, 2004.

[55] M. D. Shahbazian, B. Antalffy, D. L. Armstrong, and H. Y. Zoghbi. Insight into Rett Syndrome: MeCP2 levels display tissue- and cell-specific differences and correlate with neuronal maturation. *Hum Mol Genet*, 11(2):115–24, 2002.

[56] N. Kishi and J. D. Macklis. MeCP2 is progressively expressed in post-migratory neurons and is involved in neuronal maturation rather than cell fate decisions. *Mol Cell Neurosci*, 27(3):306–21, 2004.

[57] J. M. LaSalle, J. Goldstine, D. Balmer, and C. M. Greco. Quantitative localization of heterogeneous methyl-CpG-binding protein 2 (MeCP2) expression phenotypes in normal and Rett Syndrome brain by laser scanning cytometry. *Hum Mol Genet*, 10(17):1729–40, 2001.

[58] U. Ritz and B. Seliger. The transporter associated with antigen processing (TAP): structural integrity, expression, function, and its clinical relevance. *Mol Med*, 7(3):149–58, 2001.

[59] I. A. York and K. L. Rock. Antigen processing and presentation by the class I major histocompatibility complex. *Annu Rev Immunol*, 14:369–96, 1996.

[60] T. Nikitina, X. Shi, R. P. Ghosh, R. A. Horowitz-Scherer, J. C. Hansen, and C. L. Woodcock. Multiple modes of interaction between the methylated DNA binding protein MeCP2 and chromatin. *Mol Cell Biol*, 27(3):864–77, 2007.

[61] T. Nikitina, R. P. Ghosh, R. A. Horowitz-Scherer, J. C. Hansen, S. A. Grigoryev, and C. L. Woodcock. MeCP2-chromatin interactions include the formation of chromatosome-like structures and are altered in mutations causing Rett Syndrome. *J Biol Chem*, 282(38):28237–45, 2007.

[62] D. Balmer, J. Goldstine, Y. M. Rao, and J. M. LaSalle. Elevated methyl-CpG-binding protein 2 expression is acquired during postnatal human brain development and is correlated with alternative polyadenylation. *J Mol Med*, 81(1):61–8, 2003.

[63] C. Colantuoni, O. H. Jeon, K. Hyder, A. Chenchik, A. H. Khimani, V. Narayanan, E. P. Hoffman, W. E. Kaufmann, S. Naidu, and J. Pevsner. Gene expression profiling in postmortem Rett Syndrome brain: differential gene expression and patient classification. *Neurobiol Dis*, 8(5):847–65, 2001.

[64] J. Traynor, P. Agarwal, L. Lazzeroni, and U. Francke. Gene expression patterns vary in clonal cell cultures from Rett Syndrome females with eight different MeCP2 mutations. *BMC Med Genet*, 3:12, 2002.

[65] M. Tudor, S. Akbarian, R. Z. Chen, and R. Jaenisch. Transcriptional profiling of a mouse model for Rett Syndrome reveals subtle transcriptional changes in the brain. *Proc Natl Acad Sci U S A*, 99(24):15536–41, 2002.

[66] K. S. Beyer, F. Blasi, E. Bacchelli, S. M. Klauck, E. Maestrini, and A. Poustka. Mutation analysis of the coding sequence of the *mecp2* gene in infantile autism. *Hum Genet*, 111(4-5):305–9, 2002.

[67] C. W. Lam, W. L. Yeung, C. H. Ko, P. M. Poon, S. F. Tong, K. Y. Chan, I. F. Lo, L. Y. Chan, J. Hui, V. Wong, C. P. Pang, Y. M. Lo, and T. F. Fok. Spectrum of mutations in the MeCP2 gene in patients with infantile autism and Rett Syndrome. *J Med Genet*, 37(12):E41, 2000.

[68] P. Watson, G. Black, S. Ramsden, M. Barrow, M. Super, B. Kerr, and J. Clayton-Smith. Angelman Syndrome phenotype associated with mutations in MeCP2, a gene encoding a methyl CpG binding protein. *J Med Genet*, 38(4):224–8, 2001.

[69] P. Couvert, T. Bienvenu, C. Aquaviva, K. Poirier, C. Moraine, C. Gendrot, A. Verloes, C. Andres, A. C. Le Fevre, I. Souville, J. Steffann, V. des Portes, H. H. Ropers, H. G. Yntema, J. P. Fryns, S. Briault, J. Chelly, and B. Cherif. MeCP2 is highly mutated in X-linked mental retardation. *Hum Mol Genet*, 10(9):941–6, 2001.

[70] A. Orrico, C. Lam, L. Galli, M. T. Dotti, G. Hayek, S. F. Tong, P. M. Poon, M. Zappella, A. Federico, and V. Sorrentino. MeCP2 mutation in male patients with non-specific X-linked mental retardation. *FEBS Lett*, 481(3):285–8, 2000.

[71] J. Clayton-Smith, P. Watson, S. Ramsden, and G. C. Black. Somatic mutation in MeCP2 as a non-fatal neurodevelopmental disorder in males. *Lancet*, 356(9232):830–2, 2000.

[72] L. Villard, A. Kpebe, C. Cardoso, P. J. Chelly, P. M. Tardieu, and M. Fontes. Two affected boys in a Rett Syndrome family: clinical and molecular findings. *Neurology*, 55(8):1188–93, 2000.

[73] A. L. Collins, J. M. Levenson, A. P. Vilaythong, R. Richman, D. L. Armstrong, J. L. Noebels, J. David Sweatt, and H. Y. Zoghbi. Mild overexpression of MeCP2 causes a progressive neurological disorder in mice. *Hum Mol Genet*, 13(21):2679–89, 2004.

[74] F. Ariani, F. Mari, C. Pescucci, I. Longo, M. Bruttini, I. Meloni, G. Hayek, R. Rocchi, M. Zappella, and A. Renieri. Real-time quantitative PCR as a routine method for screening large rearrangements in Rett Syndrome: Report of one case of MECP2 deletion and one case of MECP2 duplication. *Hum Mutat*, 24(2):172–7, 2004.

[75] D. Lugtenberg, A. P. de Brouwer, T. Kleefstra, A. R. Oudakker, S. G. Frints, C. T. Schrander-Stumpel, J. P. Fryns, L. R. Jensen, J. Chelly, C. Moraine, G. Turner, J. A. Veltman, B. C. Hamel, B. B. de Vries, H. van Bokhoven, and H. G. Yntema. Chromosomal copy number changes in patients with non-syndromic X linked mental retardation detected by array CGH. *J Med Genet*, 43(4):362–70, 2006.

[76] M. Meins, J. Lehmann, F. Gerresheim, J. Herchenbach, M. Hagedorn, K. Hameister, and J. T. Epplen. Submicroscopic duplication in Xq28 causes increased expression of the MeCP2 gene in a boy with severe mental retardation and features of Rett Syndrome. *J Med Genet*, 42(2):e12, 2005.

A

[77] H. Van Esch, M. Bauters, J. Ignatius, M. Jansen, M. Raynaud, K. Hollanders, D. Lugtenberg, T. Bienvenu, L. R. Jensen, J. Gecz, C. Moraine, P. Marynen, J. P. Fryns, and G. Froyen. Duplication of the MeCP2 region is a frequent cause of severe mental retardation and progressive neurological symptoms in males. *Am J Hum Genet*, 77(3):442–53, 2005.

[78] J. Miralves, E. Magdeleine, and E. Joly. Design of an improved set of oligonucleotide primers for genotyping MeCP2tm1.1Bird KO mice by PCR. *Mol Neurodegener*, 2:16, 2007.

[79] B. Hendrich and A. Bird. Identification and characterization of a family of mammalian methyl-CpG binding proteins. *Mol Cell Biol*, 18(11):6538–47, 1998.

[80] R. D. Kirsch and E. Joly. An improved PCR-mutagenesis strategy for two-site mutagenesis or sequence swapping between related genes. *Nucleic Acids Res*, 26(7):1848–50, 1998.